

AD-A033 034

JET PROPULSION LAB PASADENA CALIF
NITRAMINE PROPELLANT RESEARCH. (U)
OCT 76 N S COHEN, L D STRAND

F/G 19/1

UNCLASSIFIED

1 OF 2
AD
A033034

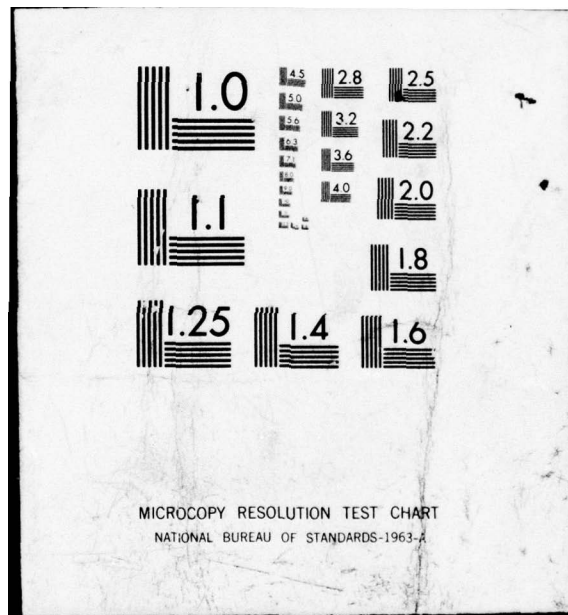


NAS7-100

AFOSR-TR-76-1163

NL





ADA 033034

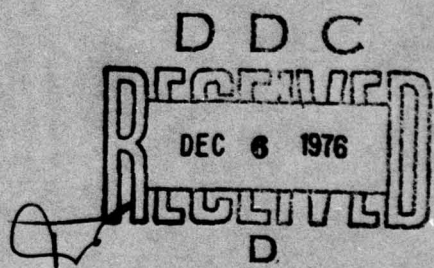
AFOSR - TR - 76 - 1168

NATIONAL AERONAUTICS AND SPACE ADMINISTRATION

CC

Technical Memorandum 33-801

Nitramine Propellant Research



JET PROPULSION LABORATORY
CALIFORNIA INSTITUTE OF TECHNOLOGY
PASADENA, CALIFORNIA

October 15, 1976

Approved for public release
distribution unlimited.

2

AIR FORCE OFFICE OF SCIENTIFIC RESEARCH (AFSC)
NOTICE OF TRANSMITTAL TO PDC
This technical report has been reviewed and is
approved for public release IAW AFR 190-12 (7b).
Distribution is unlimited.
A. D. BLOSE
Technical Information Officer

UNCLASSIFIED

SECURITY CLASSIFICATION OF THIS PAGE (When Data Entered)

(9) Final rept. 1 Jan 75-30 Jun 76

REPORT DOCUMENTATION PAGE		READ INSTRUCTIONS BEFORE COMPLETING FORM
1. REPORT NUMBER AFOSR - TR - 76 - 1163	2. GOVT ACCESSION NO.	3. RECIPIENT'S CATALOG NUMBER
4. TITLE (and Subtitle) (6) NITRAMINE PROPELLANT RESEARCH	5. TYPE OF REPORT & PERIOD COVERED FINAL 1 Jan 1975 - 30 June 1976	
7. AUTHOR(s) N. S. COHEN L. D. STRAND	6. PERFORMING ORG. REPORT NUMBER (15) NASA-100 AFOSR-TSSA-75-0005	
9. PERFORMING ORGANIZATION NAME AND ADDRESS JET PROPULSION LABORATORY, California Inst. of Tech SOLID PROPELLANT ENGINEERING PASADENA, CALIFORNIA 91103	10. PROGRAM ELEMENT, PROJECT, TASK AREA & WORK UNIT NUMBERS 681308 9711-01 61102F	
11. CONTROLLING OFFICE NAME AND ADDRESS AIR FORCE OFFICE OF SCIENTIFIC RESEARCH/NA BLDG 410 BOLLING AIR FORCE BASE, D C 20332	12. REPORT DATE (11) 15 Oct 76	
14. MONITORING AGENCY NAME & ADDRESS (if different from Controlling Office)	13. NUMBER OF PAGES 133 (12) 136p.	
	15. SECURITY CLASS. (of this report) UNCLASSIFIED	
	15a. DECLASSIFICATION/DOWNGRADING SCHEDULE	
16. DISTRIBUTION STATEMENT (of this Report) (16) 9711	(17) 01	
Approved for public release; distribution unlimited.		
17. DISTRIBUTION STATEMENT (of the abstract entered in Block 20, if different from Report) (18) AFOSR, NASA (19) TR-76-1163, TM-33-801		
18. SUPPLEMENTARY NOTES		
19. KEY WORDS (Continue on reverse side if necessary and identify by block number) GUN PROPELLANTS COMBUSTION NITRAMINE PROPELLANTS 191150		
20. ABSTRACT (Continue on reverse side if necessary and identify by block number) An extended model of the combustion of nitramine propellants is derived to account for multiple particle sizes, mixed oxidizers and active binders. Burning rates of various nitramine propellants are reported over the pressure range from 500 psi to 50,000 psi and show effects of systematic ingredient variations. A high pressure window bomb is utilized to observe the combustion process of these propellants by cinematography to a pressure of 6000 psi. The propellants are also extinguished by rapid decompression, and their surface and subsurface structures are studied with the aid of a scanning electron microscope. A computer program		

UNCLASSIFIED

SECURITY CLASSIFICATION OF THIS PAGE(When Data Entered)

cont

is developed to incorporate the model extensions and is applied to explain the experimental data. Parametric studies are performed with the model to formulate methods to achieve desirable burning rate characteristics in nitramine propellants. It is concluded that the model successfully describes the combustion of nitramine propellants and is a useful tool to evaluate combustion tailoring in association with propellant development efforts.



UNCLASSIFIED

SECURITY CLASSIFICATION OF THIS PAGE(When Data Entered)

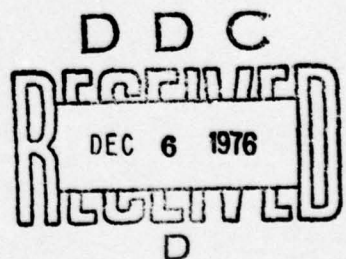
NATIONAL AERONAUTICS AND SPACE ADMINISTRATION

Technical Memorandum 33-801

Nitramine Propellant Research

N. S. Cohen and L. D. Strand

White Section	<input checked="" type="checkbox"/>
Buff Section	<input type="checkbox"/>
STANDARDIZED	<input type="checkbox"/>
SPECIFICATION	<input type="checkbox"/>
BY	
DISTRIBUTION/AVAILABILITY CODES	
DIST.	AVAIL. AND/OR SPECIAL
A	



JET PROPULSION LABORATORY
CALIFORNIA INSTITUTE OF TECHNOLOGY
PASADENA, CALIFORNIA

October 15, 1976

DISTRIBUTION STATEMENT A

Approved for public release;
Distribution Unlimited

Prepared Under Contract No. NAS 7-100
National Aeronautics and Space Administration

PREFACE

The work described in this report was performed by the Control and Energy Conversion Division of the Jet Propulsion Laboratory under Contract No. NAS 7-100, Task Order No. RD-65, Amendment No. 197. This investigation was supported by the Air Force Office of Scientific Research under AFOSR Support Agreement Nos. AFOSR-ISSA-75-0005 and AFOSR-ISSA-76-0006, and this report is submitted to AFOSR as the annual progress report for the period 1 Jan 1975 to 30 June 1976. Dr. Cohen's services as Associate Investigator were funded under JPL Contract No. 954444 to Harold Leeming & Associates.

ACKNOWLEDGEMENTS

This report was prepared by N.S. Cohen and L.D. Strand, who were the principal investigators for this research program. The work was conducted within the Solid Propulsion and Environmental Systems Section of JPL, under the supervision of W. Gin and Dr. G. Varsi. The authors hereby acknowledge the interest and support of Maj. T.C. Meier (AFOSR), Capt. L.R. Lawrence (currently at ERDA) and O.K. Heiney (AFATL), whose collaboration made this effort possible.

Propellants, low pressure burning rate data and other pertinent data were furnished by the Rocketdyne Division of Rockwell/International Corporation under the supervision of Dr. J.E. Flanagan. High pressure burning rate data for these and other related propellants were furnished by B.K. Moy of AFATL. Experiments at JPL were conducted with the assistance of A. Rasmussen and K. Schwartz (testing), R. Hanson and D. Maxeiner (cinematography), and R.E. Gauldin (scanning electron microscope). C.F. Price (currently at NWC) continued to participate in the modeling and structuring of the computer program to accommodate the model extensions.

Finally, the authors wish to express their appreciation to their many colleagues who provided valuable information in the course of this work and helped to maintain its relevance and timeliness.

TABLE OF CONTENTS

Section

1	OBJECTIVE	1
2	INTRODUCTION	2
3	PROGRAM TASKS	3
4	SUMMARY	5
5	TECHNICAL AND SCIENTIFIC ACCOMPLISHMENTS	8
5.1	TASK 1: PREPARATION	8
5.1.1	Propellants	8
5.1.2	Experimental Apparatus.	11
5.2	TASK 2: LABORATORY COMBUSTION EXPERIMENTS	13
5.2.1	Strand Burning Rate Data	13
5.2.1.1	Effect of Bimodal Particle Size in HMX-Inert Binder Propellants	13
5.2.1.2	Effect of Mixed HMX-TAGN in Inert Binder Propellants	18
5.2.1.3	Effect of HMX Particle Size in Active Binder Propellants	20
5.2.1.4	Effect of Mixed HMX-TAGN in Active Binder Propellants	22
5.2.2	Window Bomb Microcinematography Study	26
5.2.2.1	Inert Binder Propellants	26
5.2.2.2	Active Binder Propellants	28
5.2.3	Study of Extinguished Surfaces	31
5.2.3.1	HMX-Inert Binder Propellants	31
5.2.3.2	Mixed HMX and TAGN in Inert Binder . . .	46
5.2.3.3	Active Binder Propellants	49

Section

5.3 TASK 3: COMBUSTION MODELING	60
5.3.1 Discussion of Approach.	60
5.3.2 Surface Structure Modifications	65
5.3.3 Flame Structure Modifications	68
5.3.4 Energy Balance Modifications.	70
5.3.5 Provision for Metallized Propellants.	72
5.3.6 Computer Programming.	72
5.4 TASK 4: COMBUSTION MODEL APPLICATION	74
5.4.1 Combustion Model Verification	74
5.4.1.1 Bimodal HMX-Inert Binder Propellants . .	74
5.4.1.2 Effect of TAGN in Inert Binder Propellants	76
5.4.1.3 Effect of HMX Particle Size in Active Binder Propellants.	78
5.4.1.4 Effect of TAGN in Active Binder Propellants.	79
5.4.1.5 AP-Active Binder Propellants	81
5.4.2 Parametric Studies.	83
5.4.2.1 The Importance of Fine Particle Sizes. .	83
5.4.2.2 Effects of TAGN.	85
5.4.2.3 Effects of Active Binder	86
5.4.2.4 Matching Nitramine and Active Binder . .	88
5.4.2.5 Burning Rate Tailoring of Active Binder Rocket Propellants.	94
5.4.2.6 Burning Rate Tailoring of Inert Binder Rocket Propellants	97
6 PRESENTATIONS AND PUBLICATIONS.	100
7 CONCLUSIONS AND RECOMMENDATIONS	101
8 REFERENCES.	103

APPENDIX A	NOMENCLATURE	A-1
APPENDIX B	COMPUTER PROGRAM DESCRIPTION	B-1
	B-1 SUBROUTINES AND FUNCTIONS	B-1
	B-2 ITERATION PROCEDURE	B-4
	B-3 CARD INPUT SEQUENCE AND STANDARD VALUES	B-9
TABLES		
1	Inert binder propellant variations	9
2	Referenced inert binder propellants	9
3	Active binder propellant variations.	10
4	Referenced active binder propellants	10
FIGURES		
1	Effect of bimodal size in HMX-ethyl cellulose propellant	14
2	Effect of bimodal particle size in HMX-HTPB propellant	15
3	Effect of fine/coarse ratio in bimodal HMX-HTPB propellant	16
4	Burning rates of mixed HMX/TAGN-HTPB propellants	19
5	Effect of HMX particle size in active binder propellants.	21
6	Effect of TAGN in NPPU propellants	23
7	Effect of TAGN in NC propellants	24
8a	Unimodal coarse HMX/EC propellant, fractured surface, 100X.	32
8b	Bimodal coarse/fine HMX/EC propellant, fractured surface, 100X.	32
9a	Unimodal coarse HMX/EC propellant, extinguished surface, 4000 psi, 25X	33
9b	Bimodal coarse/fine HMX/EC propellant, extinguished surface, 4500 psi, 25X	33

FIGURES

10a	Unimodal coarse HMX/EC propellant, extinguished surface, 4000 psi, 100X	34
10b	Bimodal coarse/fine HMX/EC propellant, extinguished surface, 4500 psi, 100X	34
11a	Unimodal coarse HMX/EC propellant, extinguished surface, 2000 psi, 25X	35
11b	Bimodal coarse/fine HMX/EC propellant, extinguished surface, 2000 psi, 25X	35
12a	Unimodal coarse, HMX/EC propellant, extinguished surface, 1000 psi, 25X	37
12b	Bimodal coarse/fine HMX/EC propellant, extinguished surface, 1000 psi, 25X	37
13a	Magnification of lower center of Figure 12a, 50X	38
13b	Magnification of lower left region, 500X	38
14a	Edge of extinguished surface of coarse HMX/EC propellant, 1000 psi, 1000X	40
14b	Another edge view of extinguished surface of coarse HMX/EC propellant, 1000 psi, 1000X	40
15a	Edge view of extinguished surface of coarse HMX/EC propellant, 4000 psi, 100X	41
15b	Magnification of particle at crater base, 1000X	41
16a	Edge view of extinguished surface of bimodal coarse/fine HMX/EC propellant, 1000 psi, 500X.	43
16b	Magnification of central region, 1000X	43
17a	Edge view of extinguished surface of bimodal coarse/fine HMX/EC propellant, 4500 psi, 250X.	45
17b	Magnification of right-hand region, 1000X	45
18a	Unimodal fine HMX/EC propellant, extinguished surface, 4500 psi, 500X	47
18b	Edge view of extinguished surface of unimodal fine HMX/EC propellant, 4500 psi, 2000X	47

FIGURES

19a	Section showing top and edge of extinguished surface of fine HMX-fine TAGN/HTPB propellant, 3000 psi, 1000X	48
19b	A different section of the same propellant, 500X	48
20a	Section showing top and edge of extinguished surface of fine HMX-fine TAGN/HTPB propellant, 5000 psi, 500X	50
20b	Magnification of central region, 1000X	50
21a	Extinguished surface of coarse HMX/NC propellant, 3000 psi, 500X	51
21b	Section showing top and edge of extinguished surface of fine HMX/NC propellant, 4300 psi, 1000X	51
22a	Extinguished surface of coarse HMX/NC propellant, 4500 psi, 500X	52
22b	Section of extinguished surface of fine HMX/NC propellant 4800 psi, 1000X	52
23a	Section showing top and edge of extinguished surface of fine TAGN/NC propellant, 3000 psi, 1000X	54
23b	Fine TAGN/NC propellant extinguished at 5000 psi, 1000X	54
24a	Extinguished surface of fine HMX-fine TAGN/NC propellant, 3000 psi, 50X.	56
24b	Magnification of lower central region, 200X.	56
25a	Edge view of extinguished surface of fine HMX-fine TAGN/NC propellant, 3000 psi, 500X	57
25b	Magnification of central region, 2000X	57
26a	Extinguished surface of fine HMX-fine TAGN/NC propellant, 4700 psi, 500X	58
26b	Section showing top and edge of extinguished surface of fine HMX-fine TAGN/NC propellant, 4700 psi, 1000X.	58
27	Multiple flame structure for mixed oxidizers	69
28	Effect of AP in double-base propellants.	82
29	Effect of real particle size distribution on burning rate of HMX/HTPB propellant; "fine" HMX	84

FIGURES

30	Burning rates of mixed HMX/TAGN propellants in active binder; effect of active binder energy	87
31	Comparison of monopropellant burning rates and post-break propellant burning rates	90
32	Calculated reverse break points caused by low-rate nitramine.	91
33	Triple-base propellant burning rates, high solids loading.	93
34	Burning rate tailorability of energetic active binder propellants; effects of ingredient variations.	95
35	Burning rate tailorability of HMX and HMX/TAGN propellants in HTPB binder; effects of ingredient variations	98
36	Burning rate tailorability of mixed HMX/AP propellant in HTPB binder; effects of ingredient variations	99
B-1	Outer loop control logic	B-2
B-2	Inner loop solution logic.	B-3

ABSTRACT

An extended model of the combustion of nitramine propellants is derived to account for multiple particle sizes, mixed oxidizers and active binders. Burning rates of various nitramine propellants are reported over the pressure range from 500 psi to 50,000 psi and show effects of systematic ingredient variations. A high pressure window bomb is utilized to observe the combustion process of these propellants by cinematography to a pressure of 6000 psi. The propellants are also extinguished by rapid decompression, and their surface and subsurface structures are studied with the aid of a scanning electron microscope. A computer program is developed to incorporate the model extensions and is applied to explain the experimental data. Parametric studies are performed with the model to formulate methods to achieve desirable burning rate characteristics in nitramine propellants. It is concluded that the model successfully describes the combustion of nitramine propellants and is a useful tool to evaluate combustion tailoring in association with propellant development efforts.

33-801

Section 1

OBJECTIVE

The objective of this research program is to develop an improved general model of the combustion of Nitramine propellants that would accommodate a multiple of active ingredients. The basis for the approach are the combustion models developed by Kumar and Strand under AFATL MIPR No. FY7621-73-90062 (Refs. 1, 2), and by Cohen and Price under AFOSR Contract F44620-74-C-0031 (Refs. 3, 4), for simple Nitramine propellants. The research reported herein served to investigate more complicated propellants.

33-801
Section 2

INTRODUCTION

Nitramine propellants are of interest in applications seeking to optimize propellant impetus and flame temperature under constraints of propellant sensitivity, cost, smokelessness, flash and corrosivity (Refs. 5,6). However, the incorporation of Nitramines into either inert or active binder formulations has been found to produce a detrimental combustion anomaly (Ref. 7). A marked increase in the pressure-dependence of burning rate occurs at pressures in the range of 1Kpsi-7Kpsi, and persists regardless of the type of Nitramine (Refs. 8, 9). This anomaly impairs ballistics efficiency and reproducibility (Ref. 10).

Studies of Nitramine propellant combustion conducted in 1974 related this "slope-break" phenomenon to the inhomogeneity of the propellant (Refs. 1, 2), and more specifically to changes in propellant surface and flame structure dependent upon ingredient properties and particle size (Refs. 3, 4). An ideal phenomenological model and a detailed comprehensive model of the combustion process were developed which explained burning rate and slope trends in simple Nitramine propellants. These models were applied to propose formulation tailoring criteria, e.g., changes in ingredient properties and particle size, that would promote desired burning rate characteristics (Refs. 1, 3).

It is recognized that practical Nitramine propellants often contain a blend of particle sizes, mixtures of types of powder, and active nitrate binders. The modeling to date has been limited to simple propellants, consisting of a single powder of one particle size in inert hydrocarbon binders. Such was a logical first step, and provided much useful information. However, to the extent that mixed active ingredients are required for certain purposes, and can furnish an additional dimension to combustion tailoring, it is necessary to study and model their combination. Therefore, this research program served to extend the recent work to more complicated propellants of practical interest.

Section 3

PROGRAM TASKS

This research program was conducted as four tasks:

- (1) Preparation of Materials and Equipment
- (2) Laboratory Combustion Experiments
- (3) Combustion Modeling
- (4) Combustion Model Application

Task 1 involved the following subtasks:

- (a) Preparation of specified Nitramine propellant formulations¹
- (b) Transfer of high pressure combustion apparatus to JPL, and installation at JPL
- (c) Procurement of test materials

Task 2 involved the following subtasks:

- (a) Strand burning rate measurements¹, to 50Kpsi²
- (b) Window bomb movies of the combustion zone
- (c) Scanning electron microscope study of unburned and extinguished propellant surfaces and subsurfaces

Task 3 involved the following subtasks:

- (a) Conversion and check-out of prior combustion model computer program on UNIVAC 1108 computer
- (b) Modeling of mixed powders of bimodal particle sizes for a 2X2 type-size matrix (e.g., could calculate a tetramodal size for a single powder) in inert binder
- (c) Model modifications to incorporate active binder
- (d) Associated computer programming and debugging

¹ Furnished by the Rocketdyne Division of Rockwell/International Corp.

² Furnished by the Air Force Armament Laboratory, Eglin AFB.

Task 4 involved the following subtasks:

- (a) Comparison of experimental burning rates with model results
- (b) Parametric variation of model parameters to explore methods of combustion tailoring

Section 4

SUMMARY

Propellants consisting of mixtures and various particle sizes of nitramines, in active and in inert binders, were studied analytically and experimentally.

Burning rates of bimodal HMX propellants were found to be dominated by the behavior of the coarse fraction. Increasing the fine/coarse ratio slightly reduces the break point pressure attributable to the coarse size, increases pre-break burning rates and reduces post-break burning rates. Replacing HMX with TAGN raises pre-break burning rates, but effects on post-break burning rates are inconsistent. If the TAGN itself exhibits a break point, the burning rates become very high; if not, the burning rates may remain about the same or decrease. Such adjustments of burning rate levels on either side of the break point affects the apparent pressure exponent that results over the transition pressure region. These levels are further affected by the use of active binders of differing energies. Increasing the energy of the active binder raises pre-break burning rates more so than post-break burning rates. The appearance of the slope break is mitigated by combinations of these ingredients.

Motion picture observations of the combustion, and scanning electron microscope observations of extinguished propellant surfaces, confirmed the basic break point mechanism reported previously (Ref. 3). It is associated with a surface structure shift, from a decomposing planar melt at low pressures to cratering at high pressures that results from pronounced particle deflagration and propagation in depth. Bimodal HMX propellants superpose fine size and coarse size particle behavior; the post-break cratering from the coarse component is smoothed and lined by the melt layer from the fine component. Active binder propellants eject molten HMX agglomerates from the surface melt at low pressures, and the cratering at high pressures is less extensive than with inert binders.

TAGN appears to melt and decompose more readily than does HMX; there are no particle ejections from active binder, and some decomposition is evident in the melt layer. Mixtures of TAGN and HMX appear to superpose the behavior of each.

The combustion model and computer program were extended to provide for bimodal distributions, mixed oxidizers and active binder. Application to the various propellants studied showed satisfactory agreement with the burning rate data. Bimodal particle size effects at high pressure are predicted to be consistent with the experimental observations of surface structure. Effects in inert binder propellants at low pressure are determined by the diffusion flame above the melt layer, whose characteristic dimension is dominated by the coarse fraction. There is little particle size effect in active binder propellants at low pressure because the stoichiometry of each ingredient is presumed to preclude diffusion interaction. The effects of TAGN are explained by its lower melting point, faster decomposition and monopropellant reaction kinetics, and higher net surface exothermicity relative to HMX. The effects of active binder are explained by its own burning rate and energy contributions. The model also was verified by application to active binder propellants containing AP; the effect of AP on low pressure rates is significant and particle size dependent because of the diffusion flame.

Parametric studies were conducted with the model to discern methods to avoid break points in nitramine propellants. Fine particle size is the most effective approach because it extends the melt layer to higher pressure. However, production lots of fine material are found to include excessive coarse sizes which limit this approach as a practical matter. Careful combinations of HMX and TAGN can be used to mitigate the appearance of break points which do appear at higher pressures with available fine material. An alternate approach is

suggested based upon better matching of the monopropellant combustion properties of the nitramine and active binder; EDNA and tailored active binder are proposed for evaluation. Additional parametric studies were performed to show the limited combustion tailoring potential of nitramine rocket propellants unless AP is included.

It is concluded that the extended steady-state model has been successfully developed, and it is recommended that future work address the transient combustion properties of nitramine propellants.

Section 5

TECHNICAL AND SCIENTIFIC ACCOMPLISHMENTS

5.1 TASK 1: PREPARATION

5.1.1 Propellants

Propellant formulations were selected for the experimental program to afford systematic variations in bimodal particle size distribution and mixed Nitramine oxidizer in each inert-binder and active-binder systems. High solids loadings consistent with practical interest and processing constraints were utilized. The principal oxidizers selected were HMX³ and TAGN⁴, in accordance with propellant developments of recent years. Propellants processed for this program were processed and furnished to JPL and AFATL by the Rocketdyne Division of North American/Rockwell, Inc. A summary of inert binder formulations is presented in Table 1, and of active binder formulations in Table 3.

Tables 2 and 4 present additional inert binder and active binder formulations, respectively. These formulations were not tested at JPL, but were referenced in the course of this work. Burning rate data were furnished by AFATL to afford a more extensive model verification for biomodal, mixed oxidizer and active binder propellants.

Two types of inert binders were employed. First, a series of three formulations contained ethyl cellulose (EC), which was selected as a polyurethane-type binder capable of extrusion. However, the quality of the propellant samples was suspect and full complements of burning rate data were not acquired. Therefore, a second series was prepared containing

³ - Cyclotetramethylenetrinitramine

⁴ - Triaminoguanidine Nitrate

TABLE 1 - INERT BINDER PROPELLANT VARIATIONS

	<u>39-1</u>	<u>39-2</u>	<u>39-3</u>	<u>138-1</u>	<u>138-2</u>	<u>138-3</u>	<u>137-1</u>
Wt. -% 5 μ HMX	82.0	-	41.0	75.0	39.2	-	39.2
WT. -% 125 μ HMX	-	82.0	41.0	-	39.2	81.7	-
WT. -% 5 μ TAGN	-	-	-	-	-	-	39.2
Binder Type	EC	EC	HTPB*	HTPB	HTPB	HTPB	HTPB

TABLE 2 - REFERENCED INERT BINDER PROPELLANTS

	<u>GP-9</u>	<u>GP-6A</u>	<u>GP-5A</u>	<u>GP-7</u>	<u>RHT-7</u>
Wt. -% 15 μ HMX	-	24.0	40.0	56.0	74.0
Wt. -% 150 μ HMX	80.0	56.0	40.0	24.0	-
WT. -% 5 μ TAGN	-	-	-	-	13.0
Binder Type	HTPB	HTPB	HTPB	HTPB	HTPB

* - R-45 with IDP

TABLE 3 - ACTIVE BINDER PROPELLANT VARIATIONS

	<u>128-1</u>	<u>148-2</u>	<u>148-3</u>	<u>149-1</u>	<u>149-2</u>	<u>9-1</u>	<u>9-2</u>
Wt. -% 5 _μ HMX	-	75.0	-	46.0	-	-	-
Wt. -% 125 _μ HMX	-	-	75.0	-	46.0	-	-
Wt. -% 5 _μ TAGN	75.0	-	-	29.0	29.0	62.7	-
Wt. -% EDNA	-	-	-	-	-	-	75.0
Binder Type	NC*	NC	NC	NC	NPPU**	NC	

TABLE 4 - REFERENCED ACTIVE BINDER PROPELLANTS

	<u>RGP-150</u>	<u>GAU-8</u>	<u>CLASS E</u>	<u>CLASS A</u>
Wt. -% 5 _μ HMX	24.0	46.0	75.0(7 _μ)	-
Wt. -% 125 _μ HMX	-	-	-	75.0
Wt. -% 5 _μ TAGN	50.0	29.0	-	-
Binder Type	NC	NPPU	NPPU	NPPU

* - 12.6N with inert plasticizer
 ** - R-18 with TMETN plasticizer

hydroxyl-terminated polybutadiene (HTPB). Solids loading was decreased with increasing content of fine particles in order to best assure quality samples. These two series sought to study bimodal particle size in comparison to the unimodal constituents. The last formulation sought to study a mixed nitramine propellant. The referenced propellants (Table 2) provide further bimodal size variations, and an additional mixed nitramine variation.

The principal active binder was nitrocellulose (12.6% nitrogen). Five basic formulations were selected to study nitramine type and size effects. A sixth formulation varied the binder by using nitroplasticized polyurethane. The last (EDNA⁵) formulation was added to verify an aspect of model parametric study. The referenced propellants (Table 4) provide further mixed nitramine and active binder variations, although not entirely systematic.

5.1.2 Experimental Apparatus

The high pressure window bomb described in Ref. (3) was removed from the Lockheed Propulsion Company facility and reassembled at JPL. Associated plumbing and electrical work were performed to install this device at the JPL test facility and connect it with the inert gas supply and control system. A timing system was included to sequence camera, ignition and rapid decompression for each test. A 1 KW xenon light source and a Hycam camera, similar to those used at Lockheed (Ref. 3), were furnished by JPL.

Motion pictures were acquired over the range of 1-5 Kpsi for each propellant. The high pressure was enough to capture the breakpoint for coarse propellants, but not fine propellants. Magnification was constrained to 1.5/1 by the distance from the window assembly to the sample. In

practice, however, higher magnification would not be desirable at high burning rates associated with high pressure work, and where igniter or propellant smoke produce intermittent view interference. The low magnification is adequate to resolve details in coarse propellants and, based on Reference (3), a magnification of 4/1 would still be inadequate to resolve fine details in fine propellants. These fine details tend to be obscured by the surface melt layer, anyway, which is seen well enough at the low magnification. Motion pictures were acquired at framing rates of from 2-4 Kfps.

Extinguished surfaces were obtained by rapid decompression, as described in Reference (3). Motion pictures captured the extinguishment in some cases, and revealed the surface regression to be stopped immediately without major upheavals that are sometimes noted in aluminized propellants. Particle ejections were never observed to result from the rapid decompression. However, some lifting and blow holes were observed in thin portions of the surface melt when viewed under the scanning electron microscope (SEM), and this appears to be the only fault of the rapid decompression. The JPL SEM facility was used to study extinguished surfaces, microtomed sections of burned propellants and sections of unburned propellants, at various magnifications.

Burning rates at pressures below 2Kpsi were acquired in the Rocketdyne Crawford Bomb apparatus. Data at pressures above 2Kpsi, and to as high as 50Kpsi, were acquired in the AFATL high pressure strand burner facility.

Particle size distributions for fine particle ingredients, which turned out to have some significance in model applications, were furnished by Hercules/ABL and by Rocketdyne based upon MSA measurements. Attempts to measure distributions optically with the SEM proved unsuccessful because of the coagulation tendencies of the powder samples. Use of the SEM was

limited to a gross confirmation of the sizes as they existed in the propellant samples.

5.2 TASK 2: LABORATORY COMBUSTION EXPERIMENTS

5.2.1 Strand Burning Rate Data

The following discusses the burning rate data acquired and used in this program for model development and verification. Data are displayed in series of plots to show effects of various formulation variables. The plots also include the results of analytical computations based upon the extended combustion model to be discussed in Section 5.3. The general agreement between theory and experiment constitutes a form of model verification, to be discussed in the context of explanations for the burning rate trends in Subsection 5.4.1. Additional burning rate behavior exhibited by Nitramine propellants will be discussed in the context of analytical parametric study in Subsection 5.4.2.

5.2.1.1 Effect of Bimodal Particle Size in HMX-Inert Binder Propellants

The first aspect of the model extension is to consider effects of bimodal particle size distributions in HMX-inert binder propellants.

Effects of unimodal particle size were well-characterized in References (3, 4). Bimodal particle size effects are shown in Figures 1-3.

Figures 1 and 3 show systematic particle size effects in that HMX concentration remained constant at 82% and 80%, respectively. Concentration varied with particle size in the Figure 2 data, decreasing with increasing percentage of fines to promote propellant quality, which has a significant effect upon flame temperature; however, important low pressure data were acquired with this series. The Figure 1 and Figure 3 data appear to have commenced in the course of exponent transitions, such that the bimodal effect upon the approach to transition could not be discerned in those two series.

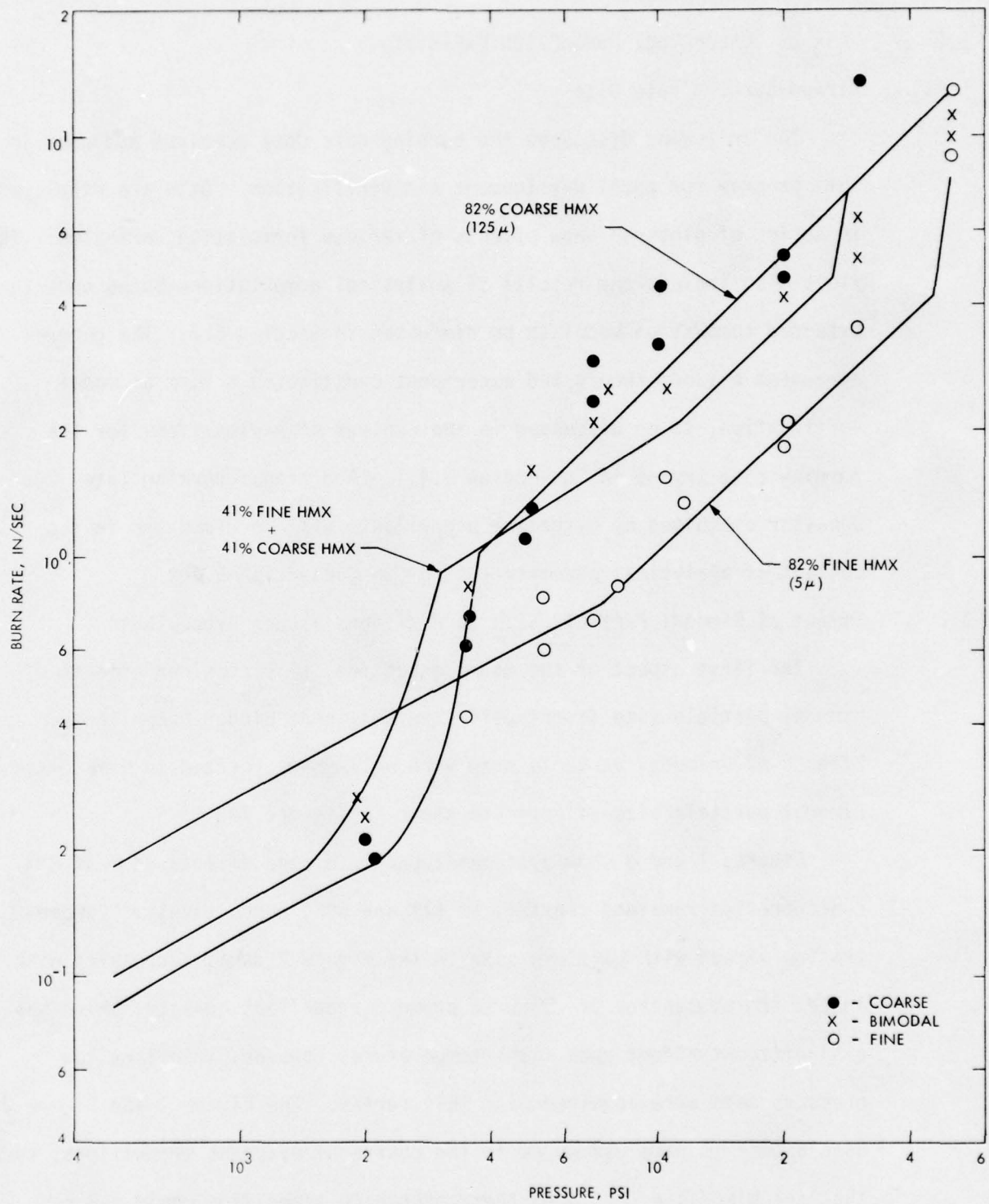


Fig. 1. Effect of bimodal particle size in HMX-ethyl cellulose propellant

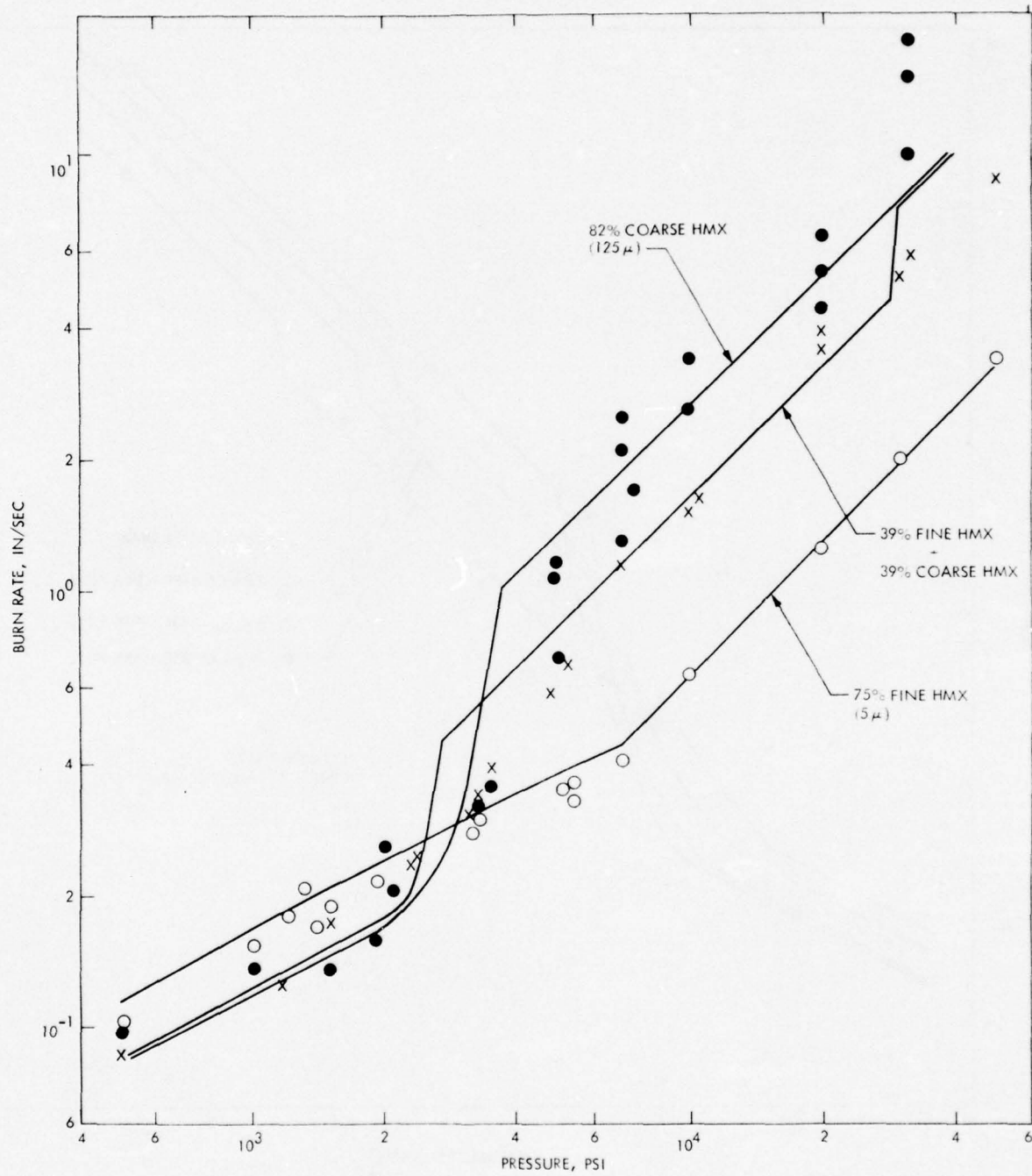


Fig. 2. Effect of bimodal particle size in HMX-HTPB propellant

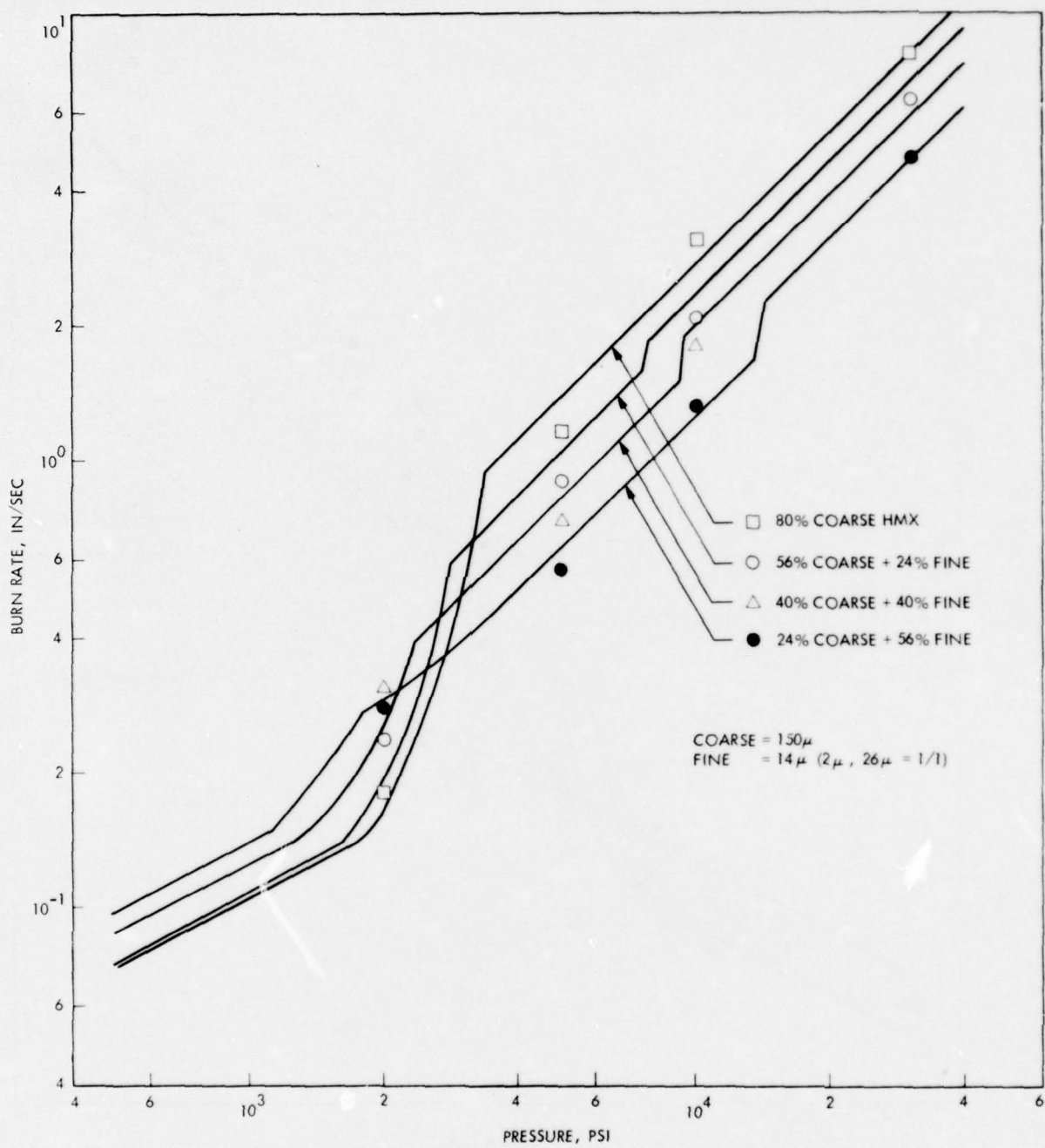


Fig. 3. Effect of fine/coarse ratio in bimodal HMX-HTPB propellant

In each figure, it is clear that increasing the percentage of the coarse size increases post-transition high pressure burning rates.

Figures 1 and 3 reveal that the transition regions of bimodal propellants are proximately located to the transition region of the unimodal coarse propellant. In other words, the pressure at which the exponent increase occurs does not decrease significantly in going from a unimodal coarse propellant to a bimodal coarse/fine propellant. This effect is clarified in Figure 2, which shows that low pressure behavior leading to the transition is dominated by the coarse particle size. Making allowance for the flame temperature differences, which are important at low pressure (References 3, 4), the unimodal fine propellant has a much higher burning rate than the unimodal coarse propellant; but, the bimodal propellant does not show a proportionate increase reflecting its fine content.

Analytically, this effect is shown at constant solids loading in Figure 1: the low pressure burning rate of the bimodal propellant is closer to that of the unimodal coarse. This behavior contrasts with AP propellants, which are dominated by the fines (Reference 14). Since the transition of a coarse particle depends upon burning rate (References 3, 4), and the burning rate of the propellant is not increased significantly by resort to a bimodal distribution, it follows that the transition pressure does not decrease significantly. The coarse particles also appear to exert a disproportionate influence at high pressure.

To the extent that fine particles tend to increase pre-transition (low pressure) rates and decrease post-transition (high-pressure) rates, the exponent shifts of bimodal propellants tend to be less abrupt, severe or extensive than those of unimodal coarse propellants. The corresponding cross-overs in burning rates between low pressure and high pressure are clearly evident in all three figures. Note, however, that even unimodal

fine propellants can exhibit exponent shifts, as explained previously (References 3, 4).

5.2.1.2 Effect of Mixed HMX-TAGN in Inert Binder Propellants

The second aspect of the model extension is to consider mixed Nitramines, in particular mixed HMX-TAGN which is of interest for practical gun propellants. Although inert binder propellants containing substantial TAGN would lack adequate energy, they are useful to provide a next step in the modeling progression. The active binder propellants of greater interest are considered later.

Results for two mixed oxidizer propellants are presented in Figure 4. Although they do not provide a systematic variation in HMX/TAGN ratio because total solids and HMX particle size also vary, there is sufficient basis for concluding that TAGN substitution for HMX increases burning rate. First of all, TAGN substitution for HMX decreases flame temperature, and reduced total solids decreases flame temperature in inert binder propellants. Notwithstanding the considerable reduction in flame temperature, the propellant with the higher TAGN/HMX ratio has a significantly higher burning rate at pressures below the transitions of the propellant containing more and coarser HMX. Secondly, this burning rate increase is greater than would be expected from the mere reduction in HMX particle size indicated.

The propellant containing the equal division of TAGN and HMX at 78% total solids exhibits a burning rate curve of similar character to the 75% fine HMX propellant of Figure 2. In that sense, it behaves like an all-fine HMX propellant. However, the burning rates are everywhere doubled by comparison notwithstanding a flame temperature reduction from 1700°K to 1580°K. Indeed, the burning rates are even higher than those of the 82% fine HMX propellant (2180°K) of Figure 1. Therefore, the fine TAGN appears to behave like a catalyzed fine HMX.

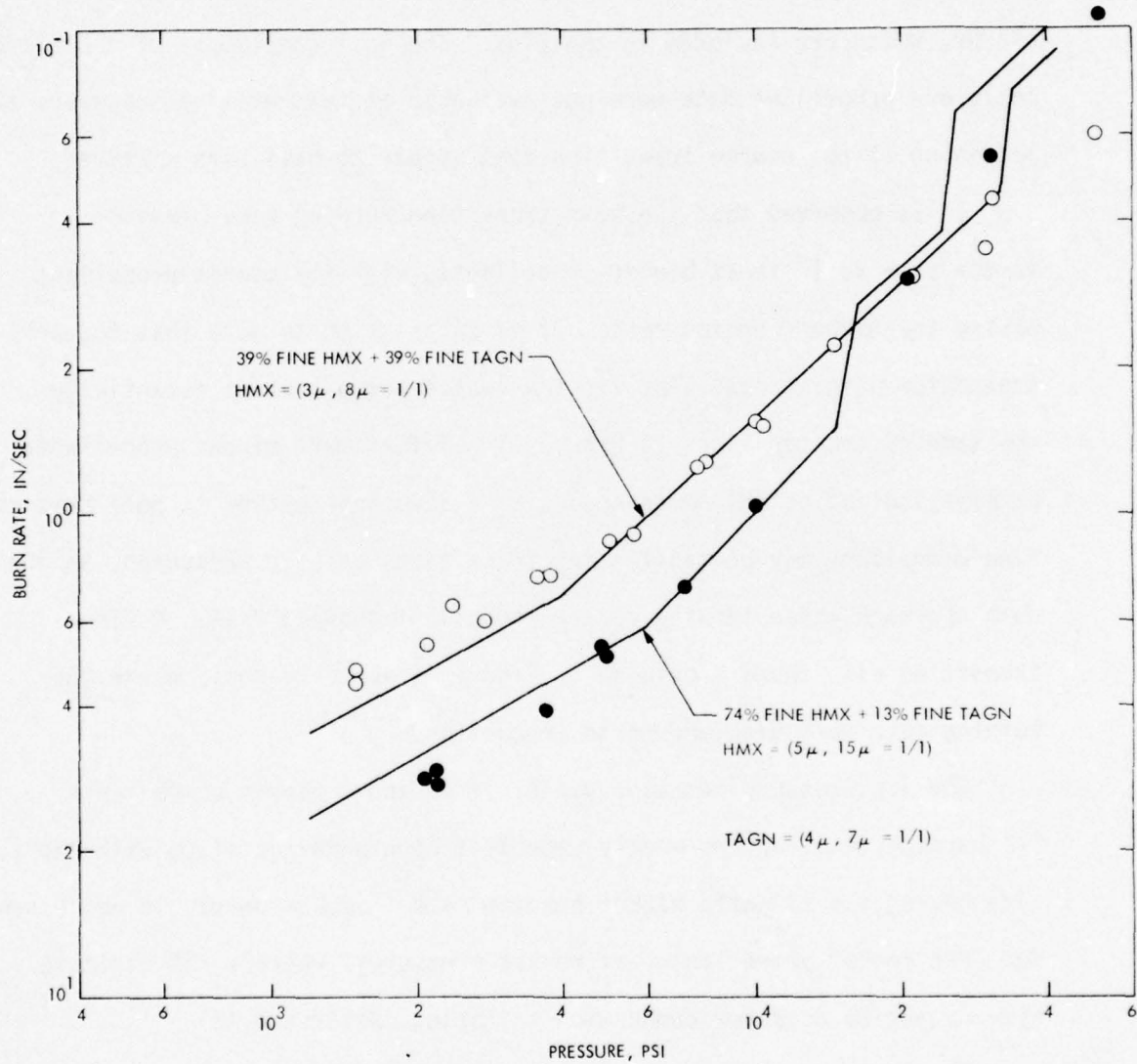


Fig. 4. Burning rates of mixed HMX/TAGN - HTPB propellants

5.2.1.3 Effect of HMX Particle Size in Active Binder Propellants

The effect of HMX particle size in active binder propellants is shown in Figure 5. High pressure data, beyond the transition of the coarse size, are shown for nitroplasticized polyurethane binder. The important low pressure data leading to the transition were not obtained for these propellants (Reference 11). Such data were acquired for nitrocellulose binder, which are included in the plot. The full complement of the nitrocellulose propellant data were not available at this writing; however, the beginning of the coarse transition does appear to have been captured.

It is observed that the post-transition burning rate behavior is the same as in inert binder propellants, with the coarse propellant having the higher burning rate. It is interesting to note that the post-transition burning rate line for the coarse propellant is essentially the same as the top lines in Figures 1 - 3 for inert binder propellants, perhaps indicating HMX dominance. It is also interesting to note that the fine propellant may be manifesting transitions at high pressures, as the data approach those for the coarse propellant above 30Kpsi. A fine transition also appears evident in Figure 1, above 30 Kpsi, where the burning rate gets high enough to produce one.

The low pressure behavior differs from inert binder propellants. The burning rate appears weakly dependent upon particle size, with the coarse size having the slightly higher burning rate. Such a result is well-known for CMDB rocket propellants, at rocket pressures, wherein HMX particle size cannot be used for combustion tailoring (Reference 12).

Figure 5 may also be illustrative of the effect of active binder type. The nitrocellulose propellants have higher burning rates than the nitroplasticized polyurethane. This correlates with the energy and burning rate properties of the binders themselves. Comparing the low pressure and pre-transition data with those of the inert binder propellants

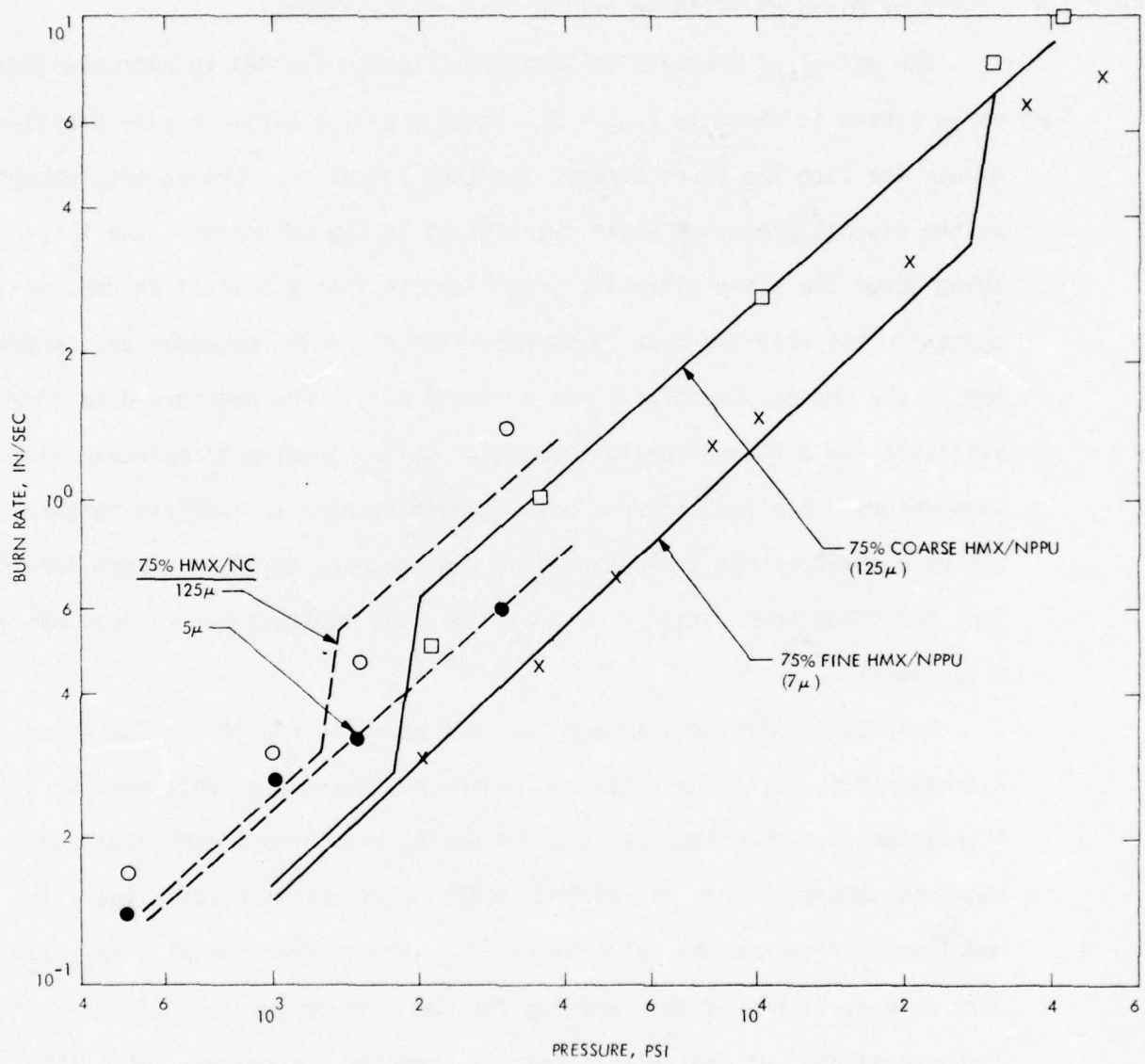


Fig. 5. Effect of HMX particle size in active binder propellants

(e.g., Figure 2), it appears that the active binder propellants have higher burning rates. Thus, the transition appears less extensive in the active binder propellants. This trend may be expected to continue with more energetic and faster burning double-base binders (see Subsection 5.4.2 for further discussion of binder parametrics).

5.2.1.4 Effect of Mixed HMX-TAGN in Active Binder Propellants

The effect of progressive TAGN substitution for HMX in nitroplasticized polyurethane is shown in Figure 6. These are fine particle size propellants. As was the case for inert binder, the TAGN raises the burning rate except at the highest pressures where transitions in the HMX occur. The interesting thing about the mixed nitramine propellant is that a transition does not appear in the reported data (Reference 11), although the model does predict one in the HMX component (see Subsection 5.4.1). Low pressure data were available for a TAGN propellant at lower solids loading to maintain flame temperature. The low pressure burning rate appears to increase further, but by a small amount indicating that the presence of TAGN is more important than the flame temperature. That also was the conclusion for inert binder propellants.

Results in nitrocellulose binder are shown in Figure 7. The mixed nitramine propellant characterized by the most extensive data does show transitions, which either casts doubt on the NPPU propellant result or suggests subtle effects of HMX/TAGN ratio or of active binder type. The model prediction appears quite persuasive here. Unfortunately, only limited data were available at this writing for the nitrocellulose analog of the NPPU propellant, at pressures below any expected transition. But, there are enough data to indicate a small effect of HMX/TAGN ratio on low pressure burning rate as long as the propellant contains substantial amounts of both nitramines. When all of the HMX is replaced by TAGN, at constant solids, a significant increase in burning rate again occurs, and at all

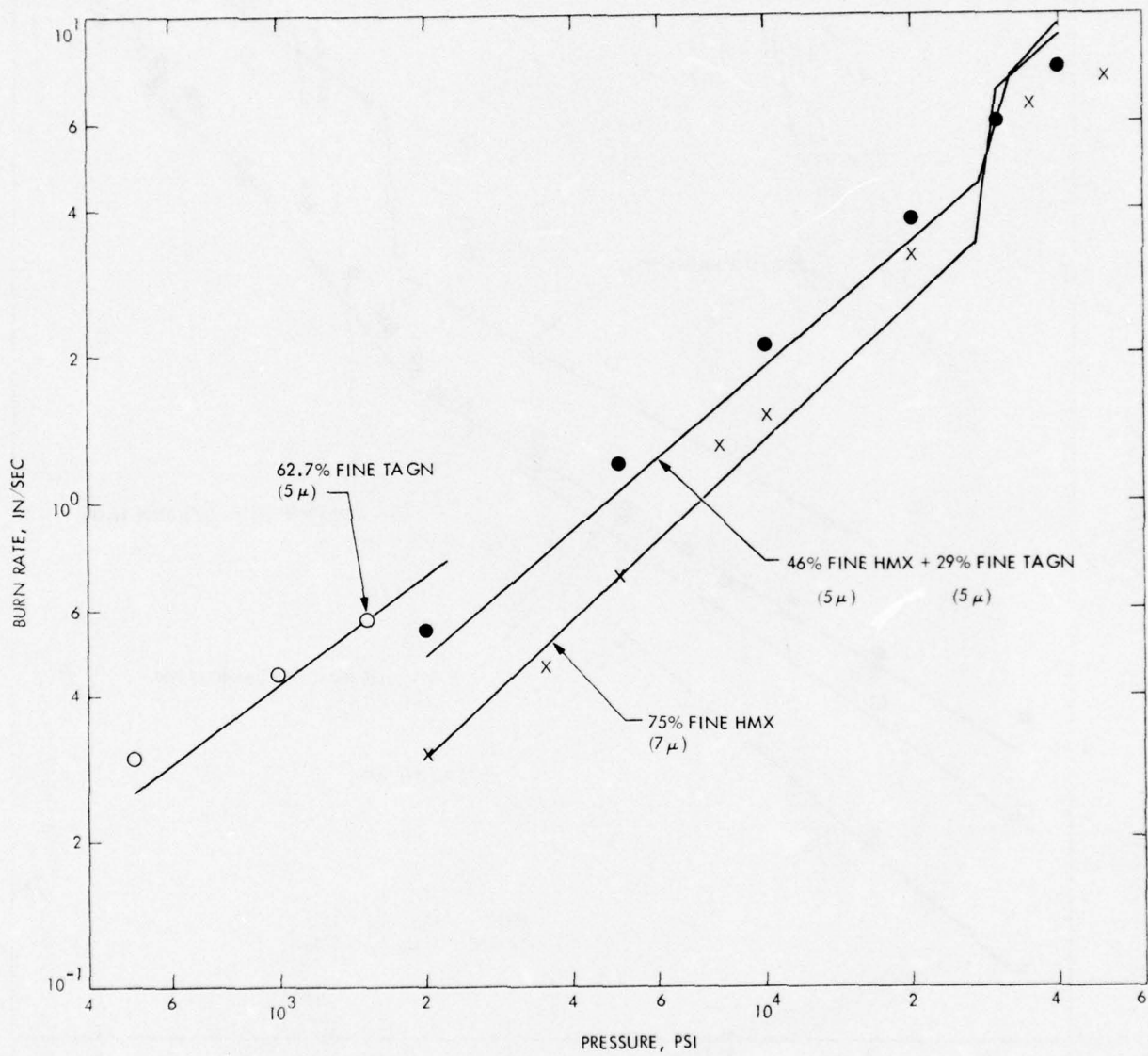


Fig. 6. Effect of TAGN in NPPU propellants

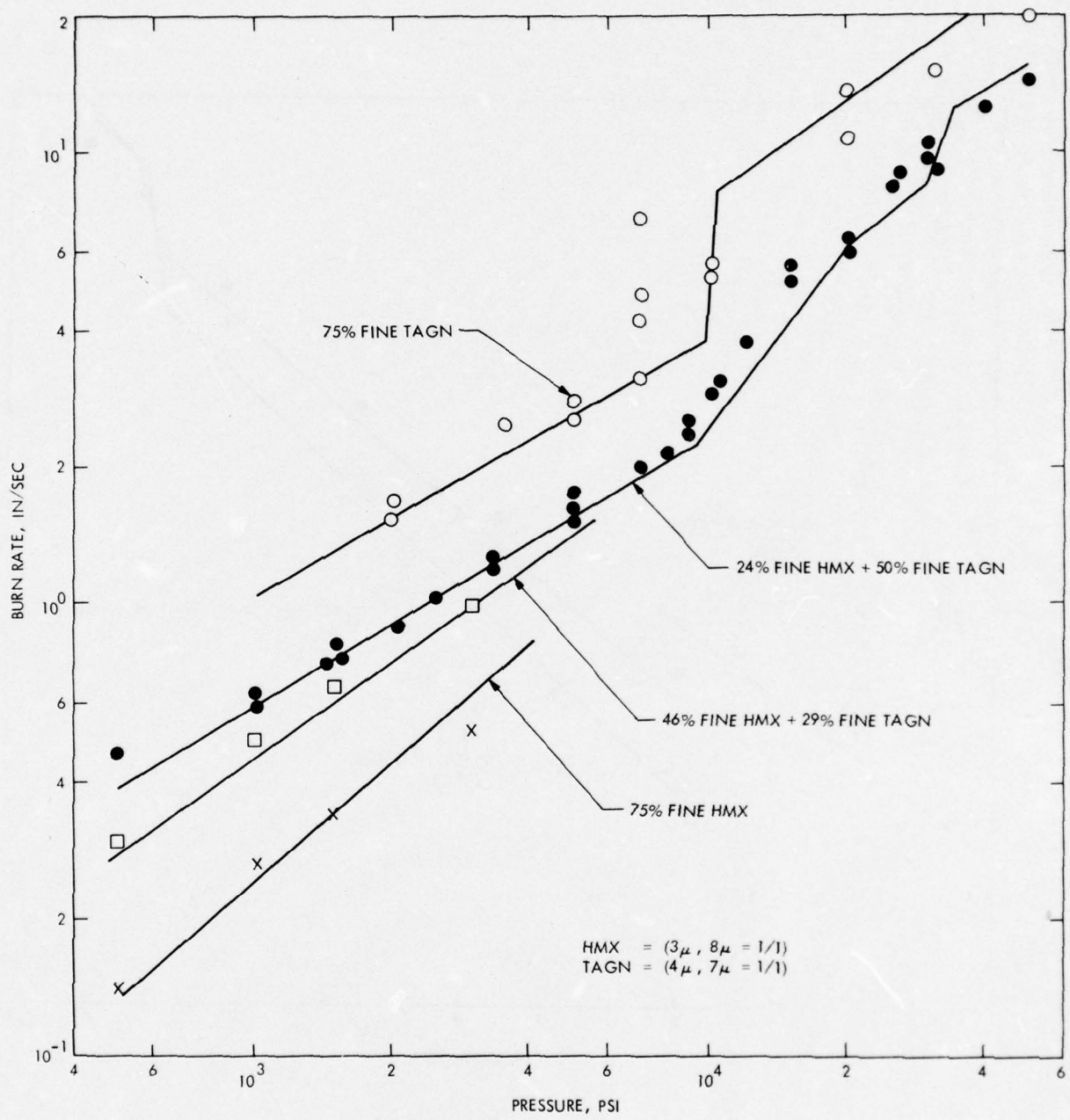


Fig. 7. Effect of TAGN in NC propellants

pressures. The data scatter at 7 Kpsi may be interpreted to be a transition in the TAGN, and the model indeed predicts one. If so, the post-transition burning rate is higher than that manifested by HMX, and is consistent with the higher burning rate of TAGN as a monopropellant.

Comparing analogous propellants in Figures 6 and 7, the nitrocellulose propellants burn faster than the NPPU propellants at the lower pressures, and the effect of the first 29% TAGN substitution is to roughly double the lower pressure burning rates in both binders. It is interesting that further increases in TAGN do not proportionally increase burning rate until the HMX is removed.

It is concluded that TAGN increases low pressure burning rates, and thereby mitigates the extent of exponent shifts when substituted for HMX. It does not, however, appear that TAGN really eliminates transitions; on the contrary, TAGN may itself transition to produce very high rates at high pressures. The TAGN substitution is more effective in mitigating transitions in active binder propellants because the active binder also serves to increase low pressure burning rates. The use of energetic plasticizers with nitrocellulose might provide further improvement in that regard. Parametrics are discussed in Subsection 5.4.2

5.2.2 Window Bomb Microcinematography Study

5.2.2.1 Inert Binder Propellants

The results of observing unimodal coarse and unimodal fine HMX propellant combustion were reported in Ref. (3). The purpose here was to try to discern any effects of combining them in a bimodal distribution.

At 1000 psi, the surface had a molten appearance with limited individual particle luminosity. The molten appearance is characteristic of both unimodal propellants, and the limited particle activity is characteristic of the coarse propellant at this pressure. It was possible to discern only coarse individual particle behavior at the available magnification. The particle activity was greater in the bimodal propellant than in the coarse propellant; the bimodal propellant has the higher burning rate at this pressure. The gas phase was essentially non-luminous, a characteristic of both unimodal propellants at this pressure, but included decomposition products in the form of white smoke which is more characteristic of the fine propellant.

At 2000 psi, the white smoke became more dense, and the particle activity increased in both the coarse and bimodal propellants. Red-orange flamelets erupted at isolated locations in greater amount and more frequently. The surface of the bimodal propellant began to have a mottled appearance, indicating the beginnings of coarse particle deflagration in depth which is responsible for the exponent shift (Ref. 3). It appeared that this change occurred first in the bimodal propellant, which had the higher pretransition burning rate (see Fig. 1). The bimodal propellant also began to exhibit a dull red continuum in the gas phase, which is characteristic of the fines (Ref. 3).

At 4000 psi, the coarse particle behavior was observed to dominate both the coarse and bimodal propellants. The entire burning surface was engulfed by turbulent red-orange flames. Rapid, pronounced regression occurred at various locations on the burning surface, and into the propellant interior; to produce a rugged surface appearance. The pressure of 4000 psi is past the transitions of these propellants (see Fig. 1).

There were two major differences between ethyl cellulose and polybutadiene propellants. The glaze of the surface melt layer had a black sheen with HTPB, but was yellowish in color with ethyl cellulose. The HTPB propellants produced some black smoke in the gas phase, the ethyl cellulose propellants did not. The polybutadiene is more carbon rich than the ethyl cellulose. These differences were evident at low pressure. At high pressure, the melt layer could not be discerned and the coarse particle flames dominated the gas phase appearance.

The HTPB propellant containing equal amounts of fine HMX and fine TGN produced a surface ash above the melt layer. This ash was more pronounced at low pressure. This propellant is much more fuel-rich and cooler than its all-HMX analog. The surface regressed smoothly and evenly, with no manifestations of heterogeneous behavior evident. The gas phase at 1000 psi consisted of dense black smoke above the ash. At 5000 psi, there was less smoke production and a bright red continuum characteristic of fine HMX (Ref. 3) could be observed. It appears that increasing pressure facilitates the decomposition and combustion of fuel-rich propellants. This fuel-richness obscured any unique behavior that might otherwise be attributable to the TGN.

5.2.2.2 Active Binder Propellants

At 1000 psi, either coarse or fine HMX in nitrocellulose produced agglomerate spheres at the surface. These spheres glowed with a red-orange color, and were periodically ejected into the gas phase. These were the first instances of particle ejections observed in the course of this study. The origin of the agglomerates appeared to be a thin surface melt layer, which regressed uniformly. The agglomerates appeared to be larger in size and fewer in number with fine HMX than with coarse HMX, and their behavior was reminiscent of aluminum behavior in solid propellant combustion (Ref. 13). In addition to the ejected agglomerates, the gas phase of the fine HMX propellant consisted of a red-orange transparent flame continuum. The coarse HMX propellant exhibited a more heterogeneous particle flame combustion which produced yellow-orange streaks through the gas phase. It may be inferred that the combustion is more heavily dominated by the binder at this pressure, and that continuity of propellant ingredients is not fully preserved in the combustion products.

At 5000 psi, the coarse HMX propellant behaved similarly to the inert binder propellant at high pressure. There were no more particle agglomerates or ejections; rather, the burning HMX particles produced visible turbulent flames and the deflagration paths propagated into the propellant. This pressure is above the transition for this propellant (see Figure 5, coarse HMX in NC), and it may be inferred that the nitramine is becoming the more dominant component at the higher pressures. The fine HMX propellant, also, no longer produced agglomerates or particle

ejections at this pressure. The gas phase consisted of a bright yellow-orange continuum, and no heterogeneous particle activity could be discerned.

The fine TAGN in nitrocellulose, without HMX, was a propellant which burned cleanly and homogeneously at 1000 psi. There were no agglomerates and no particle ejections; indeed, it appeared as though the active binder contained no powder. The gas phase was clean and transparent; no flame continuum was observed. The interesting thing about this propellant was its surface behavior. It had a thick melt layer which was undulating as though boiling or otherwise indicating gas production within or beneath. This behavior is quite different from HMX, and indicates that the TAGN is able to respond, melt and decompose more readily or rapidly. Perhaps therein lies the explanation for the higher burning rate (compare in Figure 7). At 5000 psi, the principal differences were less pronounced surface activity and the generation of considerable gray smoke in the gas phase. Even at this pressure, no visible flame or luminosity was observed. It might therefore be inferred that exothermic condensed phase decomposition plays an important role in the combustion of TAGN propellants.

Combining fine TAGN and fine HMX produced a different character of particle ejection at 1000 psi than seen with HMX alone, and less surface activity than seen with TAGN alone. The ejected particles were much smaller than the agglomerate spheres, were non-spherical and were not glowing; they were visible by the external illumination. Drawing an analogy to aluminum behavior, they may be pre-agglomerate clusters of the HMX. To the extent that HMX behaves more slowly than TAGN, the

forming HMX melt may be left behind by the TAGN-active binder melt and decomposition. The gas phase at 1000 psi was nonluminous, which is more a characteristic of the TAGN; this is consistent with the notion of bypassed HMX. At 5000 psi, the gas phase was a superposition of the flame continuum from the HMX and the smoke production from the TAGN. The brightness from the flame was dimmed considerably by the smoke. No particle ejections could be discerned at this pressure.

In order to further explore HMX and TAGN in combination, another propellant was furnished which served to replace the fine HMX with coarse HMX. The low pressure behavior showed more particle combustion and less particle agglomeration or ejection than the all coarse HMX analog; indeed, the deep penetration particle deflagration appeared to be incipient. The high pressure (5000 psi) behavior clearly showed the penetrating particle combustion as well under way, but combined with the smoke production characteristic of the TAGN. Burning rate data were not completed for this propellant; however, it can be expected with reasonable certainty that the TAGN served to raise the burning rate at 1000 psi, that an exponent break point exists and that the pressure of 5000 psi has passed it.

Motion picture film clips have been edited, labeled and combined for presentation at technical meetings. A copy may be made available through the AFOSR.

5.2.3 Study of Extinguished Surfaces

5.2.3.1 HMX-Inert Binder Propellants

Figure 8 shows fractured surfaces of the coarse unimodal and coarse/fine bimodal propellants, unburned. It should be noted that the nominally 125μ coarse fraction actually lies in an approximately 90μ - 190μ size range. Note that the effect of the bimodal distribution is to reduce the average spacing between particles, but to increase spacing between coarse particles. The coarse particles appear randomly jammed together in the unimodal propellant, which is believed to facilitate the post-transition penetration burning (Ref. 3).

Figure 9 shows the samples of the two propellants quenched at the upper test pressures. The transition to deep penetration burning has produced the heavily cratered surfaces shown, particularly in (a), penetrating three to four crystal layers deep in some areas. The bimodal propellant (b) appears to have had a smoother surface, indicating that the finer size HMX fraction probably was still melting and regressing in a normal manner. The normal burning fine fraction resulted in a smearing out of the more rugged features of the unimodal propellant (a). This appears to justify the superposition principle to be used in the theoretical modeling, in that all sizes do not transition at once. Higher magnification views are presented in Figures 10a and 10b, respectively; the relative crustiness of the bimodal propellant melt layer (b) is evidence of an HMX melt contribution.

Figure 11 shows the samples of the two propellants quenched at 2000 psi. The occurrence at this pressure of the transition to penetration burning and cratering is in agreement with the model prediction



Fig. 8a. Unimodal coarse HMX/EC propellant,
fractured surface, 100X



Fig. 8b. Bimodal coarse/fine HMX/EC propel-
lant, fractured surface, 100X

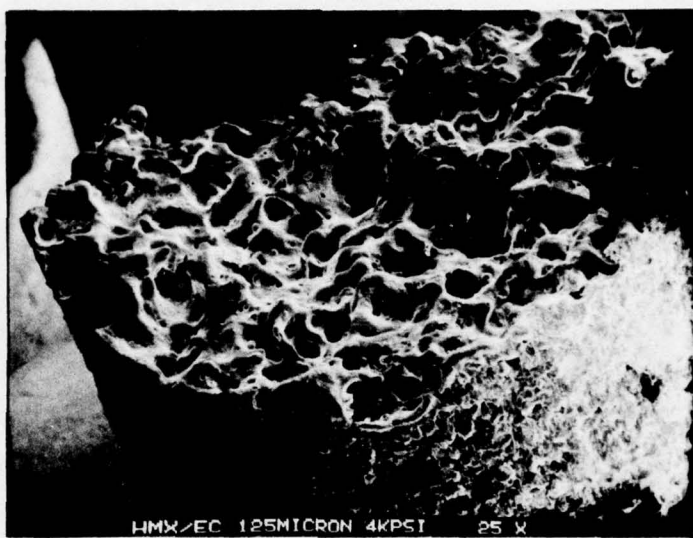


Fig. 9a. Unimodal coarse HMX/EC propellant,
extinguished surface, 4000 psi, 25X

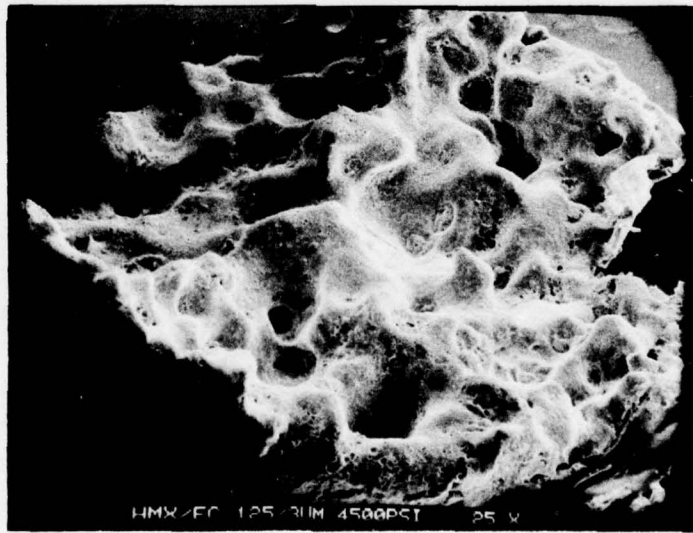


Fig. 9b. Bimodal coarse/fine HMX/EC propel-
lant, extinguished surface, 4500 psi, 25X

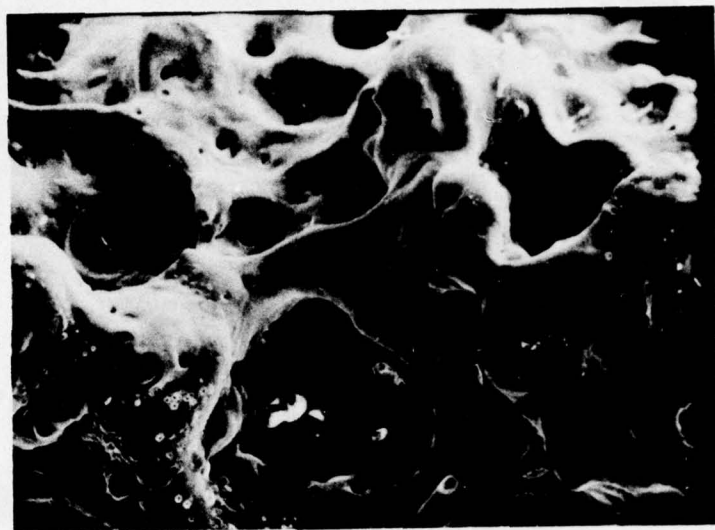


Figure 10a. Unimodal Coarse HMX/EC Propellant,
Extinguished Surface, 4000 psi, 100X

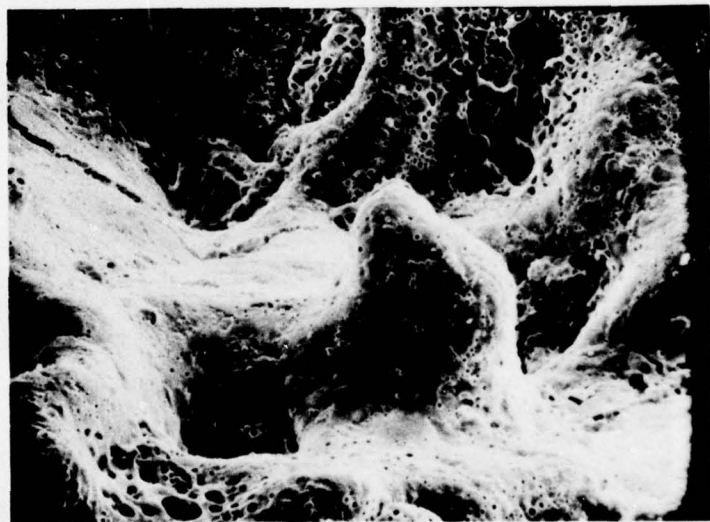


Figure 10b. Bimodal Coarse/Fine HMX/EC Propellant
Extinguished Surface, 4500 psi, 100X

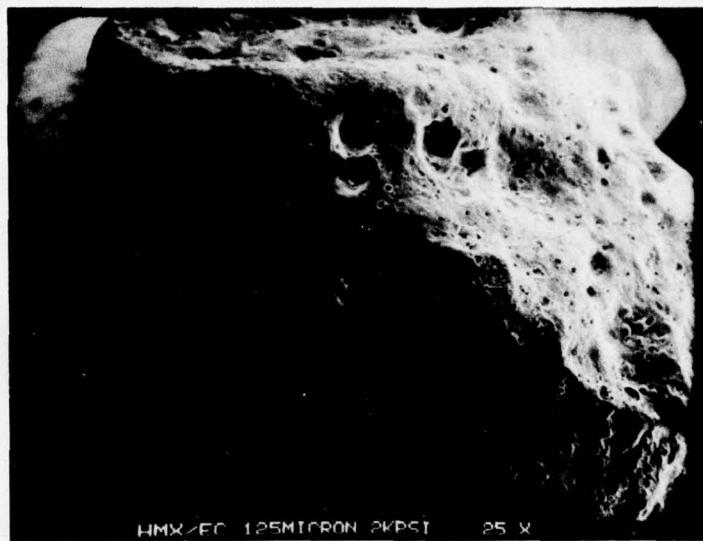


Fig. 11a. Unimodal coarse HMX/EC propellant,
extinguished surface, 2000 psi, 25X

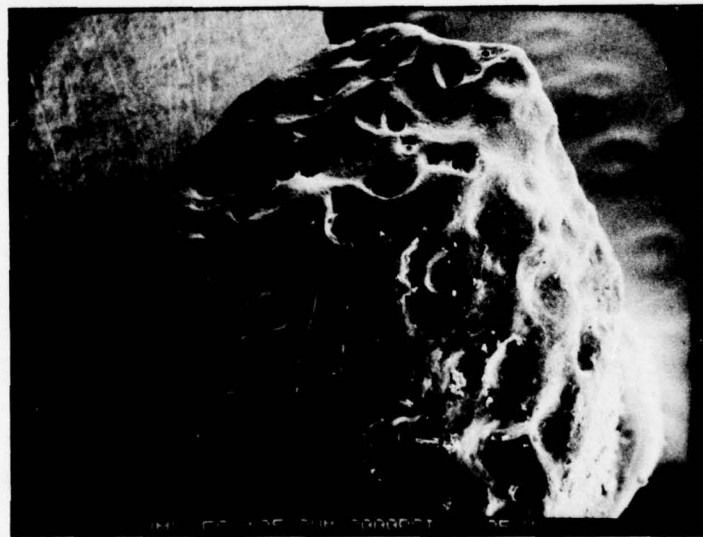


Fig. 11b. Bimodal coarse/fine HMX/EC propel-
lant, extinguished surface, 2000 psi, 25X

taken together with the data of Figure 1. The transition is seen to be further advanced in the bimodal than the unimodal propellant. This is caused by the higher pre-transition burning rate of the bimodal propellant, due to the fine size component, which lowers the pressure at which the coarse HMX crystals begin to remain frozen in accordance with the principles of Refs. (3,4).

The samples of the two propellants quenched at 1000 psi are shown in Figure 12. The smooth surface and lack of cratering of the unimodal propellant, (a), indicates that it was still burning in a normal manner. The preponderance of blow holes created during the rapid depressurization quench indicates that a substantial melt layer thickness existed. The slight amount of cratering for the bimodal propellant confirms that transition to penetration burning had already begun to occur for this more rapid burning propellant (note the similarity of Figures 12-b and 11-a), and at a lower pressure than the coarse propellant.

A closer look at the melt layer of the coarse HMX propellant is provided by Figure 13. Figure 13(a) shows the top and the unrestricted side of the propellant. The edge runs from the lower left to the upper right, and the interface of the melt can be seen to run along this edge. A magnified view of this interface is provided by Figure 13(b). The melt layer resembles a cake frosting.

Sections of these extinguished surfaces were microtomed in order to view the propellant surface structures in cross-sectional depth. Similar studies were made by Derr (Ref. 14), at low pressure, which showed melt layer depths of the order of the constituent particle size. Derr also observed that the melt was a composite of binder and recrystallized HMX.

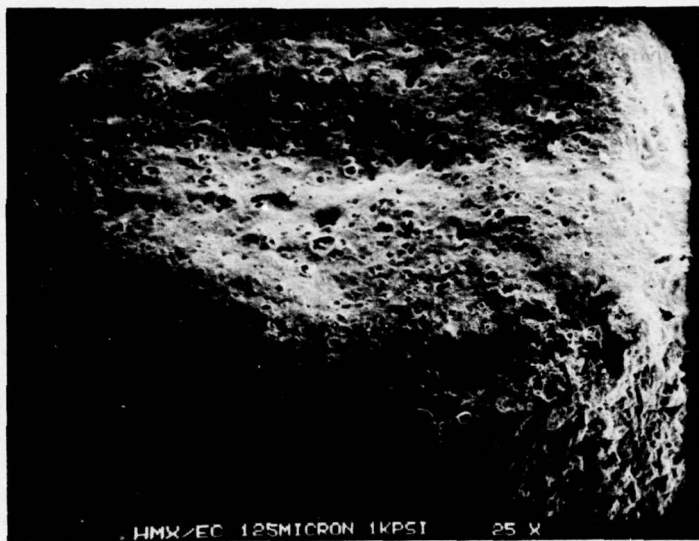


Fig. 12a. Unimodal coarse HMX/EC propellant,
extinguished surface, 1000 psi, 25X



Fig. 12b. Bimodal coarse/fine HMX/EC propel-
lant, extinguished surface, 1000 psi, 25X

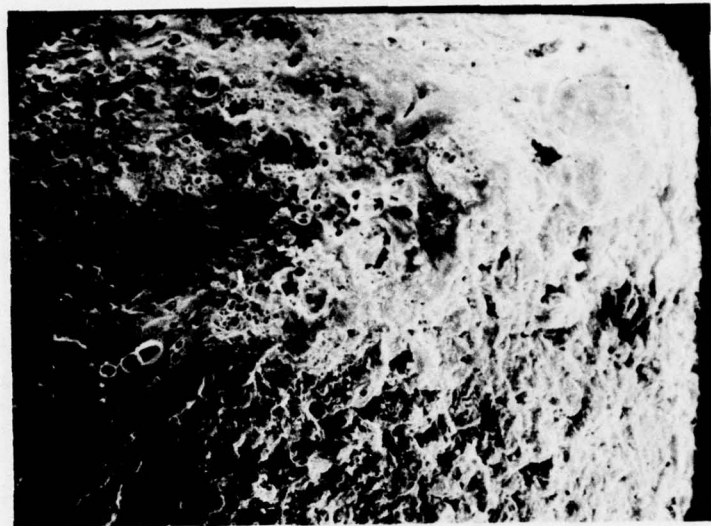


Figure 13a. Magnification of Lower Center of
Figure 12a, 50X



Figure 13b. Magnification of Lower Left Region,
500X

Cohen (Refs. 3, 15) extended these observations to high pressure, and inferred that the HMX was no longer melting in bulk at pressures above the exponent break point. The present work serves to confirm these observations and further extend them to bimodal HMX propellants.

Figure 14 presents views of two surface cross-sections of the 125μ HMX propellant that was extinguished at 1000 psi. This pressure is below but close to the break point pressure. The magnification is 1000X to show detail. There appears to be a mixture of recrystallized HMX and binder to a depth of at least 60μ . The smooth flowing surface at the top of Figure 14a is attributed to a coating of binder. This binder coat is better seen in cross-section in Figure 14b, to the right and left of top center. Another sheet of binder or admixed material appears to exist to the right of center, above the HMX crystal in the lower right-hand corner. This latter crystal does not appear to have melted. However, more indications of a melt appear to the left of that crystal at the same depth. Lower magnification views indicate the depth of the composite melt layer to vary from $100\mu - 200\mu$, in accord with Ref. (14).

Figure 15 displays a cross-sectioned region of the cratered surface that appears above the break point for the 125μ HMX propellant. This surface was extinguished at 4000 psi. Figure 15a is at a magnification of 100X, to show the crater region, and Figure 15b is at a magnification of 500X to focus upon the unburned HMX crystal at the base of one crater (right of center in Figure 15a). Bulk melting of crystals is not evident in Figure 15a. There is a very thin coating of the cratered surface, which is attributed to binder melt. Blow holes resulting from



Figure 14a. Edge of Extinguished Surface of Coarse HMX/EC Propellant, 1000 psi, 1000X



Figure 14b. Another Edge View of Extinguished Surface of Coarse HMX/EC Propellant, 1000 psi, 1000X

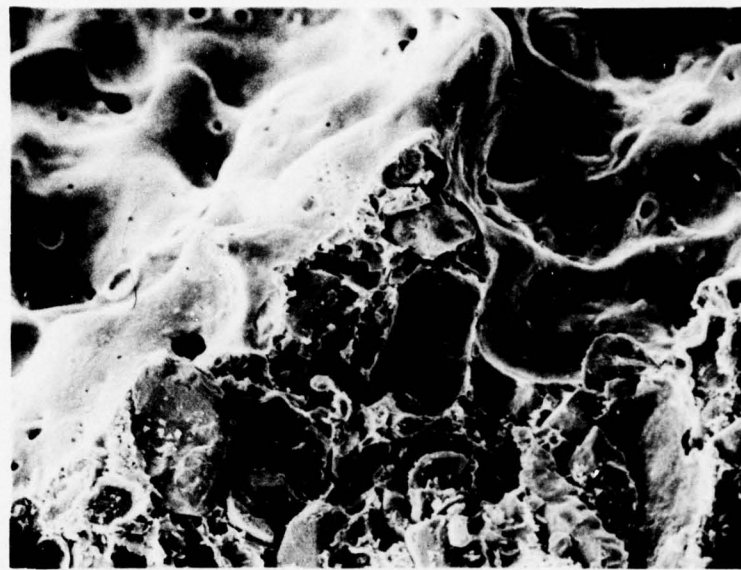


Figure 15a. Edge View of Extinguished Surface of
Coarse HMX/EC Propellant, 4000 psi, 100X



Figure 15b. Magnification of Particle at Crater
Base, 1000X

the rapid decompression appear on this melt layer. Figure 15b reveals that the HMX crystal at the base of the crater had been burning because its surface is dished concave in the classical BDP model configuration (Refs. 14, 16). Moreover, this burning appears to have taken place without bulk melting. Another crystal appears in contact at the lower left, which would have allowed the propagation to continue in depth if the propellant had not been extinguished. The cracking on the surface of the principal crystal is due to the electron beam, which was focused up to 10KX. These photos confirm the conclusions of Ref. (3), which were incorporated into the model.

Figure 16 shows a cross-sectioned region of the bimodal $125\mu /5\mu$ HMX propellant that was extinguished at 1000 psi. This pressure is at the commencement of the slope transition. Figure 16a is at a magnification of 500X to show the general vicinity, and Figure 16b is at a magnification of 1000X to show more detail. Figure 16a indicates a possible composite melt layer thickness of at least 60μ surrounding a coarse crystal at the lower center. One difficulty of interpretation is the fact that the fine size in this propellant is of the order of the dimensions of the binder melt layer and the fine structure of the recrystallized HMX that were observed in the coarse propellant. The interesting feature is at the right of center, which is magnified to the right-hand portion of Figure 16b. This appears to be a massive recrystallized coarse particle, which had partially burned away and may have been molten to a depth of 40μ , if not entirely. Note the fine structure in the upper portion of this particle, and its blending into vertical features in the lower portion. This may be indicative of a coarse



Figure 16a. Edge View of Extinguished Surface of
Bimodal Coarse/Fine HMX/EC Propellant,
1000 psi, 500X



Figure 16b. Magnification of Central Region, 1000X

particle at the borderline of bulk melting. The region to the left of this particle reveals a surface melt of the order of 10μ which has different features from the area beneath. It appears that this layer is a composite melt involving the binder and the fine size of the bimodal distribution. The theoretical model will assume that the features of the two sizes superpose, and would predict both sizes at the surface to be molten at pressures below the break point.

Figure 17 improves the distinction between the fine and coarse particles and more clearly validates the superposition. Here, a cross-section of the bimodal propellant that was extinguished at 4500 psi is shown. This pressure is above the break point for this propellant. Figure 17a shows a cratered region at the right-hand side, and the vicinity to the left, at 250X magnification. Figure 17b is a magnification of the crater wall near its top at 1000X. Here, the surface melt layer is more clearly a composite consisting of binder and recrystallized fine HMX. Below the melt layer, undisturbed fine HMX is observed in the interstices between the coarse particles. The coarse particles do not appear to have melted and, therefore, do not confuse the appearance of the fines. The cratering is less pronounced than in the coarse propellant because the coarse particles are further apart and subject to the superposed surface melt from the fines. This is precisely how the model will treat and predict the surface structure of bimodal HMX propellants above the break point. The coarse particles no longer melt in bulk, and are therefore able to produce the craters; the fine particles continue to melt in bulk and this melt layer lines the craters. As a result, high pressure burning rates are reduced in comparison to the coarse propellant (see Figures 1-3).

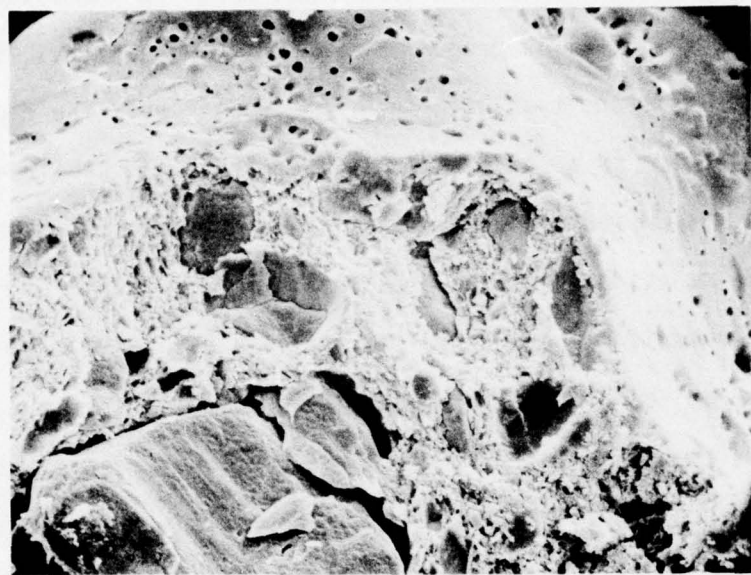


Figure 17a. Edge View of Extinguished Surface of
Bimodal Coarse/Fine HMX/EC
Propellant, 4500 psi, 250X

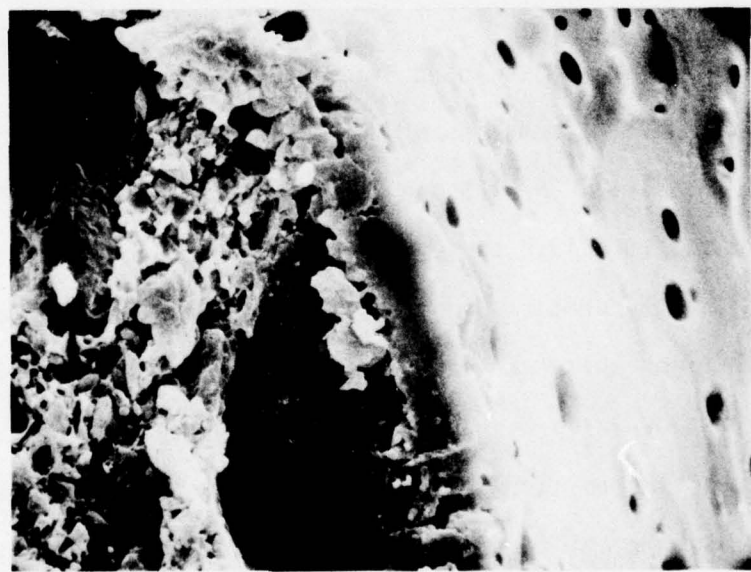


Figure 17b. Magnification of Right-Hand Region,
1000X

Extinguished surfaces for the all-fine, 5μ HMX propellant are shown in Figure 18. This propellant was extinguished at 4500 psi, which is below any transition with such fine particles. The rippled surface seen in (a) is an original melt layer that may have been affected by the rapid decompression or the particle fine structure; some below holes are also evident. The cross-section in (b) reveals a melt layer whose thickness is comparable to the particle size. No evidence of cratering could be found at this pressure. Thus, the all fine HMX propellant burns the more slowly at high pressure (see Figures 1 and 2).

The foregoing observations are consistent with the nature of the burning observed in the rate data and in the movies. It can be concluded that the individual fine size and coarse size processes superpose in a bimodal propellant, and that the fine size indeed promotes the transition burning of the coarse in such propellant.

5.2.3.2 Mixed HMX and TAGN in Inert Binder

Two different portions of the extinguished surface of the 39% fine HMX - 39% fine TAGN/HTPB propellant, extinguished at 3000 psi, are shown in Figure 19. These represent each of the two characteristic surfaces seen under the scanning electron microscope. Figure 19a shows that portion which was not covered by ash residue, and Figure 19b shows that portion which was. The portion not covered by ash shows a melt layer similar to that seen with HMX alone, but with more rugged features. There is some evidence of subsurface decomposition, by the voids immediately beneath the melt layer. These subsurface voids are more prevalent beneath the ash in (b). The ash is able to store residual heat, which can influence the subsurface during equilibration following the

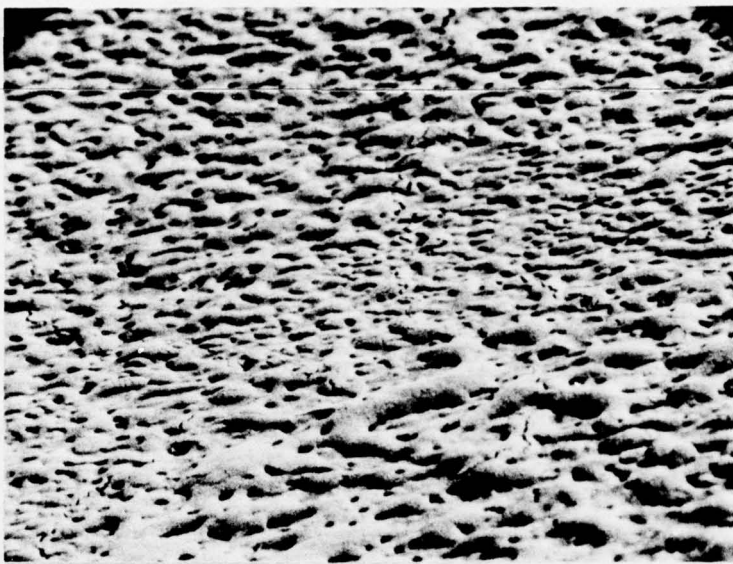


Figure 18a. Unimodal Fine HMX /EC Propellant,
Extinguished Surface, 4500 psi, 500X

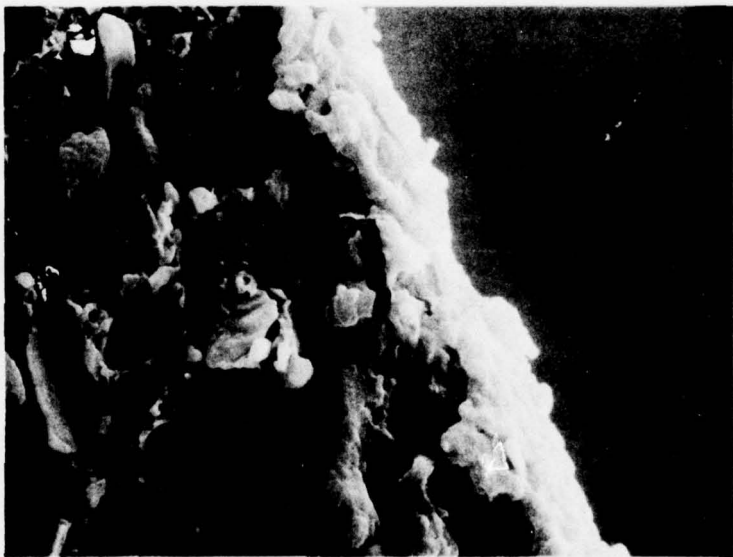


Figure 18b. Edge View of Extinguished Surface
of Unimodal Fine HMX /EC Propellant,
4500 psi, 2000X.

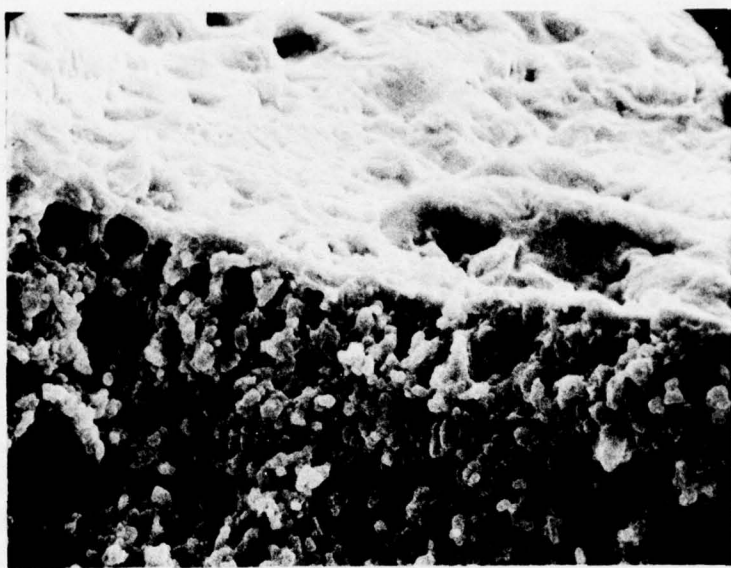


Figure 19a. Section Showing Top and Edge of Extinguished Surface of Fine HMX-Fine TAGN/HTPB Propellant, 3000 psi, 1000X.



Figure 19b. A Different Section of the Same Propellant, 500X.

decompression. Indeed, the depth of activity is much greater in (b) than in (a). Since the TAGN is able to melt and decompose more readily than the HMX, these voids may be manifestations of the TAGN. The ash appears to grow up out of the melt layer, unfurling in a sort of network consisting of bridges and holes, and would be a manifestation of the binder.

The subsurface voids are seen more clearly in Figure 20, which shows a surface extinguished at 5000psi. It is clear that the voids do not result from the microtoming. Their dimensions are larger than the particle sizes, suggesting perhaps that the fine particles exist as clusters when mixed into propellant. This assumes that the voids are manifestations of TAGN decomposition, leaving behind recrystallized HMX and solidified binder in this layer. The magnified view in (b) does indicate a recrystallized melt surrounding the voids, having a different structure than the particles seen in Figure 19a. The melt layer will be modeled as a three component admixture, each component having distinct kinetics and energetics of decomposition. The ash will not be considered in the molding.

5.2.3.3 Active Binder Propellants

Representative surface features of HMX/NC propellants are shown in Figures 21 and 22. Figure 21a shows the post-transition cratered surface characteristic of coarse HMX propellants at high pressure. The pressure of 3000 psi is above the break point (see Figure 5). Thus, the cratering appears in active binder as well as inert binder propellants. However, the cratering here does not appear quite as rugged (compare with Figures 10a and 15a, at 1/5 the magnification, and with Figure 9a



Figure 20a. Section Showing Top and Edge of Extinguished Surface of Fine HMX-Fine TAGN/HTPB Propellant, 5000 psi, 500X

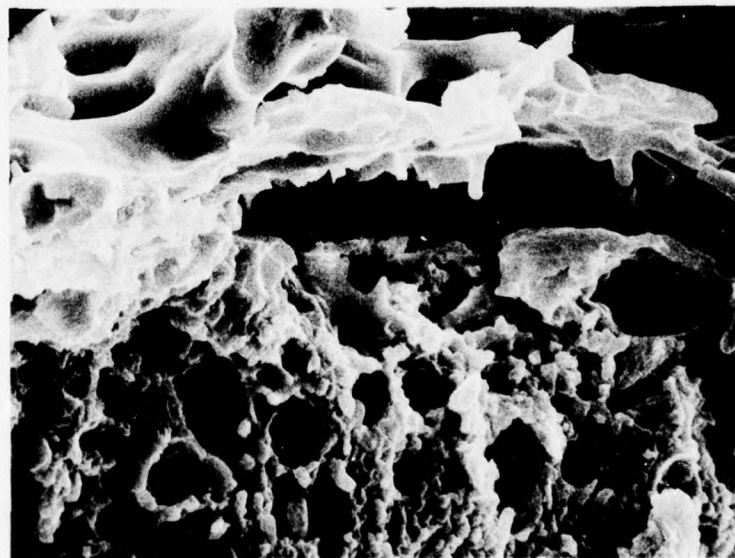


Figure 20b. Magnification of Central Region, 1000X.

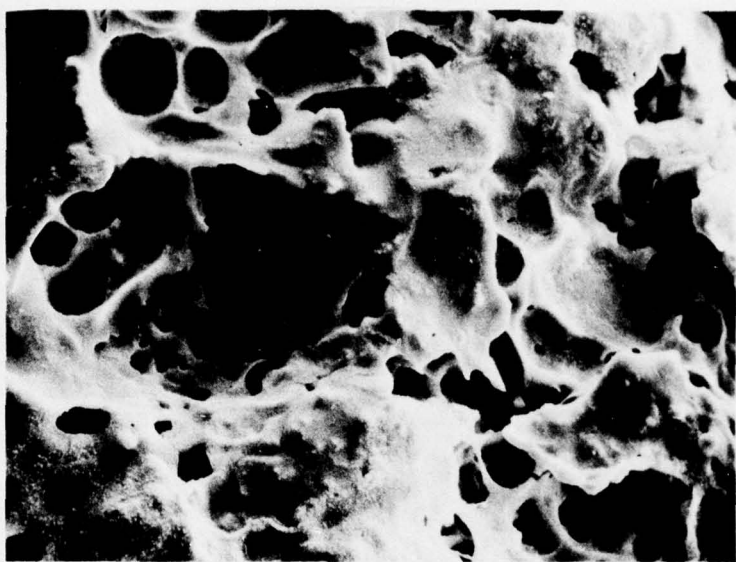


Figure 21a. Extinguished Surface of Coarse HMX/NC Propellant, 3000 psi, 500X.



Figure 21b. Section Showing Top and Edge of Extinguished Surface of Fine HMX/NC Propellant, 4300 psi, 1000X.

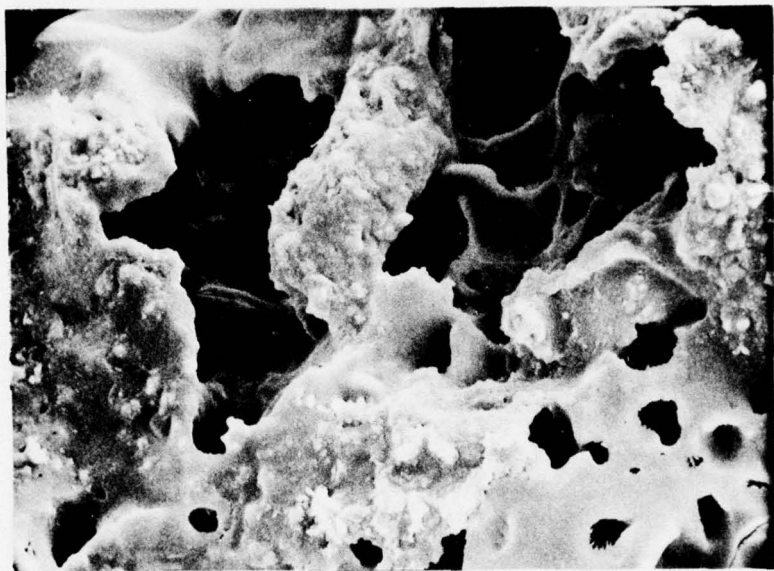


Figure 22a. Extinguished Surface of Coarse HMX/NC Propellant, 4500 psi, 500X

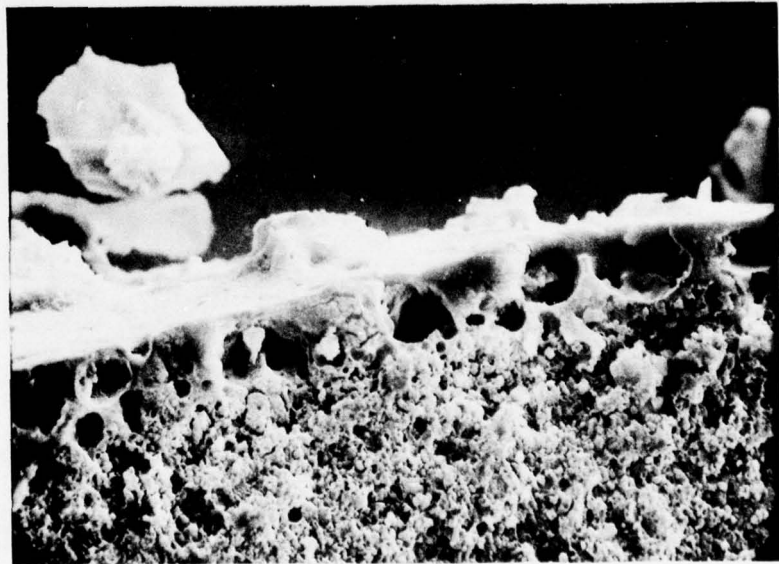


Figure 22b. Section of Extinguished Surface of Fine HMX/NC Propellant, 4800 psi, 1000X

at 1/20 the magnification). The propellant quality of the active binder is probably serving to limit the scope of penetration, tending to keep itself more even with the particle deflagration. Figure 21b shows the planar melt characteristic of fine propellants or pre-transition pressures. The interesting feature here is the apparent formation of an agglomerate at the surface, such as were seen in the movies. Note that the agglomerate is enormous compared to the fine particle size, and is partially hollow. The agglomerate appears to be balling up as the surface continues to regress, and it is known from the movies that it will eventually be ejected as a glowing sphere. That this can happen in active binder propellants, but not in inert binder propellants, may be again due to the self-deflagration propellant quality of the active binder. The surface of Figure 21b suggests that the combustion model need not draw special attention to agglomerate formation because it is an after-occurrence surrounded by surface regression in the normal planar fashion. A non-agglomerate region is shown in Figure 22b, wherein the melt layer closely resembles that characteristic of the fine size of the inert binder sample shown in Figure 16. Figure 22a shows the cratering of the coarse HMX propellant at a higher pressure compared to Figure 21a.

Extinguished surfaces of fine TAGN/NC propellant are shown in Figure 23. The features appear to be independent of pressure over the range tested. The melt layer appears to be similar to that of the fine HMX propellant, Figure 22b. It can be observed that the extinguishment has captured some of the boiling-like surface eruptions that were seen in the movies. There is no ash because the binder is chemically balanced.

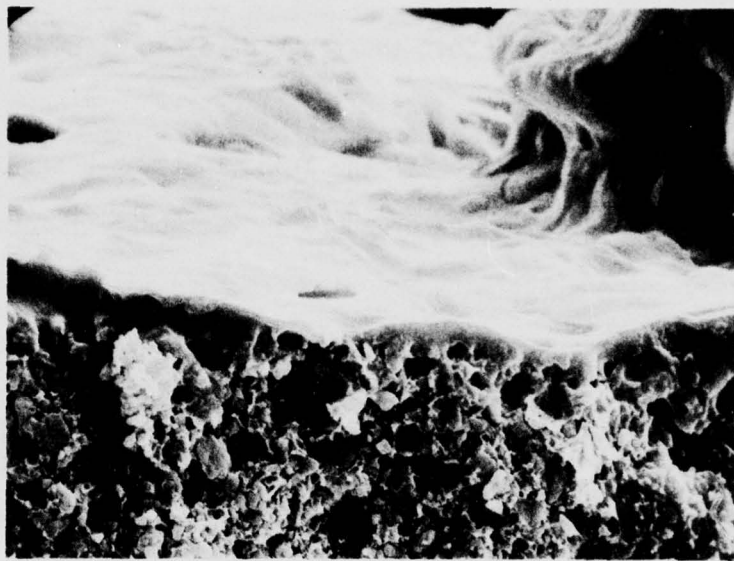


Figure 23a. Section Showing Top and Edge of Extinguished Surface of Fine TAGN/NC Propellant, 3000 psi, 1000X.

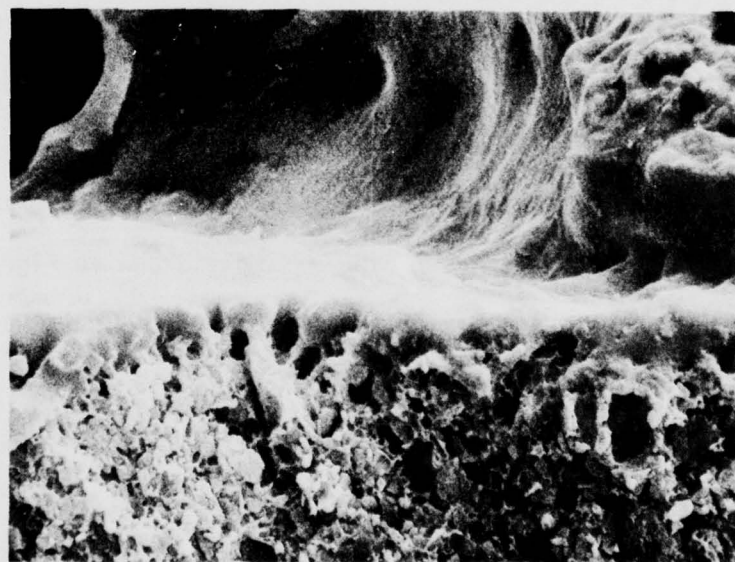


Figure 23b. Fine TAGN/NC Propellant Extinguished at 5000 psi, 1000X.

The effects of combining HMX and TAGN (46% and 29%, respectively) are shown in Figures 24-26. Figure 24(a) is a low magnification view of the surface to give a general picture of the cluster-like particles that were observed to be ejected in the movies. Figure 24(b) shows these clusters at higher magnification. They appear to be grouped recrystallized melts situated upon a melt layer and protruding slightly above this melt layer. These clusters are presumably HMX, which melts and decomposes less readily or rapidly than TAGN. The cluster size is, roughly, about six mean particle diameters, similar to the size of the voids attributed to TAGN clusters in the HTPB propellant (Figure 20). It is difficult to ascertain such particle groupings in unburned propellant, but they appear to show up in burned mixed nitramine propellant as hypothesized. The melt layer here would then be TAGN or an admixture of TAGN and binder. It is situated beneath the HMX, and eventually ejects the HMX, because it decomposes more rapidly. Figure 25 shows an edge view of a sectioned surface, (b) being at higher magnification. There are more pervasive voids in the melt layer than seen with HMX or TAGN alone, which may indicate trapped decomposition of the TAGN-binder admixture. The upper features appear to be the HMX clusters being left behind. The thickness of the melt sublayer beneath the voids is comparable to that of the TAGN/NC propellant (Figure 23), but the overall melt layer thickness (including the voids and the top layer) is much greater. Figure 26 repeats these features at a higher pressure. Figure 26a may be considered essentially as Figure 24 at higher magnification, and better reveals the recrystallized melt clusters intermingled with a smooth melt layer. Figure 26b is similar to Figure 25, except



Figure 24a. Extinguished Surface of Fine HMX - Fine TAGN/NC Propellant, 3000 psi, 50X.



Figure 24b. Magnification of Lower Central Region, 200X.



Figure 25a. Edge View of Extinguished Surface of Fine HMX-Fine TAGN /NC Propellant, 3000 psi, 500X.



Figure 25b. Magnification of Central Region, 2000X.

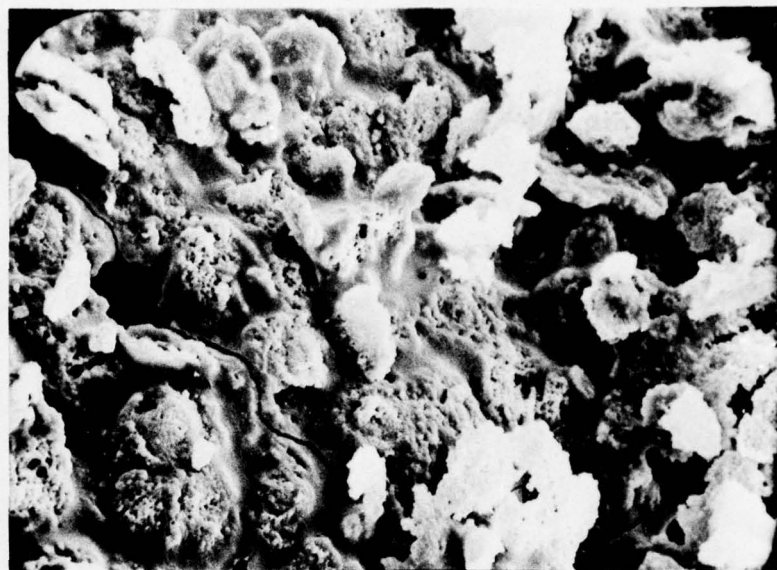


Figure 26a. Extinguished Surface of Fine HMX-Fine TAGN/NC Propellant, 4700 psi, 500X

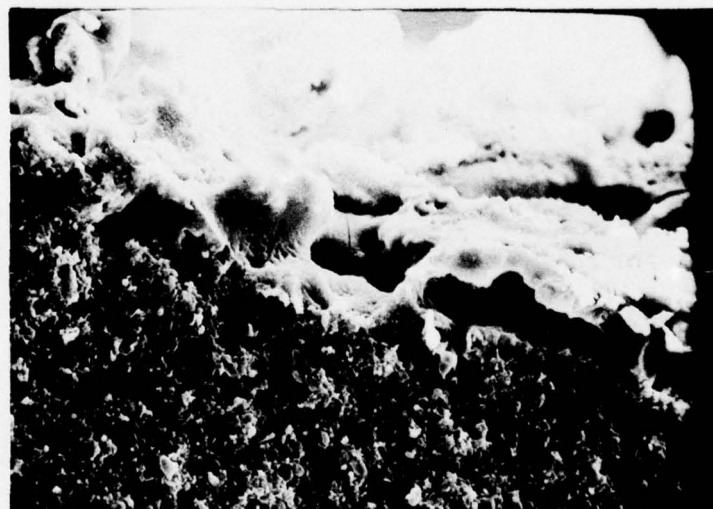


Figure 26b. Section Showing Top and Edge of Extinguished Surface of Fine HMX-Fine TAGN/NC Propellant, 4700 psi, 1000X

that the view angle is changed to better reveal more of the top of the surface along with the subsurface. Viewing both parts of Figure 26 in tandem gives a better indication of the nature of this composite surface.

It can be concluded that the steady burning surface of mixed fine ingredient propellants consists of a melt of one nitramine situated on a melt of the other nitramine admixed with the binder melt. Relative positions depend upon relative rates of decomposition. It appears that these features can be superposed, approximately, for modeling purposes, as in the manner described for bimodal particle sizes.

5.3 TASK 3: COMBUSTION MODELING

5.3.1 Discussion of Approach

The initial problem was to extend the detailed nitramine propellant combustion model (Refs. 3,4) to include mixed nitramines and bimodal particle size distributions in inert binder. These extensions to the model impacted the surface structure, flame structure and energy equations set forth in Subsection 5.3 of Ref. (3). The mixed oxidizer approach was subsequently generalized for mixtures of nitramine and ammonium perchlorate (AP), which are of interest for rocket propellants. The features of the original BDP model (Ref. 16), derived for AP propellants, were retained for this purpose. Finally, the model was extended to incorporate active binders in a simplified manner. The result is a general combustion model that is useful to evaluate combustion tailoring approaches for gun and rocket propellants.

It is assumed that the ingredients are uniformly dispersed in the binder medium, allowing a statistical representation of the surface structure. The form of this representation follows Ref. (3), which is in turn based upon Ref. (16). It should be noted that the statistical representation is presently undergoing a detailed and critical review by Glick (Ref. 17), and may take on other forms in the future. Nevertheless, the form used here has been accepted at this time and has proven satisfactory.

The model extension is limited to two particle sizes for each of two oxidizers. If desired, this can be interpreted as up to four particle sizes for a single oxidizer. This limitation is in due regard for computational complexities, and is acceptable in the light of propellant developments and in view of the purpose of the model to study combustion

tailoring. The disadvantages are that real particle size distributions cannot be represented in detail, and that exponent break points will tend to appear as stepped discontinuities (cf. Ref. 4) in the results. Glick (Ref. 17) has adopted a "pseudopropellant" approach which incorporates up to 60 particles, but decouples them to avoid computational complexity; burning rates are independently calculated for each of 60 pseudopropellants (particles), and then averaged. On balance, it is considered important to couple the particles and that a 2×2 type-size matrix should be adequate.

The melt criterion of Ref. (3), which is the key mechanism for the nitramine break point in pressure exponent, is applied to each particle size for each nitramine. Thus there is a possible total of four tests, with four possible results. It is assumed that multiple surface solutions may be superposed according to the volume fraction of each particle; this assumption was supported by the experimental work. Thus the surface may consist of melt layers, melt layers lining craters, craters within craters, or these nitramine features combined with the particle protrusion-recession features associated with AP (Ref. 16).

Because the propellant contains more than one type or size of particle, the existence of multiple geometry diffusion flames in the gas phase must be addressed. The models representing a single particle size (Refs. 4, 16) base the characteristic dimension for diffusional mixing upon that size. However, in the case of AP, it was found that the important characteristic was not so much the particle size but the spacings between particles (Ref. 18). The size and spacing are easily related in a unimodal propellant, so may be expressed interchangeably, but in a multimodal propellant the relationship is complex because of the

packing of particles. Use of the statistical average particle spacing would afford the simplification of a single characteristic dimension for the mixing. However, it is found that such a description is not correct for nitramine propellants. Use of the spacing tends to give disproportionate weight to the presence of fine particles, which appears correct for AP. However, in the case of nitramines, the surface structure will be dominated by the coarse size whether molten or cratered. Furthermore, low pressure burning rate data for bimodal nitramine propellants reveal the relative importance of the coarse size. Therefore, it is necessary to model two primary diffusion flames, one for each oxidizer on the ground that diffusional behavior stems from different sources.

There are additional reasons for the requirement of two primary diffusion flames. First, the decomposition species of nitramines and AP are different such that the primary flame kinetics should differ. Diffusion flames in AP propellants are believed to involve perchloric acid or chlorine oxides, and in nitramine propellants they probably involve nitrogen oxides. Although kinetics times are often small compared to diffusion times, and the values of the kinetics constants are not so well known for nitramine propellants, nevertheless provision for two sets of kinetics data appears warranted. Secondly, initial model developments predicated on a single averaged primary diffusion flame encountered computational difficulties at nitramine break points, which at times precluded convergence of the iterations. It was found that forcing a transitioning and non-transitioning nitramine to couple with a single primary flame could produce instabilities in the iterations or in the solutions that did converge. Thus resort to two primary flames to accommodate mixed nitramine-AP produced the added benefits of well-behaved answers and shorter computer times in general.

The two primary flames are presumed to interact by assigning each the same adiabatic thermochemical properties of the propellant gases. This assumption seems valid as long as flame heights are large compared to interstitial spacings, which is computed to be true wherever diffusion flame heat feedback is significant, and serves to avoid complications of variable stoichiometries and thermochemistries. Thus the two primary flames have the same temperature, but are free to occur at different heights above the surface. The two primary flames will also influence one another in the course of the iterations for both oxidizers to achieve the burning rate solution.

The final diffusion flame of the multiple flame model is retained as a single averaged flame. Physically, it is plausible to combine all residual reactants into a single flame because it exists at relatively large distances from the surface. Quantitatively, it has little impact upon the energy balance so that its treatment is not important, nor does it upset the iterations for mixed oxidizers.

Two monopropellant flames are necessary because of differing energetics, surface decomposition and gas phase reaction rates, and particle burning rates for different oxidizers. These two flames are treated as independent premixed flames, and are presumed non-interacting. For purposes of the energy balance, two tests are employed comparing associated monopropellant and primary flame heights in order to distribute the heat feedback from these flames to the surface. It is, therefore, possible that different oxidizers will be controlled by different flames at a given pressure.

The essence of the model is the computation of the oxidizer surface temperature from the energy equation, whose components are developed in terms of the multiple flame model. This surface temperature establishes

the oxidizer regression rate, and combined with the oxidizer surface structure the oxidizer mass flux is determined. In the case of inert binder propellants, it is postulated that the oxidizer controls and that continuity is satisfied. In other words, the mass consumption rate of the binder must follow that of the oxidizer and in such relation that the propellant is conserved macroscopically. This postulate, binding the ingredients, establishes the propellant burning rate. When there are two oxidizers, the existence of two surface temperatures must be addressed. This is approached by a double computational iteration of the energy balance for each oxidizer, such that the total mass flux is converged. The inert binder is still constrained to obey continuity in its relation to the summation of oxidizer. However, multiple active ingredients are not constrained to continuity as to each other such that one may dominate or lead where appropriate.

Where one oxidizer has two particle sizes (i.e., bimodal distribution), it is assumed that their surface temperatures are the same. There can be two surface structures superposed, but only one monopropellant flame and one primary diffusion flame with the appropriate averaged characteristic dimension (depending upon AP or nitramine, as discussed earlier). This approach was validated by computing the same 2-particle propellant as a bimodal propellant, as a mixed oxidizer propellant with a single primary flame and as a mixed oxidizer propellant with two primary flames. This exercise also showed that a single primary flame would be adequate for mixed oxidizers, at least where the flame-related inputs are the same, but for the iteration problems alluded to earlier. Where there are two bimodal oxidizers, the approaches for bimodal and mixed oxidizer propellants are combined. A tetramodal single oxidizer propellant would be calculated in that manner.

Provision for active binders is accomplished in four ways. First, it is assumed that the regression rate of the binder at any pressure is its intrinsic value as though no fillers or powders were present. Second, the constraint of oxidizer-binder continuity is removed to allow the binder to govern where appropriate. Third, the binder surface heat of decomposition changes sign, becoming exothermic. Fourth, it is assumed that there is no heat release in the primary diffusion flame when the powder and binder are each balanced stoichiometrically, or nearly so, as would be the case with HMX or RDX combined with active binders. In other words, a primary diffusion flame, reflecting component interaction, can exist only when one component is significantly fuel-rich or oxidizer-rich compared to the other. This premise may be stated more fundamentally in terms of the absence of interactions in laboratory decomposition experiments (Ref. 6), or in terms of the decomposition chemistry of the ingredients. Data were not received with which to study this premise in more detail here, and it will be a subject of future research elsewhere (Refs. 19, 20). The foregoing provides an initial basis for the modeling of filled active binder propellants, without the complications of a Rice-Ginnel (Ref. 21) model. It is sufficient to evaluate combustion tailoring in terms of particle size, certain ingredient types, binder energy level and binder burning rate level; but it may be deficient in terms of the interaction chemistry for other ingredient types not considered here. Nitroplasticized polyurethane binders capable of self-deflagration are treated qualitatively as active binders.

5.3.2 Surface Structure Modifications

Referring to the unimodal, single oxidizer model, Eq. (1) of Ref (3) is expanded as follows:

$$\left(\frac{S_{ox}}{S_0}\right)_F = \sum_{i=1}^2 \left(\frac{3\zeta_i(1-\sigma_i) \left[\left(\frac{h}{D_{i1}}\right)_P^2 + \left(\frac{h}{D_{i1}}\right)_N^2 + \frac{1}{3} \right]}{1 + 3\zeta_i \left[\left(\frac{h}{D_{i1}}\right)_P^2 + \left(\frac{h}{D_{i1}}\right)_N^2 \right]} + \frac{3\zeta_i \sigma_i \left[\left(\frac{h}{D_{i2}}\right)_P^2 + \left(\frac{h}{D_{i2}}\right)_N^2 + \frac{1}{3} \right]}{1+3\zeta_i \left[\left(\frac{h}{D_{i2}}\right)_P^2 + \left(\frac{h}{D_{i2}}\right)_N^2 \right]} \right) \quad (1)$$

A nomenclature is provided as Appendix A. This expression applies if all particles are frozen. In this context, an ammonium perchlorate particle is always frozen but a nitramine particle may or may not be. If all particles are melted, Eq. (3) of Ref. (3) becomes:

$$\left(\frac{S_{ox}}{S_0}\right)_M = \sum_{i=1}^2 \left(\zeta_i \left[(1-\sigma_i) C D_{i1}^a + \sigma_i C D_{i2}^a \right] \right) \quad (2)$$

If some particles are melted and some frozen, it is assumed that the contributions can continue to be superposed by volume fraction. Thus a portion of Eq. (2) may be summed with a portion of Eq. (1).

For an ammonium perchlorate particle, which is always frozen, the protrusion (positive h/D) above the surface is given by Eq. (4a) of Ref. (3) which follows Eq. (4) of Ref. (16). The penetration (negative h/D) is given by the negative form of that equation. For a frozen nitramine particle, any protrusion is again given by that Eq. (4a) but the penetration is given by Eq. (4b) of Ref. (3). This equation also appears as Eq. (3) in Ref. (4), and models the penetration producing the cratered surface that is

observed. These equations are applied to each frozen particle, and the appropriate substitution for h/D is made in Eq. (1). If a particle is melted, Eq. (2) applies for that particle and h/D is zero. Whether a nitramine particle is melted or frozen is determined by Eq. (5) of Ref. (3); this equation also appears as Eq. (4) in Ref. (4).

The spacing between particles is used in the Burke-Schumann model for diffusional mixing. It is derived by subtracting the total unit lengths of statistically intersected particles from unity, following Ref. (14), and then expressing the result in terms of volume fractions. The Ref. (14) result is thereby expanded to:

$$\frac{\delta}{D_{11}} = \frac{\left(\frac{\pi}{6\zeta}\right)^{1/3} \frac{FAC1}{(1-\sigma_1)} - \sqrt{2/3} \left[1 + \left(\frac{\sigma_1}{1-\sigma_1}\right) + \left(\frac{1}{1-\sigma_1}\right) \frac{FAC1}{FAC2} \right]}{1 + \left(\frac{\sigma_1}{1-\sigma_1}\right) \frac{D_{11}}{D_{12}} + \frac{FAC1}{FAC2} \left[\left(\frac{1-\sigma_2}{1-\sigma_1}\right) \frac{D_{11}}{D_{21}} + \left(\frac{\sigma_2}{1-\sigma_1}\right) \frac{D_{11}}{D_{12}} \right]} \quad (3)$$

where

$$FAC1 = 1 + \frac{\alpha_2}{\alpha_1} \frac{\rho_1}{\rho_2} \quad FAC2 = 1 + \frac{\alpha_1}{\alpha_2} \frac{\rho_2}{\rho_1}$$

For the implementation of the Burke-Schumann model, Eq. (14) of Ref. (16) is written in terms of δ and expanded as follows for each oxidizer:

$$b_i^2 = (1-\sigma_i) \frac{D_{i1}}{6}^2 \left[1 + \sqrt{1.5} \frac{\delta}{D_{i1}} \right]^2 + \sigma_i \frac{D_{i2}}{6}^2 \left[1 + \sqrt{1.5} \frac{\delta}{D_{i2}} \right]^2 \quad (4)$$

In the case of ammonium perchlorate, only the first term is used (with $\sigma = 0$) to give weight to the particle spacing in terms of the fine particle size (Ref. 18). Both terms are used for nitramines to give the necessary weight to the coarse size which dominates either the melt or cratered surface structure.

5.3.3 Flame Structure Modifications

What may be termed the multiple-multiple flame model for mixed oxidizers is shown depicted in Fig. 27. Each oxidizer has its own monopropellant flame. The expression for each monopropellant flame height is still given by Eq. (18) of Ref. (16). The value of M_{ox} that is used is the result for each corresponding oxidizer. The order of the reaction is taken to be 2 for nitramines (Ref. 22), but has been optimized as 1.8 for AP (Refs. 16, 22). The final diffusion flame is given by Eq. (16) of Ref. (16), averaged by weighting the result for each oxidizer by the mass flow rate of that oxidizer ($(M_{ox}S_o)_i/S_o$).

Each primary diffusion flame consists of its own diffusion and reaction heights. The reaction height is given by Eq. (8) of Ref. (16). Kinetics constants differ between AP and nitramines, and reaction orders are specified as 1.5 and 2.0, respectively (Refs. 16, 22). In general, the diffusion height would be obtained by substituting Eq. (14) of Ref. (16) (now Eq. (4) here) into Eq. (13) of Ref. (16). However, the Burke-Schumann model has been simplified by the "short flame" assumption (Ref. 22) which provides a characteristic dimension in terms of b . For AP, the diffusion flame height becomes roughly proportional to the fine particle size and independent of pressure:

$$x^*_{PD_i} \approx D_{il} \quad (5a)$$

This was modified for nitramines to account for the binder interference in the melt layer and a pressure-dependence (Eq. (6) of Ref. (3)). Thus the diffusion height becomes roughly proportional to a weighted particle size, and varies inversely with pressure:

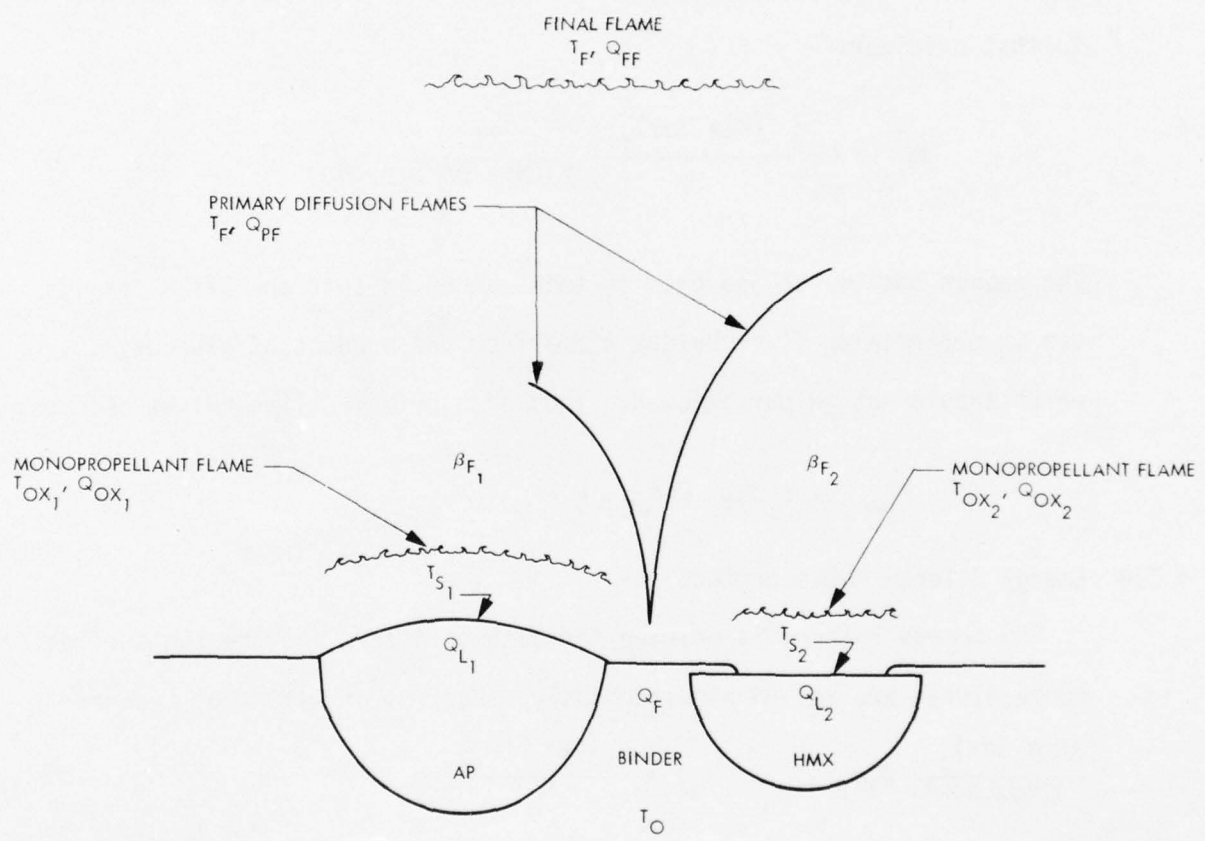


Figure 27. Multiple Flame Structure for Mixed Oxidizers.

$$x^*_{PD_i} \sim \frac{[(1-\sigma_i) D_{i1}^2 + \sigma_i D_{i2}^2]^{a/2}}{p^n} \quad (5b)$$

The two heights are summed in accordance with Eq. (7) of Ref. (3) to establish the flame height. That equation also appears as Eq. (17) in Ref. (16). For each oxidizer, the M_T in that equation is written in terms of a total propellant mass flow rate that would be attributable to that oxidizer:

$$M_{T_i} = M_T \cdot \frac{(Mox\ Sox)_i}{\alpha_i} \cdot \frac{\alpha_T}{\sum (Mox\ Sox)_i} \quad (6)$$

- The reason that M_T is assigned in this manner is that the basis for its use in determining flame height stems from the product of gaseous ρu , which should not be partitioned. Thus each primary flame height becomes:

$$\xi_{PF_i} = c_p M_{T_i} (x^*_{PD_i} + x^*_{PF_i}) / \lambda \quad (7)$$

5.3.4 Energy Balance Modifications

The energy balance is written for each oxidizer, and the two surface temperatures are solved simultaneously. Eq. (6) of Ref. (16) becomes:

$$\begin{aligned} \frac{(Mox\ Sox)_i}{\sum (Mox\ Sox)_i} M_T c_p (T_{S_i} - T_0) &= - \frac{(Mox\ Sox)_i}{S_0} Q_{L_i} \\ &\quad - [M_T - \sum (Mox\ Sox)_i / S_0] \frac{(Mox\ Sox)_i}{\sum (Mox\ Sox)_i} Q_F \\ &\quad + \frac{(Mox\ Sox)_i}{S_0} (1 - \beta_{F_i}) [Q_{Ox_i} \exp(-\xi_{Ox_i}) + Q_{FF_i} \exp(-\xi_{FF})] \\ &\quad + \frac{(Mox\ Sox)_i}{\sum (Mox\ Sox)_i} M_T \beta_{F_i} Q_{PF_i} \exp(-\xi_{PF_i}) \end{aligned} \quad (8)$$

For inert binders, the following relation is specified:

$$M_T = \frac{\sum (M_{ox} S_{ox})_i / S_0}{\alpha_T} \quad (9)$$

For active binders, the general relation is retained:

$$M_T = \sum (M_{ox} S_{ox})_i / S_0 + [1 - \sum (S_{ox})_i / S_0] \rho_F r_F \quad (10)$$

Thus Eq. (8) has the following general form:

$$\begin{aligned} T_{S_i} &= T_0 - K Q_{L_i} / c_p - (1 - K) Q_F / c_p \\ &+ K (1 - \beta_{F_i}) [Q_{ox_i} \exp(-\xi_{ox_i}) + Q_{FF_i} \exp(-\xi_{FF})] / c_p \\ &+ K \beta_{F_i} Q_{PF_i} \exp(-\xi_{PF_i}) / c_p \end{aligned} \quad (11)$$

where $K = \alpha_T$ for inert binders and

$$K = \frac{\sum (M_{ox} S_{ox})_i}{S_0 M_T} \text{ for active binders}$$

Eqs. (20), (21), and (22) of Ref. (16) become:

$$Q_{ox_i} = c_p (T_{ox_i} - T_0) + Q_{L_i} \quad (12)$$

$$Q_{FF_i} = \frac{c_p}{K} [(T_F - T_0) - K (T_{ox_i} - T_0) + (1 - K) Q_F / c_p] \quad (13)$$

$$Q_{PF_i} = c_p (T_F - T_0) + K Q_{L_i} + (1 - K) Q_F \quad (14)$$

Once T_{S_i} is determined, M_{ox_i} is established by an Arrhenius law, Eq. (5) of Ref. (16). Upon solution for both, M_T is determined by Eq. (9) for inert binders and Eq. (10) for active binders. The r_F for active binders is an input at any pressure. The propellant burning rate is then given by Eq. (1) of Ref. (16):

$$r = M_T / \rho_p \quad (15)$$

The T_{S_i} and M_T are solved iteratively.

5.3.5 Provision for Metallized Propellants

Although metals, like AP, would not be of interest for gun propellants, both metals and AP are of interest for rocket propellants. The provision for metals reported in Ref. (18) has been retained in the extended model. Basically, the metal occupies space, absorbs energy at the surface, and affects the propellant flame temperature. Distinctive combustion mechanisms attributable to the metal, as would affect burning rate, are not included. This simplified provision has been found to be satisfactory for practical rocket propellants (Ref. 18).

5.3.6 Computer Programming

A detailed description of the extended model computer program is presented in Appendix B. At the commencement of this research program, the computer program consisted of the unimodal single oxidizer model for nitramines (Refs. 3, 4) and the bimodal single oxidizer model for AP (Ref. 18) in separate branches. The programming effort consisted of incorporating the bimodal expressions for nitramines as differing from AP, incorporating the active binder model as an additional branch, dimensioning variables for dual oxidizer, incorporating the new expressions for bimodal dual oxidizer and devising an iteration scheme for dual oxidizer. Additionally, new input and output formats were devised as appropriate for the extensions, and vestigial statements were removed.

Difficulties in the iterations were sometimes encountered at nitramine break points, due to the discontinuous nature of the criterion for a melted nitramine particle transitioning to a frozen particle. The attempt to force

an answer under such conditions resulted in jagged burning rate curves about the break point. As noted earlier, this difficulty was compounded by forcing a transitioning particle and a non-transitioning particle to follow a single averaged primary flame. The difficulty was resolved by the two-flame model and by devising a new iteration procedure that would logically control the physical state of the particle. The method of forcing an answer as a last resort was retained in order to assure sets of answers within allotted computer times. In addition, coding for diagnostics or debug was devised whereby the iterations could be traced through output of certain key parameters at each step if desired.

A source deck and listing can be furnished upon request.

5.4 TASK 4: COMBUSTION MODEL APPLICATION

5.4.1 Combustion Model Verification

5.4.1.1 Bimodal HMX - Inert Binder Propellants

Figures 1-3 included the results of model calculations together with the data for each propellant. The agreement is generally quite good. The important things to note are the bimodal effects upon the location of the first break point and the high pressure line. Unimodal particle size effects were explained earlier (Refs. 3,4). It is apparent that the model successfully predicts these locations, correctly describing the relative dominance of the coarse particle size in the superposed surface structure and diffusion flame characteristic dimension. The planar surface structure and the primary diffusion flame govern low pressure burning rates and the approach to the transition in the coarse size. The cratered surface structure and the monopropellant flame govern high pressure burning rates. The greater the coarse fraction, the greater the cratering and the higher the high pressure rates. Low pressure rates are reduced because of the greater flame standoff as brought about by the coarse size; the coarse size dominates to the extent that the first break point location does not change significantly.

Figures 1 and 2 show break points in the fine propellants at about 7 Kpsi, and Figure 1 shows a break point in the bimodal propellant at about 10 Kpsi. These are due to a flame structure shift above the planar surface of the fine size or fine fraction. The monopropellant flame is moving inside of and taking over from the diffusion flame. Note, however, that the fine size is also predicted to undergo a surface structure shift eventually to produce another upward break point.

These appear in Fig. 1 at 25 Kpsi for the bimodal propellant and at 45 Kpsi for the fine propellant. Data at 50 Kpsi for the fine propellant appear to confirm this second break. The second break does not appear in the fine propellant of Fig. 2 because its burning rate is too low, a result of the lower solids loading.

The low pressure data of Fig. 2 are very close together because increasing fine fraction is trading off with lower solids loading. The lower solids loading reduces flame temperature and increases the diffusion flame characteristic dimension, which lower burning rate. The increasing fine fraction reduces the characteristic dimension, which raises burning rate. The changing solids loading spreads the high pressure data, however, relative to Figure 1, because lower solids and reduced cratering are complementary.

Figure 3 shows a more systematic variation in fine/coarse ratio. The first break points are due to the surface structure shift in the coarse size, and the second upward break points are due to the surface structure shift in the input coarser component of the fine size. Breaking up the fine size into two components is found to improve the prediction of high pressure characteristics dependent upon them, and better simulates real distributions in a given lot of material. Had a single mean size (14μ) been input to represent the fines, the second break would have occurred at roughly 0.3 in./sec. burning rate and would have jumped all the way to the top line. Rather, the 2μ component remains planar and keeps the lines properly separated at high pressure. It is found to be more important to break up the fine size in this manner than the coarse size to interpret nuances in data

brought about by broad-banded size distributions. This problem will be discussed further in its combustion tailoring implications in Subsection 5.4.2. An important thing to note in Figure 3 is the continuing increment in low pressure rate and decrement in high pressure rate as fine fraction increases. The net result is a lower effective post-transition slope with increasing fine fraction, which appears in the model as less extensive jumps in burning rate.

5.4.1.2 Effect of TAGN in Inert Binder Propellants

The model treats TAGN as HMX with different input constants. Unknown constants for TAGN were deduced by fitting the model to GAU-8 propellant data. This deduction was subsequently verified by predicting the burning rate of pressed TAGN, using the model in its degenerative 100% oxidizer form, when that data became available. Ordinarily, the constants should be determined by first fitting the model to the oxidizer only (Ref. 22) unless experimental measurements are available for them. The TAGN burns roughly twice as fast as HMX. It was found that the decomposition kinetics prefactor had to be increased an order of magnitude above that for HMX, and that the net surface heat release when melted had to be about 50% higher. Its melting point is known to be 150°C lower, and its flame temperature is about 20% lower than for HMX.

Figure 4 presented data for RHT-7 propellant (high total solids) and formulation 137-1 (higher TAGN/HMX ratio). The RHT-7 data were originally predicted by parametric variation of particle size, before the particle size data became available. It was found that the assumed particle sizes differed from the actual particle sizes by a factor of

two (TGN assumed too fine, HMX too coarse). When the model was re-run with the actual sizes, which is the result shown in Figure 4, the only real change was in the nuances of the multiple break points. Thus, the analysis can tolerate some particle size uncertainty, which is known to exist from quality control experience. Note that the inputs break up each fine oxidizer into two components, reflecting the 25% and 75% weight positions in the distribution, rather than use the mean. This serves to straddle the data better, as discussed earlier. The predicted break points in the HMX sizes precede those in the TGN because the TGN is finer and has a lower melting point. Note that a line which would average out the analytical zig-zags for the RHT-7 propellant would closely align with the data.

The higher burning rate of the 137-1 propellant is due to the higher proportion of TGN, notwithstanding its lower flame temperature and lower solids loading. The HMX is finer, but this is less important than the surface decomposition kinetics and surface heat release of the TGN. The first analytical exponent break is due to a flame structure shift, and the second is due to a surface structure shift in the coarser HMX component which then triggers shifts in all but the finer TGN component. The cross-over at high pressure, whereby the 137-1 propellant rates become lower, is predicted to be due to the fact that there is less cratering because of the lower total solids and lower HMX fraction. Also, the finer HMX causes the predicted shift to begin at higher pressure; however, this high pressure shift is not fully evident in the data.

It is predicted that TAGN can be effective to diminish exponent shifts by its surface decomposition properties, which raise low pressure rates, and by its ability to remain molten to higher pressures, which lowers high pressure rates. However, it is cautioned that the higher rates from the TAGN can induce an earlier shift in the HMX that is mixed with it if the HMX is not sufficiently fine. It is concluded that there is good agreement between theory and experiment for these propellants.

5.4.1.3 Effect of HMX Particle Size in Active Binder Propellants

Active binder burning rates for input purposes were furnished by Rocketdyne. The standard nitrocellulose binder was represented as having the burning rate of M-1 gun propellant. Its surface heat of decomposition was assumed to be in proportion to that of HMX, ratioed according to monopropellant flame temperatures. The burning rate of the nitroplasticized polyurethane was somewhat lower, in accordance with active binder energy-burn rate correlations and its heat of decomposition was averaged from the components. Data for energetic active binders were also furnished for parametric study, and surface heats of decomposition were similarly derived.

The effect of HMX particle size in active binders was shown in Figure 5. The predicted small effect at low pressure results from the absence of the diffusion flame; the rationale was that there could be no component interaction when both oxidizer and binder are stoichiometrically balanced. What little effect there is stems from the model for binder interference with oxidizer in the admixture surface melt. This small effect appears to be predicted correctly. Burning rates at high pressure are dominated by the transition in the coarse size, the

same as for inert binders. Note the zig-zags in the data for the 7 μ HMX/NPPU propellant. These indicate the presence of coarser sizes in the distribution, and could have been better represented by the model by inputting several sizes as was done for the RHT-7 propellant discussed earlier. The Figure 5 result compares the effect of not doing so.

The burning rates for the NC propellants are predicted to be higher than for the NPPU propellants because of the higher binder burning rates and energy. This effect is predicted to diminish at high pressure when the transitioning nitramine becomes more dominant. Thus, the higher burning rates at low pressure serve to reduce the extent of the transition. High pressure data for the NC propellants were not available to verify this prediction in the case of HMX alone.

5.4.1.4 Effect of TAGN in Active Binder Propellants

The addition of TAGN to active binder propellants is predicted to raise burning rate, as was the case for inert binder propellants.

Results for NPPU propellants were shown in Figure 6. Exponent shifts are predicted to occur at about 30 Kpsi, due to transition in the fine HMX. The similar location of the post-transition lines is due to the increased cratering in the HMX propellant and the increased decomposition kinetics of the TAGN in the mixed propellant. The data also merge at these very high pressures. The more rapid decomposition of the TAGN is also reflected in the low pressure data for the TAGN propellant. High pressure data were not available for this propellant. It is apparent that the relative reactivity of the TAGN prevents the active binder from dominating the low pressure combustion, a result which is consistent with the motion picture observations.

Predictions for the NC propellants were shown in Figure 7. The most interesting data are those for the RGP-150 propellant because so many data points were taken. These data clearly show, within the scatter, the kind of zig-zags at high pressure that are calculated by the model to reflect multiple transitions. The model is closely aligned with those zig-zags when each oxidizer is represented by the 25% and 75% weight sizes of the distribution. The first upward break is due to transition in the coarse HMX, which then triggers all but the fine TAGN. The second upward break is due to the fine TAGN. Each break leads to a new line representing a new burning rate level dependent upon the extent of cratering. It is observed that the model successfully predicts the increasing burning rates with increasing proportions of TAGN.

The data for the all-TAGN propellant in Figure 7 are also interesting because of the significant data scatter at 7 Kpsi. This scatter may be interpreted as a break point location, which is predicted reasonably well by the model. The post-break burning rate line is seen to be relatively high. This is predicted to be caused by a combination of full cratering and rapid TAGN decomposition, which will be most complementary with TAGN alone.

The proximity of the two intermediate burning rate propellants in Figure 7 is predicted to result from a tradeoff of propellant energy and surface decomposition. The replacement of HMX with TAGN lowers energy but increases decomposition rates, and the proximity derives from the coupling of the two. When all TAGN is removed, burning rate drops considerably at low pressure because the important surface

decomposition is slowed. When all HMX is removed, burning rate jumps considerably because there is no coupling to hold back the TAGN decomposition effect. It is predicted that the 46% HMX propellant will eventually cross over and burn faster than the 24% HMX propellant. This will occur when the HMX transitions, and the greater HMX concentration will produce more cratering. The lines will then interweave at very high pressures where the TAGN also transitions. This high pressure prediction is not shown, to avoid confusing the figure, and because high pressure data for the 46% HMX propellant were not available.

It is concluded that TAGN can serve to mitigate exponent shifts in active binder nitramine propellants, but doing so involves walking a tightrope. There should be enough to raise low pressure burning rates, but not so much as would trigger the HMX present. It should be fine enough to avoid its own transitioning, and its concentration should be limited so that post-break burning rates do not get too high if it does transition. The TAGN itself can transition, and is not a cure-all panacea. Further adjustments of burning rate are available by tailoring the burning rate and energy level of the active binder component.

5.4.1.5 AP-Active Binder Propellants

AP propellants were not studied in the experimental portions of this program. However, in view of the model extension to active binders, it was deemed appropriate to verify a case of AP addition to an active binder. Data for a CMDB propellant containing AP and energetic active binder were furnished by Hercules. These data, together with model results, are shown in Figure 28. The data are over a low pressure regime consistent with rocket applications. Data and model results are

AD-A033 034

JET PROPULSION LAB PASADENA CALIF
NITRAMINE PROPELLANT RESEARCH. (U)
OCT 76 N S COHEN, L D STRAND

F/G 19/1

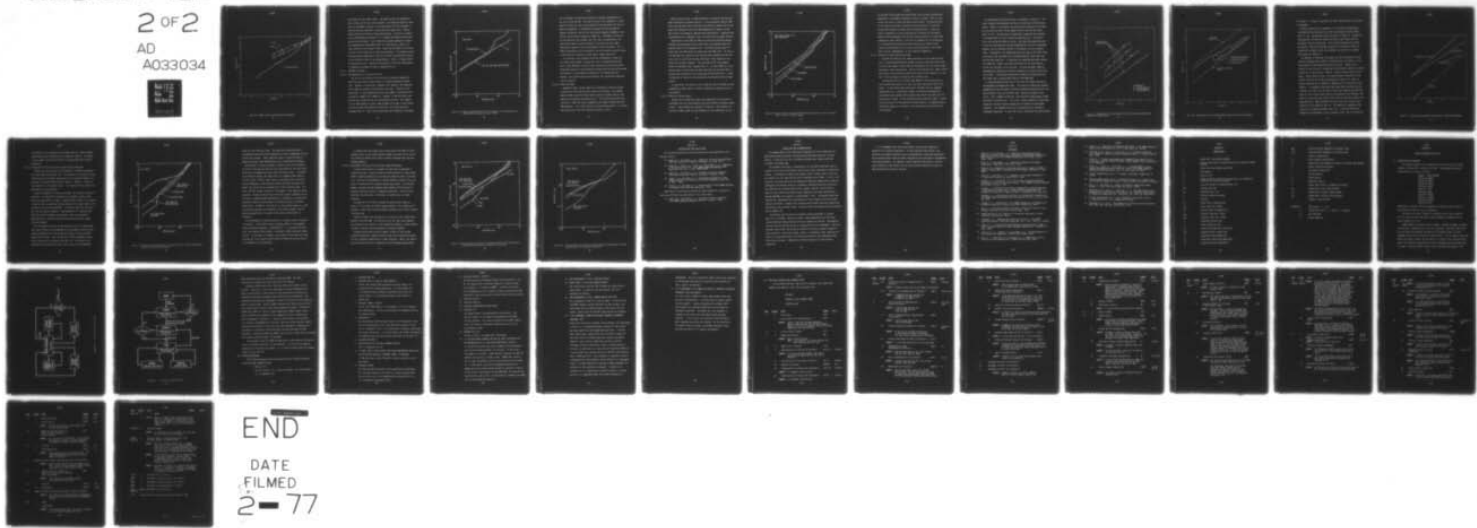
UNCLASSIFIED

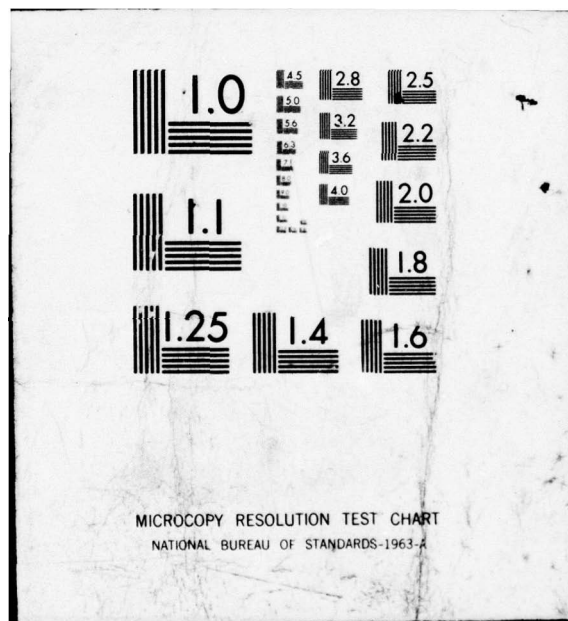
2 OF 2
AD
A033034

NAS7-100

AFOSR-TR-76-1163

NL





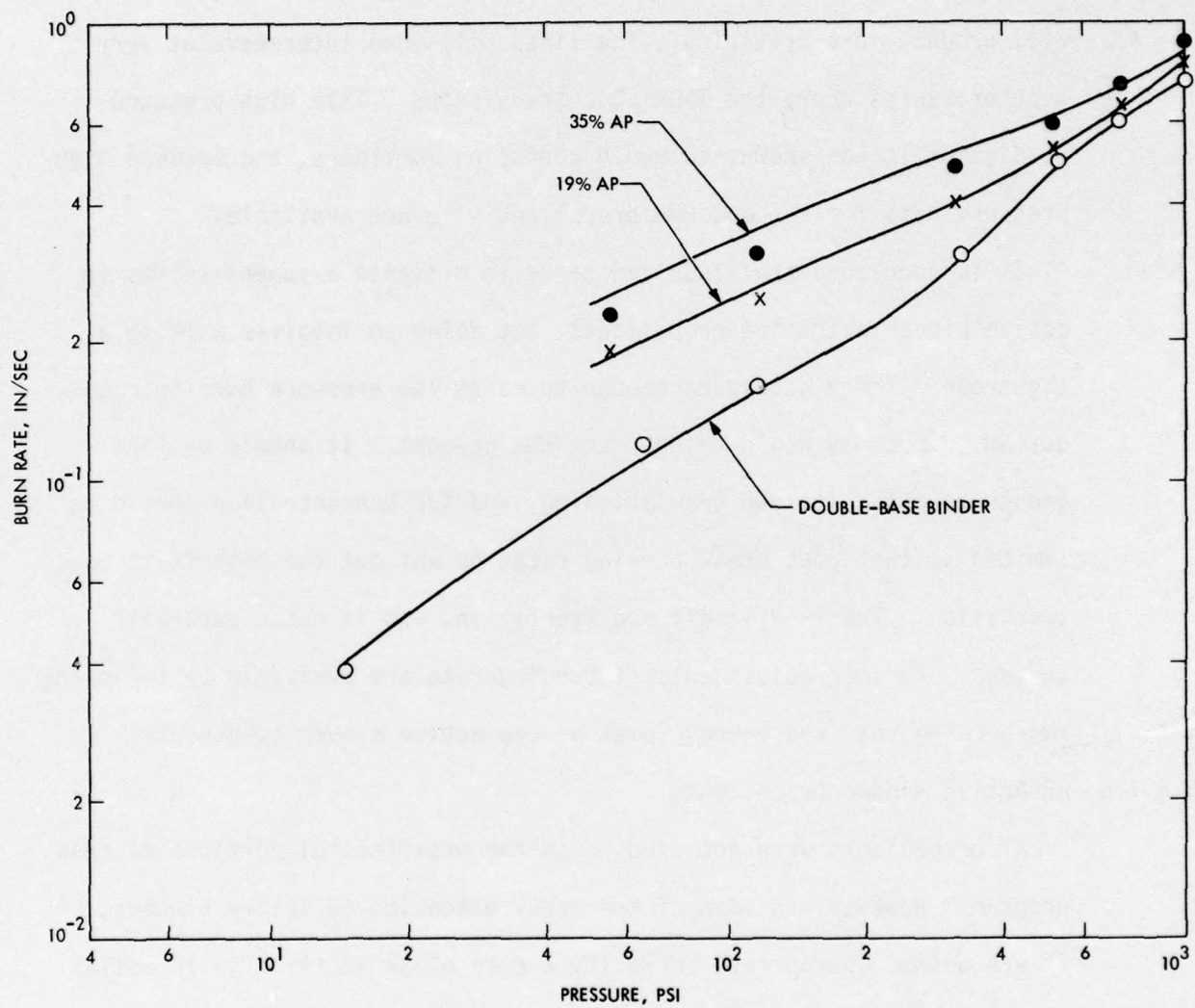


Fig. 28. Effect of AP in double-base propellants

also shown for the binder itself. The model results are essentially data in-data out for zero solids loading. The important things to note with the systematic increase in AP concentration are the increases in burning rate and reductions in slope over the range 50 psi - 500 psi. These reflect the diffusion flame contributions. Since AP is oxidizer rich, and therefore unbalanced, it is presumed that there can be interaction with the binder. Such interaction has been measured in laboratory decomposition experiments (Ref. 6); significantly, there is no such interaction in the case of HMX. Note also the merger of the lines with the active binder line at the upper pressures. This merger results from the growing importance of the active binder contributions relative to the diffusion flame in the energy balance. There is no deep cratering mechanism for AP. Additional discussion of diffusion flame effects is deferred to parametric study in Subsection 5.4.2.

5.4.2 Parametric Studies

5.4.2.1 The Importance of Fine Particle Size

The use of fine particle size should be an effective approach to defer the occurrence of break points in nitramine propellants (Refs. 3,4). However, to effectively implement this approach, the propellant must indeed be limited to sufficiently fine sizes. Figure 29 illustrates why. If the propellant contains only 5μ HMX, a break point will not begin to appear until 35000 psi. However, in the real world, production lots of HMX consist of a distribution of sizes. For example, a lot of HMX reported to have a mean diameter of 5μ may in fact consist of sizes ranging from submicron to 50μ (Ref. 23) unless carefully screened (Ref. 3). Such a size distribution was simulated in the model

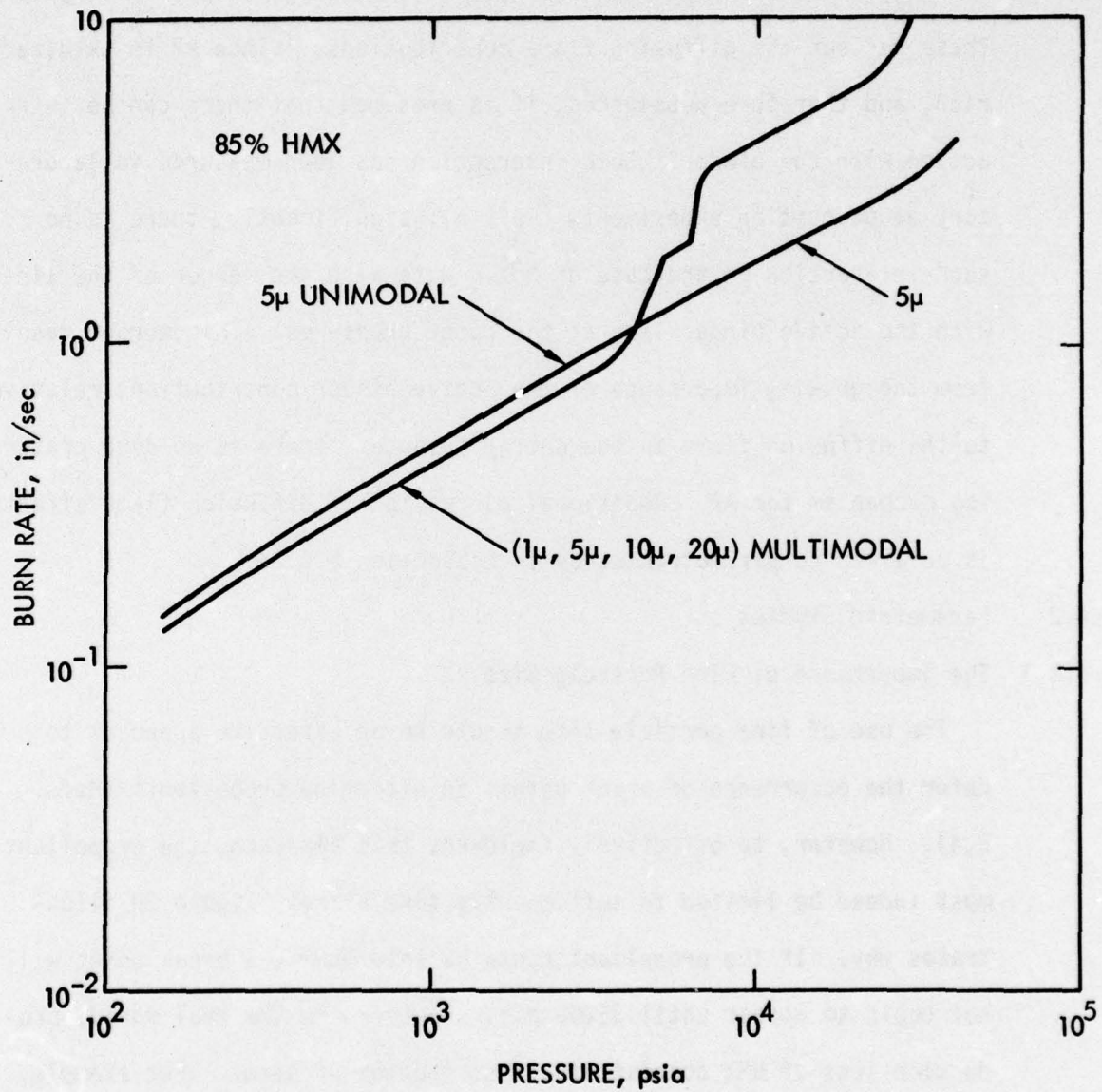


Figure 29. Effect of Real Particle Size Distribution on Burning Rate of HMX/HTPB Propellant; "Fine" HMX

by a tetramodal distribution consisting of unequal concentrations of 1μ , 5μ , 10μ and 20μ HMX. The result for this " 5μ " propellant is superposed in Figure 29, and is quite different from the result for the unimodal 5μ propellant. A break point assignable to the 20μ particle appears at 4000 psi, one for the 10μ particle appears at 6000 psi, and one for the 5μ particle appears at 20000 psi. The effects of the 10μ and 20μ particles are stronger than their small concentrations (17% total) would seem to warrant because of the impact of their deep-penetration combustion upon the propellant surface structure. For a smooth (continuous) size distribution, the real propellant would display a long, drawn-out transition, rather than a staged transition.

In conclusion, some procedure should be implemented to screen out the coarse sizes present in production lots of purportedly fine HMX. This is more important in inert binder propellants than active binder propellants because of the mitigations brought about by the active binder contributions to the propellant combustion, as discussed earlier. However, this approach may not be practical for applications requiring low cost material.

5.4.2.2 Effects of TAGN

Compared to HMX, coarser TAGN can be tolerated in order to prevent a break point from occurring below some given pressure. For example, where the HMX size distribution should extend no further than 4μ , the TAGN size distribution may extend to 8μ . This reflects the lower melting point of TAGN, but offset somewhat by the higher burning rate that TAGN produces. For a given particle size and melting point, it is really the burning rate level that induces the break to occur.

Break points do occur in TAGN propellants, as shown by the data and model applications discussed earlier. If the propellant contains TAGN alone, burning rates reach relatively high levels on either side of the break point because of the rapid TAGN decomposition compared to HMX. These levels are reduced by reducing TAGN concentration. Reducing TAGN concentration will, therefore, shift its break point to higher pressure.

Combinations of fine HMX and TAGN can pinch the difference between pre-break and post-break burning rate levels, and thereby reduce the apparent extent of the exponent shift. Pre-break burning rates are higher than with HMX alone, but lower than with TAGN alone. As long as the TAGN does not transition, the burning rates following the HMX transition will be lower than ordinary post-break levels because of the planar melt surface component. This pinching of the lines appears optimal at HMX/TAGN ratios ranging from 1-2. Too much TAGN will raise burning rates to facilitate the TAGN transition, and too much HMX will produce more cratering of the surface upon the HMX transition. A good illustration of this pinch was provided by the Figure 6 data and model results.

In conclusion, the judicious use of TAGN can serve to smooth out the appearance of break points if further reductions in particle size are not possible.

5.4.2.3 Effects of Active Binder

Another way to smooth out break point appearance is by the use of multimodal fine size distributions and active binders of greater energy content. These effects are combined in Figure 30. The oxidizer is a mixture of TAGN and HMX to take advantage of that combination as well.

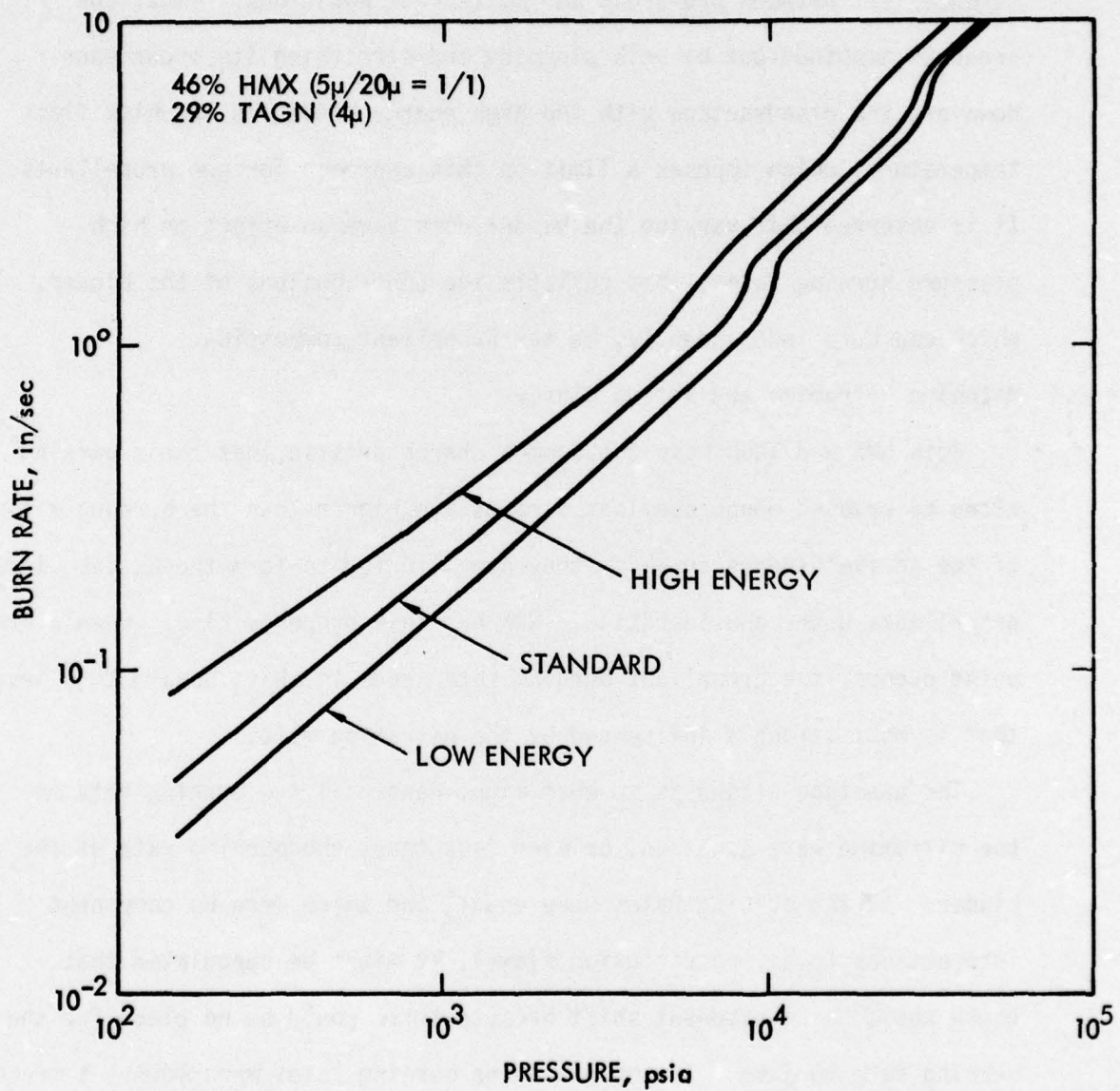


Figure 30. Burning Rates of Mixed HMX/TAGN Propellants in Active Binder;
Effect of Active Binder Energy

The two HMX sizes produce two break points, but the overall break point appearance is stretched out because it occurs in stages. Note, in particular the result in the high energy active binder. The burning rates at low pressure have been increased so much that there is little difference left between pre-break and post-break positions. Thus, the break is smoothed out by both pinching and stretching its occurrence. However, the disadvantage with the high energy binder is its high flame temperature, which imposes a limit on this approach for gun propellants. It is observed that varying the binder does have an effect on high pressure burning rates; this reflects the contributions of the binder, which can burn independently, to the propellant combustion.

5.4.2.4 Matching Nitramine and Active Binder

Both HMX and TAGN have the common characteristic that their burning rates as pressed monopropellant strands are higher than the burning rates of the active binders in which they are situated to form the active binder propellants under consideration. RDX has this property also. When a break point occurs, the propellant burning rate tends to shift upward to a level that is most strongly influenced by the nitramine rate.

The question arises as to what might happen if the burning rate of the nitramine were equal to, or even less than, the burning rate of the binder. If the burning rates were equal, and there were no component interactions (e.g., no diffusion flame), it might be speculated that there would be no exponent shift because there would be no place for the burning rate to jump. If the nitramine burning rates were lower, a transition could result in the prediction of mesa behavior, or downward breaks, which would appear as low slopes in real propellants having broad size distributions.

An interesting correlation of data is presented in Figure 31. The lines represent the monopropellant data, including the nitrocellulose binder. EDNA is a low energy, low melting point nitramine, like TAGN, but with burning rates falling between those of HMX and the binder (Refs. 8, 24). The data are for propellants containing 75% nitramine in nitrocellulose, and are limited to post-break data. The TAGN is fine, and the HMX and EDNA are coarse. Note that the propellant data follow the corresponding nitramine monopropellant line as if dominated thereby, and are therefore ordered in accordance with the nitramine rates. Consequently, the EDNA propellant rates jump to the least level. Low pressure data confirmed that the EDNA propellant rates jump less than the HMX propellant. A propellant was requested that would contain fine EDNA and a higher rate binder that would try to match the two, but was not available at this writing. In using the model, EDNA was represented by reducing the kinetics constants by a factor of two relative to HMX. A calculation predicted the break to be negligible when the binder rate is approximately equal to the EDNA rate.

A nitramine whose burning rate is less than the binder rate may be represented by nitroguanidine (NQ). This type of situation was studied parametrically with the model, arbitrarily selecting input constants that would produce a very low nitramine rate. Results are shown in Figure 32. For a unimodal propellant, the transition indeed causes a downward shift in burning rate. The binder is more influential at the lower pressures, and the nitramine becomes most influential at the higher pressures. This downward break can be stretched out by assuming a tetramodal propellant. In the limit, with a continuous size distribution,

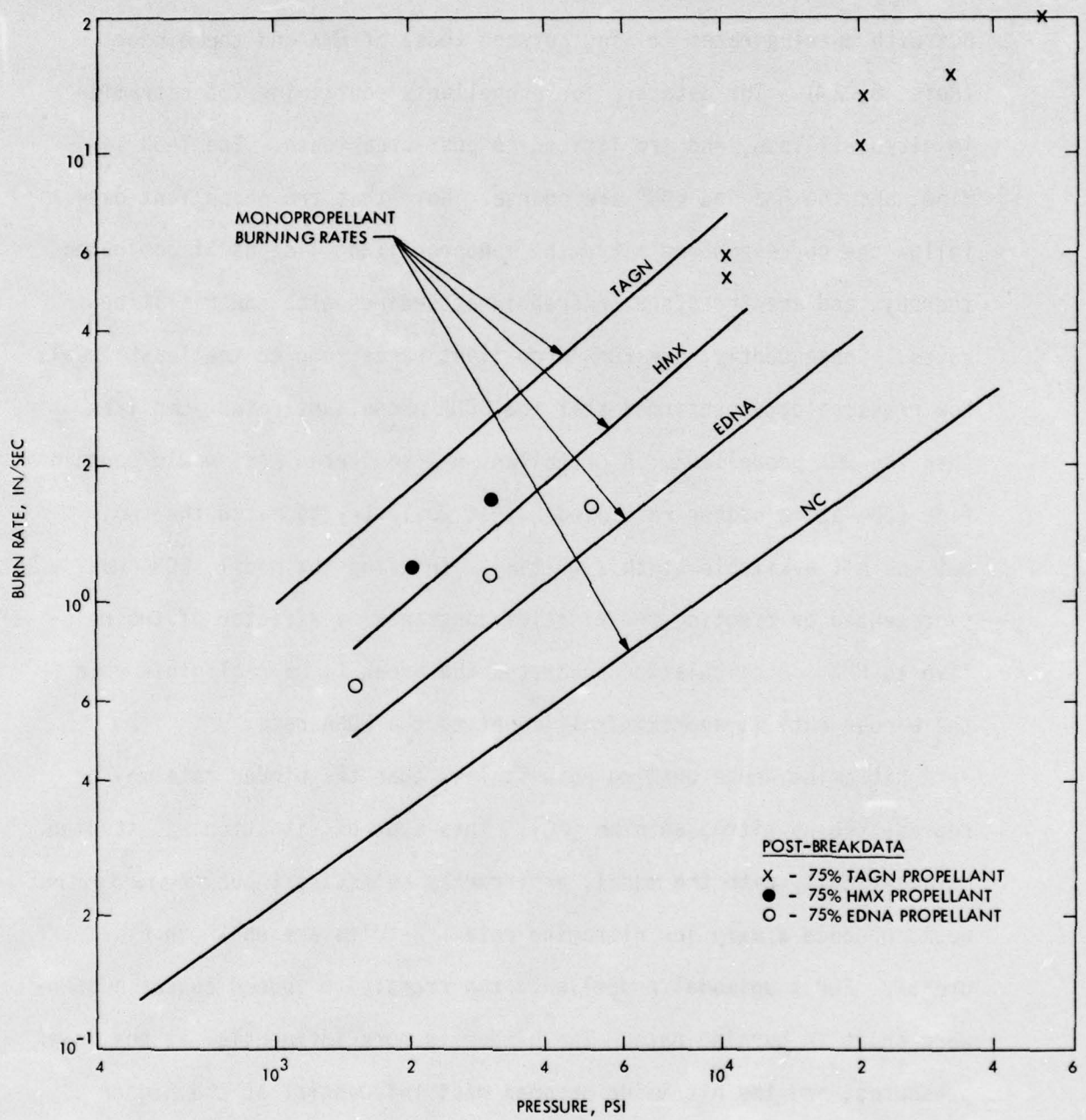


Fig. 31. Comparison of monopropellant burning rates and post-break propellant burning rates

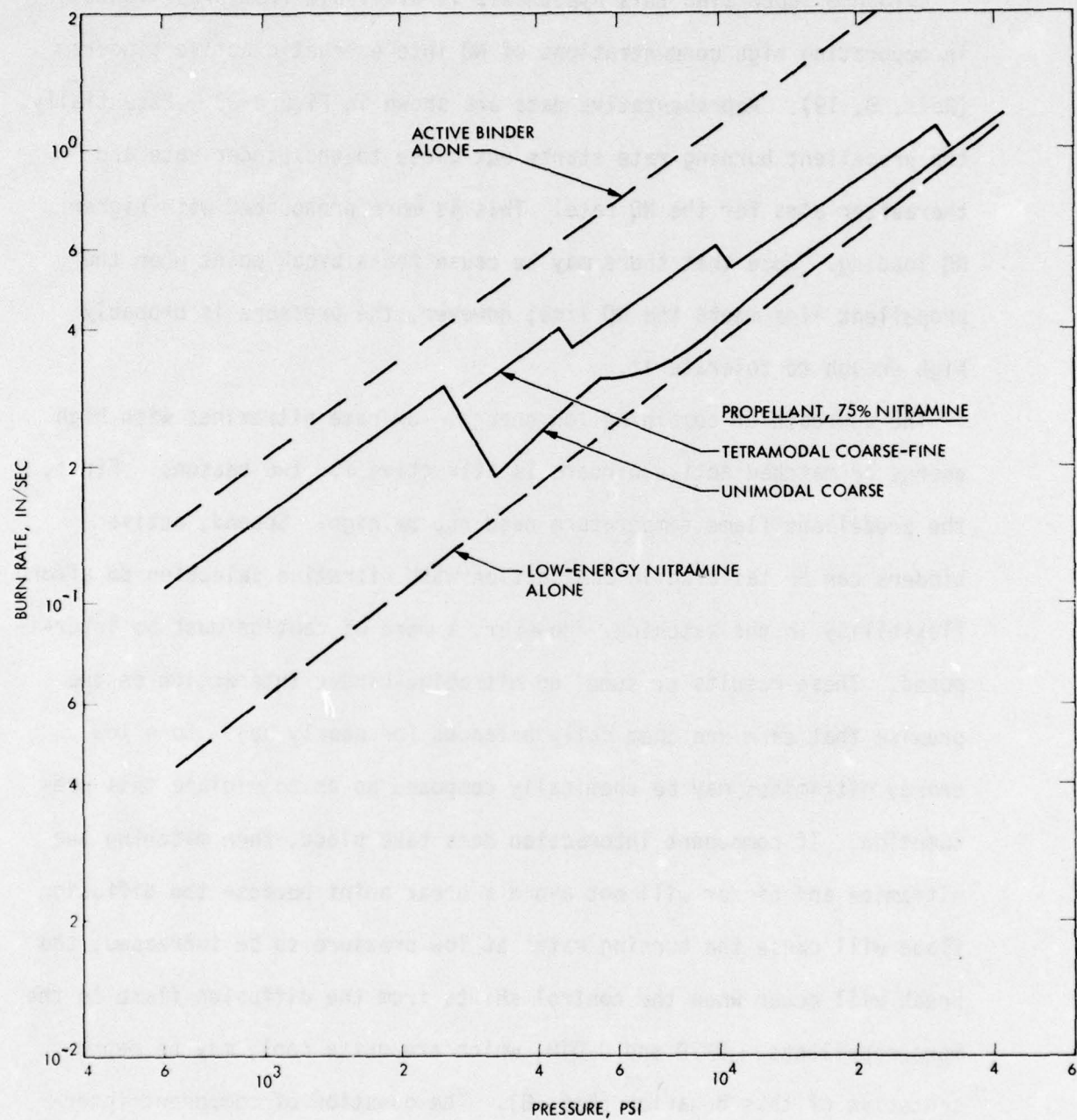


Fig. 32. Calculated reverse break points caused by low-rate nitramine

the result is a range of pressures over which there would be a continuous low exponent.

Evidence supporting this hypothesis is available from propellants incorporating high concentrations of NQ into energetic active binders (Refs. 8, 19). Representative data are shown in Figure 33. Essentially, the propellant burning rate starts out close to the binder rate and thereafter aims for the NQ rate. This is more pronounced with higher NQ loading. Note that there may be cause for a break point when the propellant line meets the NQ line; however, the pressure is probably high enough to tolerate it.

The approach of combining low energy, low rate nitramines with high energy or matched active binders is attractive for two reasons. First, the propellant flame temperature need not be high. Second, active binders can be tailored in conjunction with nitramine selection to afford flexibility in the matching. However, a word of caution must be interposed. These results presume no nitramine-binder interaction on the premise that each are chemically balanced (or nearly so). Some low energy nitramines may be chemically composed so as to violate this presumption. If component interaction does take place, then matching the nitramine and binder will not avoid a break point because the diffusion flame will cause the burning rates at low pressure to be increased; the break will occur when the control shifts from the diffusion flame to the monopropellants. DMED and DMDTH, which are quite cool, may be representative of this behavior (Ref. 8). The question of component interaction will be studied elsewhere (Ref. 19). It may be evaluated by decomposition experiments, such as reported in Ref. (6), or by particle

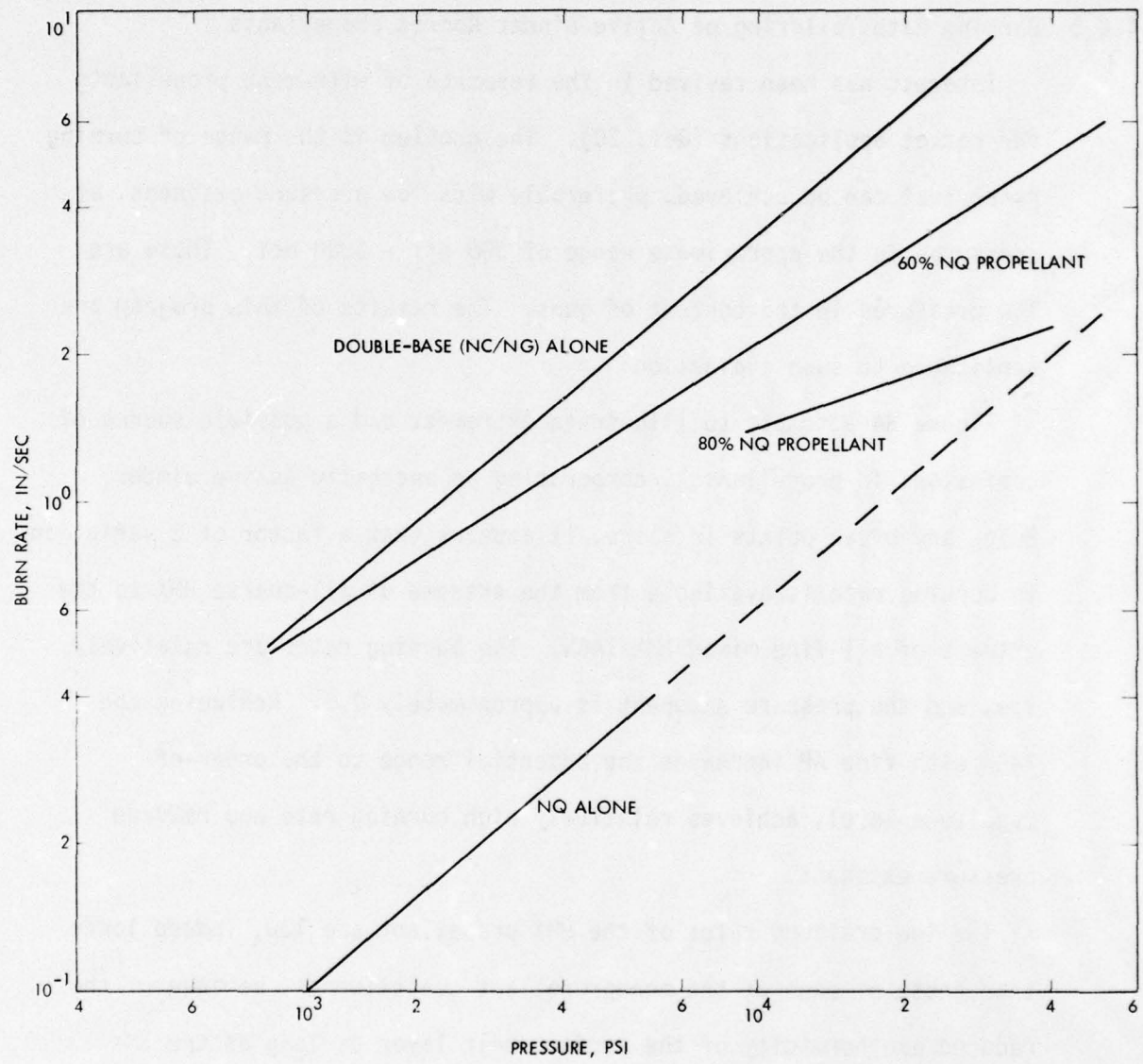


Fig. 33. Triple-base propellant burning rates, high solids loading

size effects at low pressure as are present with AP. Many nitramine derivatives may be processed for such chemistry studies. At present, it would appear that tailoring EDNA or NQ propellants would be most productive.

5.4.2.5 Burning Rate Tailoring of Active Binder Rocket Propellants

Interest has been revived in the research of nitramine propellants for rocket applications (Ref. 20). The problem is the range of burning rates that can be achieved, preferably with low pressure exponent, at pressures in the approximate range of 300 psi - 3000 psi. These are low pressures in the context of guns. The results of this program are applicable to such evaluation.

Figure 34 attempts to illustrate extremes, and a possible source of confusion, in propellants incorporating an energetic active binder. Below any break points in slope, it appears that a factor of 2 variation in burning rate is available from the extreme of all-coarse HMX to the extreme of all-fine mixed HMX/TAGN. The burning rates are relatively low, and the pressure exponent is approximately 0.6. Replacing the TAGN with fine AP increases the potential range to the order-of-magnitude level, achieves relatively high burning rate and reduced pressure exponent.

The low pressure rates of the HMX propellant are low, indeed lower than those of each of the monopropellant constituents, because of the reduced exothermicity of the surface melt layer as long as the HMX remains fully molten. Thus, the addition of HMX to energetic active binder reduces the low pressure rate (Ref. 12). The rates of the propellant containing AP are high, and are particle size-dependent,

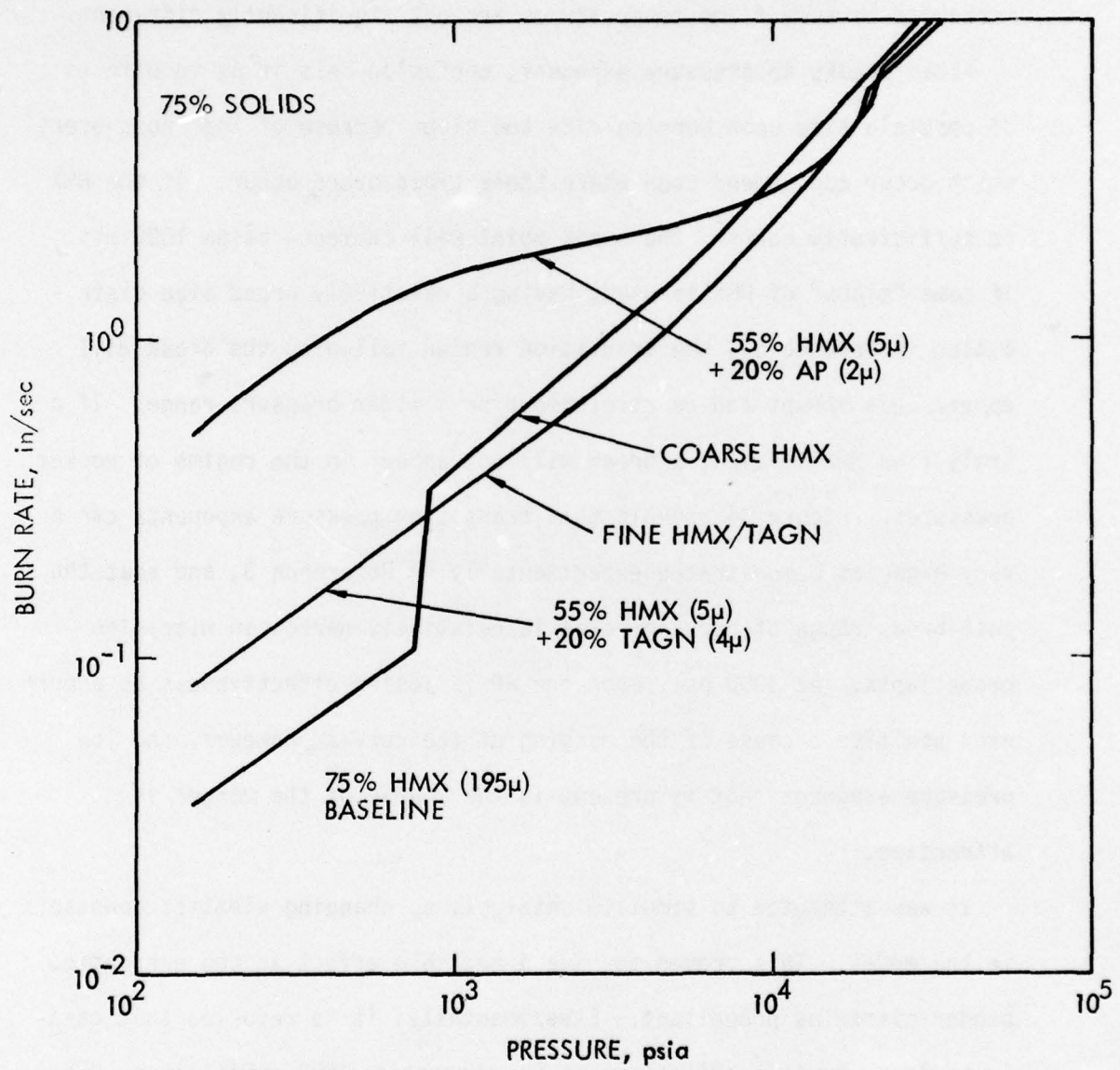


Figure 34. Burning Rate Tailorability of Energetic Active Binder Propellants;
Effects of Ingredient Variations

because of the diffusion flame. The propellant containing TAGN is intermediate because the fast decomposition kinetics compensates for the surface heat release. These propellants show a strong influence of mechanism because flame temperatures are not significantly different.

Above breaks in pressure exponent, confusion sets in as to effects of particle size upon burning rate and slope because of the cross-overs which occur and depend upon where these cross-overs occur. If the HMX is sufficiently coarse, the break point will commence below 1000 psi. If some "class" of HMX is used, having a relatively broad size distribution (Reference 6), the transition region following the break will appear less abrupt and be stretched over a wider pressure range. If a truly fine HMX is used, a break will not appear in the regime of rocket pressures. Figure 34 reveals that transition pressure exponents can be very high, as demonstrated experimentally in Reference 3, and that the post-break range of burning rates is relatively narrow in nitramine propellants. At 3000 psi, even the AP is losing effectiveness as a burn rate additive because of the merging of the curves; however, the low pressure exponent that is present in the course of the merger is attractive.

It was attempted to simulate catalysts by changing kinetics constants in the model. This proved to have a negligible effect in the energetic binder-nitramine propellant. Experimentally, it is reported that catalysts lose chemical effectiveness in energetic CMDB propellants (Reference 6). In the model, it appears to be a matter of how high the binder burning rate is (by itself) and how high the propellant burning rate is in the absence of the simulation.

It appears that the careful use of sufficiently fine HMX will avoid exponent shifts in the rocket pressure regime, and that fine AP is the most effective additive with which to achieve increased burn rate and reduced exponent.

5.4.2.6 Burning Rate Tailoring of Inert Binder Rocket Propellants

A set of curves similar in purpose to Figure 34 are presented in Figures 35 and 36. Figure 35 shows tailoring potential in inert binder (HTPB) nitramine propellants, and Figure 36 shows the effect of AP addition. Particle size adjustment of the HMX affords a factor of two variations in burning rate at pressures below break points. The fine HMX appears to reduce pressure exponent when compared with the coarse at pressures where the coarse is undergoing transition. The use of sufficiently fine HMX avoids a transition, or break point, at rocket pressures.

The addition of fine TAGN increases the burning rate range to a factor of 3, but does not further reduce exponent. The simulation of a catalyst in that mixed oxidizer propellant produces only a minor increase in burning rate.

Figure 36 reveals that the addition of fine AP is only slightly more effective than the TAGN in raising burn rate, but does lower exponent. The simulation of a catalyst in that propellant produces a slight further increase in burning rate and reduction in pressure exponent.

Although burning rate tailoring appears limited in inert binder nitramine propellants, moderate burning rates can be achieved by operating fine ingredient propellants at higher pressures. Again, the careful use of fine particle size is necessary to avoid exponent break points.

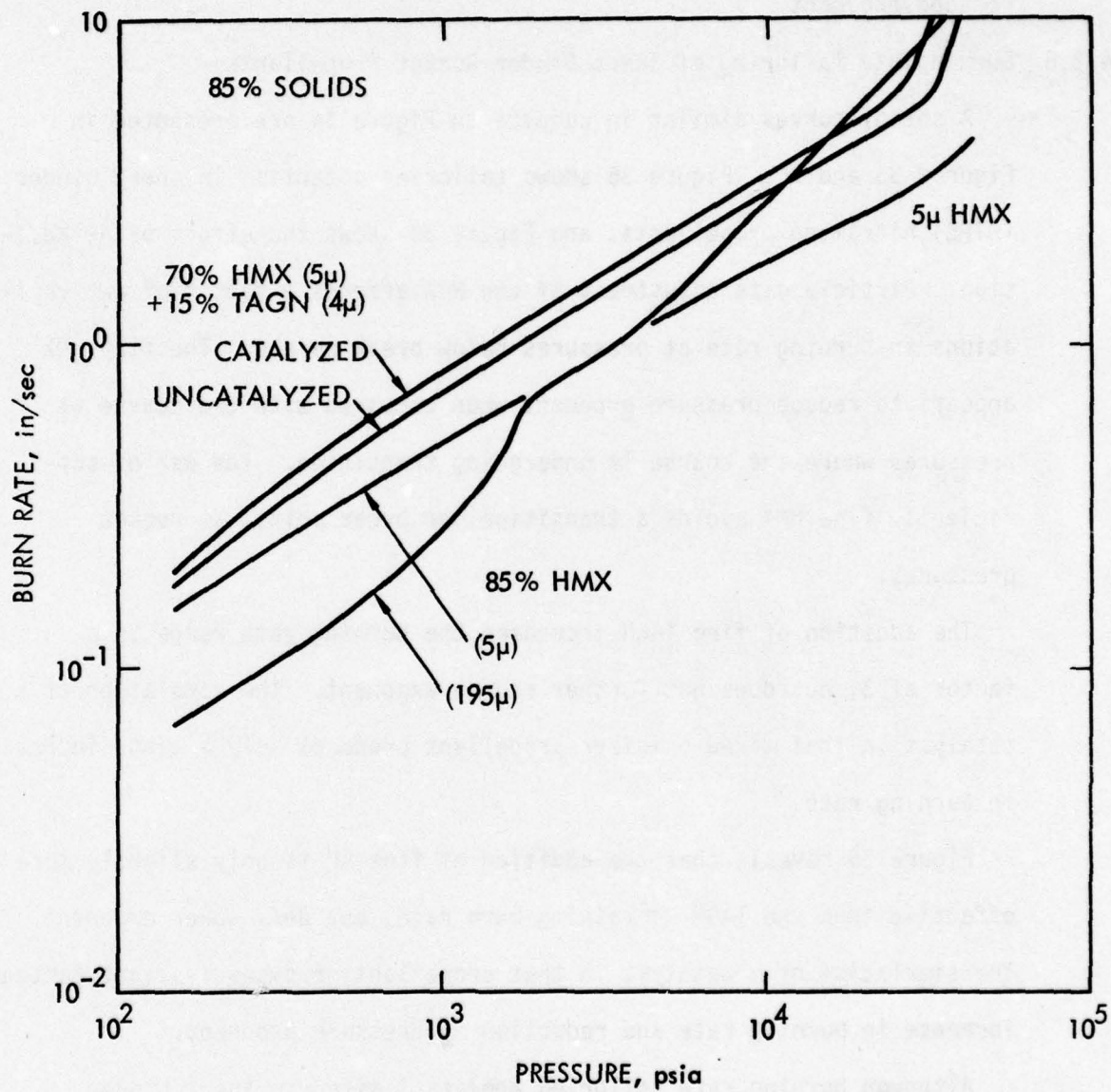


Figure 35. Burning Rate Tailorability of HMX and HMX/TAGN Propellants in HTPB Binder; Effects of Ingredient Variations

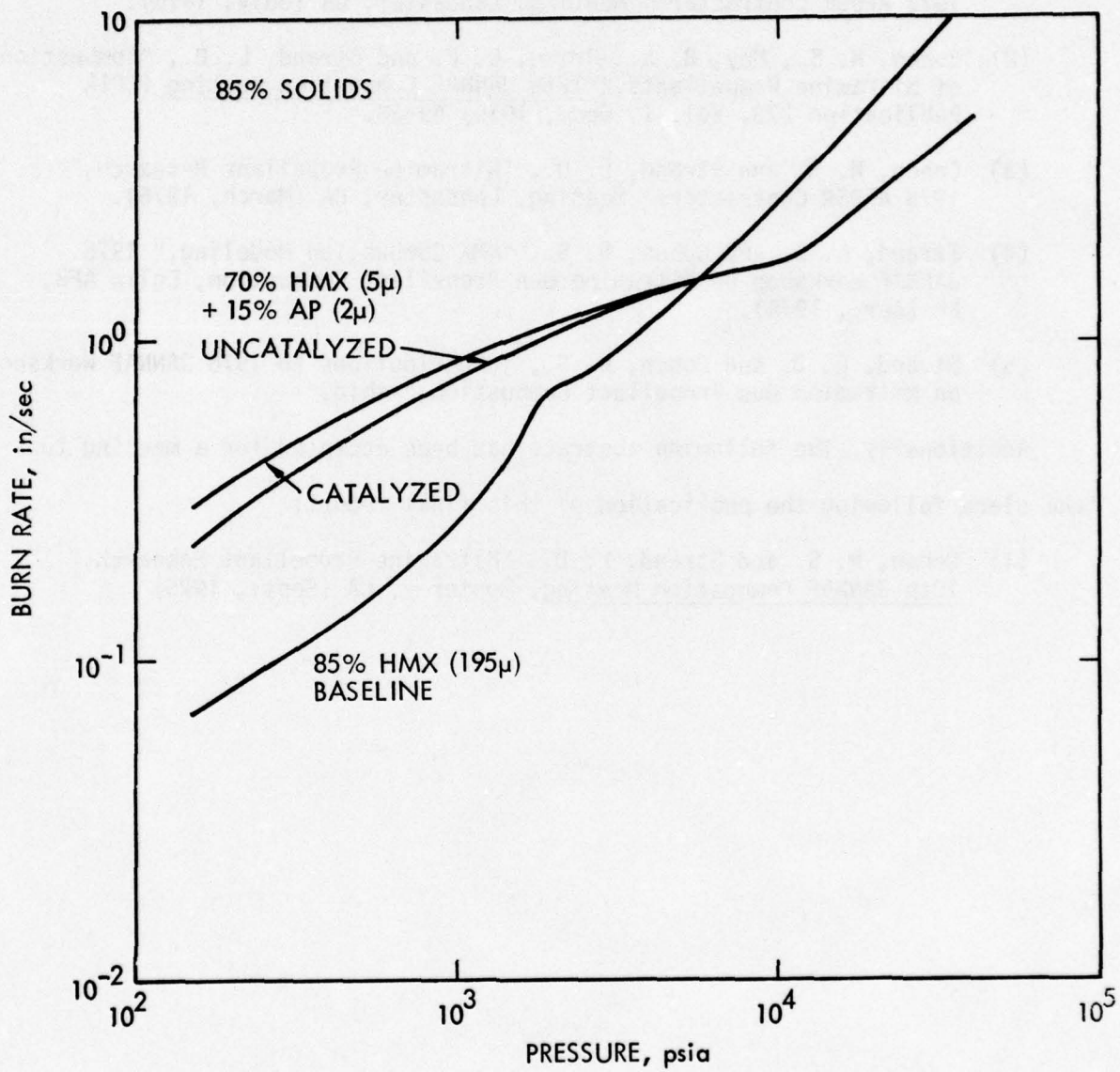


Figure 36. Burning Rate Tailorability of Mixed HMX/AP Propellant in HTPB Binder; Effects of Ingredient Variations

Section 6

PRESENTATIONS AND PUBLICATIONS

The following presentations and publications have been generated by this research contract:

- (1) Cohen, N. S. and Strand, L. D., "Combustion of Nitramine Propellants," 1975 AFOSR Contractors' Meeting, Lancaster, CA (July, 1975).
- (2) Cohen, N. S., Moy, B. K., Price, C. F. and Strand, L. D., "Combustion of Nitramine Propellants," 12th JANNAF Combustion Meeting (CPIA Publication 273, Vol. I, Dec., 1975) 49-58.
- (3) Cohen, N. S. and Strand, L. D., "Nitramine Propellant Research," 1976 AFOSR Contractors' Meeting, Lancaster, CA (March, 1976).
- (4) Strand, L. D. and Cohen, N. S., "HMX Combustion Modeling," 1976 JANNAF Workshop on Nitramine Gun Propellant Combustion, Eglin AFB, FL (Apr., 1976).
- (5) Strand, L. D. and Cohen, N. S., "Contributions to 1976 JANNAF Workshop on Nitramine Gun Propellant Combustion," *ibid.*

Additionally, the following abstract has been accepted for a meeting to take place following the publication of this final report:

- (1) Cohen, N. S. and Strand, L. D., "Nitramine Propellant Research," 13th JANNAF Combustion Meeting, Monterey, CA (Sept., 1976).

Section 7

CONCLUSIONS AND RECOMMENDATIONS

An extended model of the steady-state combustion of solid propellants has been developed which explains observed burning rate characteristics, and the effects of particle size, AP or nitramine oxidizer type, bimodal and mixed oxidizers, and binder type.

The exponent break that is characteristic of nitramine propellants may be avoided by the use of sufficiently fine particle sizes to maintain a planar melt surface. Distributions of HMX should contain sizes no larger than 4μ ; this may be relaxed to 8μ for lower melting point nitramines such as TAGN. If this is not practical, the break point can be mitigated by judicious combinations of HMX and TAGN because the burning rates are increased at pressures below the break point. The TAGN does not eliminate break points, however, and will itself exhibit a break at sufficiently high burning rates promoted by high TAGN concentrations. Optimum HMX/TAGN ratios appear to range between 1 and 2. An approach based upon matching the monopropellant characteristics of the nitramine and active binder should be evaluated. Although this approach would produce excessive temperatures and burning rates with HMX or RDX, it would not with low energy-low rate nitramines such as EDNA or NQ.

The burning rate tailoring of nitramine rocket propellants is limited unless AP is included. With inert binder, flame temperatures are relatively low and diffusion flame processes are not as powerful as with AP. Consequently, burning rates are low and are not as strongly particle size dependent. Similarly, catalysts which affect the diffusion flame will not have as great an impact as they do with AP. With active binder, there is no diffusion flame interaction so there is no significant basis for tailoring by particle size adjustment below break point pressures. TAGN would be helpful because of its own kinetics properties.

It is recommended that future work address the transient combustion properties of nitramine propellants. For gun propellant applications, the transient environment produced by guns and conventional closed bomb experiments may be causing effects which should be accounted for and described in recommending tailoring approaches. For smokeless rocket propellant applications, the melt layers observed in the present work may have favorable combustion instability implications which should be verified.

Section 8

REFERENCES

1. Kumar, R. N., and Strand, L. D., "Analytical Investigation of the Combustion Processes Occurring in Advanced Nitramine-Based Propellants," AFATL-TR-74-155, Air Force Armament Laboratory, Eglin AFB, Florida (Sept. 1974).
2. Kumar, R. N. and Strand, L. D., "Combustion Problems of Nitramine Propellants," AIAA Paper 75-239 (Jan., 1975).
3. Cohen, N. S., "Combustion of Nitramine Propellants," Report LPC-744F on Contract F44620-C-0031, Lockheed Propulsion Company, Redlands, CA (Jan., 1975).
4. Cohen, N. S. and Price, C. F., "Combustion of Nitramine Propellants," J. Spacecraft & Rockets 12, 608-612 (Oct. 1975).
5. Baumann, R. P., and Picard, J.P., "The Transfer of Rocket Propellant Technology to Gun Propellant Applications," 1973 JANNAF Propulsion Meeting, New Orleans, LA (Oct., 1972).
6. Stiefel, L., "A Review of the Effect of Composition on the Burning Rate of HMX-Containing Propellants," R-2046, Munitions Development and Engineering Directorate, Frankfort Arsenal, Philadelphia, PA (June 1972).
7. Simmons, R. L., "High Pressure Ballistics of Nitramine Gun Propellants," 9th JANNAF Combustion Meeting (CPIA Publication 231, Vol. III, Dec. 1972), pp. 41-59.
8. Simmons, R. L., Presentation at the JANNAF Workshop on the Combustion of Nitramine Propellants for Guns, Eglin AFB, Florida (Jan. 1973).
9. Moy, B. K., "Nitramine Combustion Problems," AFATL-TR-72-190, Air Force Armament Laboratory, Eglin AFB, Florida (Sept. 1972).
10. JANNAF Workshop on the Combustion of Nitramine Propellants for Guns, Eglin AFB, Florida (Jan. 1973).
11. Flanagan, J. E., "Advanced Gun Propellant for Gau-8," 11th JANNAF Combustion Meeting" (CPIA Publication 261, Vol. I, Dec. 1974), pp. 285-291.
12. Cohen, N. S., "Solid Propellant Combustion Literature Review," Report 835-S-1 Contract F04611-67-C-0089, Lockheed Propulsion Co., Redlands, CA (May, 1968).
13. Churchill, H. L., Fleming, R. W. and Cohen, N. S., "Aluminum Behavior in Solid Propellant Combustion," AFRPL-TR-74-13 (May, 1974).
14. Derr, R. L., Beckstead, M. W. and Cohen, N. S., "Combustion Tailoring Criteria for Solid Propellants," AFRPL-TR-69-190 (May, 1969).

15. Cohen, N. S., "Combustion of Nitramine Propellants," 11th JANNAF Combustion Meeting (CPIA Publication 261, Vol. I, Dec. 1974), pp. 267-283.
16. Beckstead, M. W., Derr, R. L. and Price, C. F., "A Model of Composite Solid Propellant Combustion Based on Multiple Flames," J. AIAA 8, 2200-2207 (Dec. 1970).
17. Glick, R. L. "Steady State Combustion of Nonmetallized Composite Solid Propellant," Contract F44620-74-C-0080, Thiokol Chemical Corp., Huntsville, AL (in progress).
18. Cohen, N. S., Derr, R. L. and Price, C. F., "Extended Model of Solid Propellant Combustion Based on Multiple Flames," 9th JANNAF Combustion Meeting (CPIA Publication 231, Vol. II, Dec. 1972), pp. 25-42.
19. Private communication with J. E. Flanagan, Rocketdyne, Canoga Park, CA (1976).
20. Private communication with M. W. Beckstead, Hercules, Inc., Magna, Utah, "HMX Propellant Combustion Studies," Contract F04611-76-C-0019 (in progress).
21. Rice, O. K. and Ginnel, R., "Theory of Burning of Double-Base Rocket Powders," J. Phys. and Colloid Chem. 54, 863-871 (1950).
22. Beckstead, M. W., Derr, R. L. and Price, C. F., "The Combustion of Solid Monopropellants and Composite Propellants," 13th Symposium (International) on Combustion (Combustion Inst., Pittsburgh, Pa., 1971), pp. 1047-1056.
23. Private communication with J. Gray, Rocketdyne, Canoga Park, CA and N. Stanley, Hercules, Inc., Cumberland, MD (1976).
24. Fogelzang, A. E., et al., "The Combustion of Nitramines and Nitrosamines," Dokl. Akad. Nauk SSSR 216, 603-606 (May, 1974).

APPENDIX A

NOMENCLATURE

a	binder melt interference exponent
b	distance from center of oxidizer particle to center of binder spacing
c	binder melt interference coefficient
c_p	heat capacity
D	particle size
h	height of particle protrusion (subscript p) or penetration (subscript N) relative to binder
K	ratio of oxidizer to propellant mass flux
M_{ox}	oxidizer mass flux
M_T	propellant mass flux
n	diffusion pressure exponent
P	pressure
Q_F	binder heat of decomposition
Q_{FF}	final flame heat release
Q_L	oxidizer heat of decomposition
Q_{ox}	oxidizer flame heat release
Q_{PF}	diffusion flame heat release
r	propellant burning rate
r_F	binder regression rate
S_o	normalizing propellant surface area
S_{ox}	exposed oxidizer surface area
T_F	propellant flame temperature
T_o	propellant conditioning temperature
T_s	propellant surface temperature

x_{PD}^*	diffusion height component of diffusion flame
x_{PF}^*	reaction height component of diffusion flame
α	oxidizer concentration
α_T	total oxidizer concentration
β_F	energy partition parameter according to relative flame heights
δ	binder interstitial spacing
λ	gas thermal conductivity
ρ	oxidizer density
ρ_F	binder density
ρ_P	propellant density
σ	coarse size fraction in bimodal distribution
ξ_{FF}	dimensionless final flame standoff
ξ_{ox}	dimensionless oxidizer flame standoff
ξ_{PF}	dimensionless diffusion flame standoff
ζ	oxidizer volume fraction

Subscript i	i^{th} oxidizer ($i = 1, 2$)
j	j^{th} particle size ($j = 1$, fine; $j = 2$, coarse)
M	melt condition
F	frozen condition

APPENDIX B

COMPUTER PROGRAM DESCRIPTION

B-1 SUBROUTINES AND FUNCTIONS

The computer program file is identified as KR, and its map of linked elements for execution is identified as KRUT. The component subroutines and functions are listed as follows:

Segment	MAIN PROGRAM
Subroutine	CONCAL
Subroutine	INPUT
Subroutine	OUTPUT
Subroutine	STEMP
Function	DON
Subroutine	HDCAL
Subroutine	SOXCAL
Function	CONVR2
Subroutine	BESSEL
Subroutine	FIND

Additionally, external library subroutines for heading, dating, plotting, math functions, controls, etc. are employed.

The outer loop control elements are depicted in the logic diagram of Fig. B-1, and the inner loop model solution elements are depicted in the logic diagram of Fig. B-2.

Segment MAIN is the master control element. Subroutine CONCAL increments the pressures at which burning rates are calculated. Subroutine INPUT reads the card inputs and performs calculations to establish values for other parameters which are in the nature of model inputs. In this regard, subroutine BESSEL calculates a Bessel function which is an input to the diffusion flame model, and subroutine FIND performs certain interpolations and extrapolations of inputs. Subroutine OUTPUT stores, writes and plots the results of the

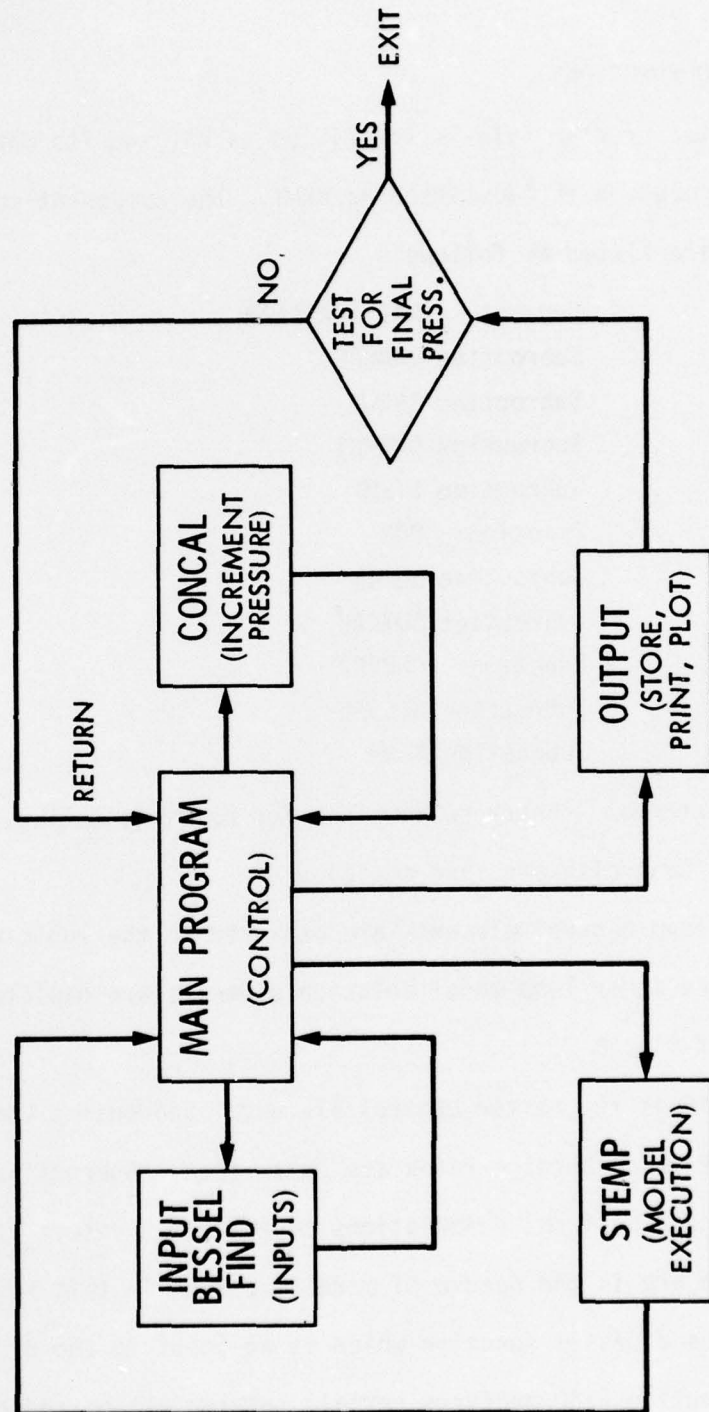


Figure B-1. Outer Loop Control Logic

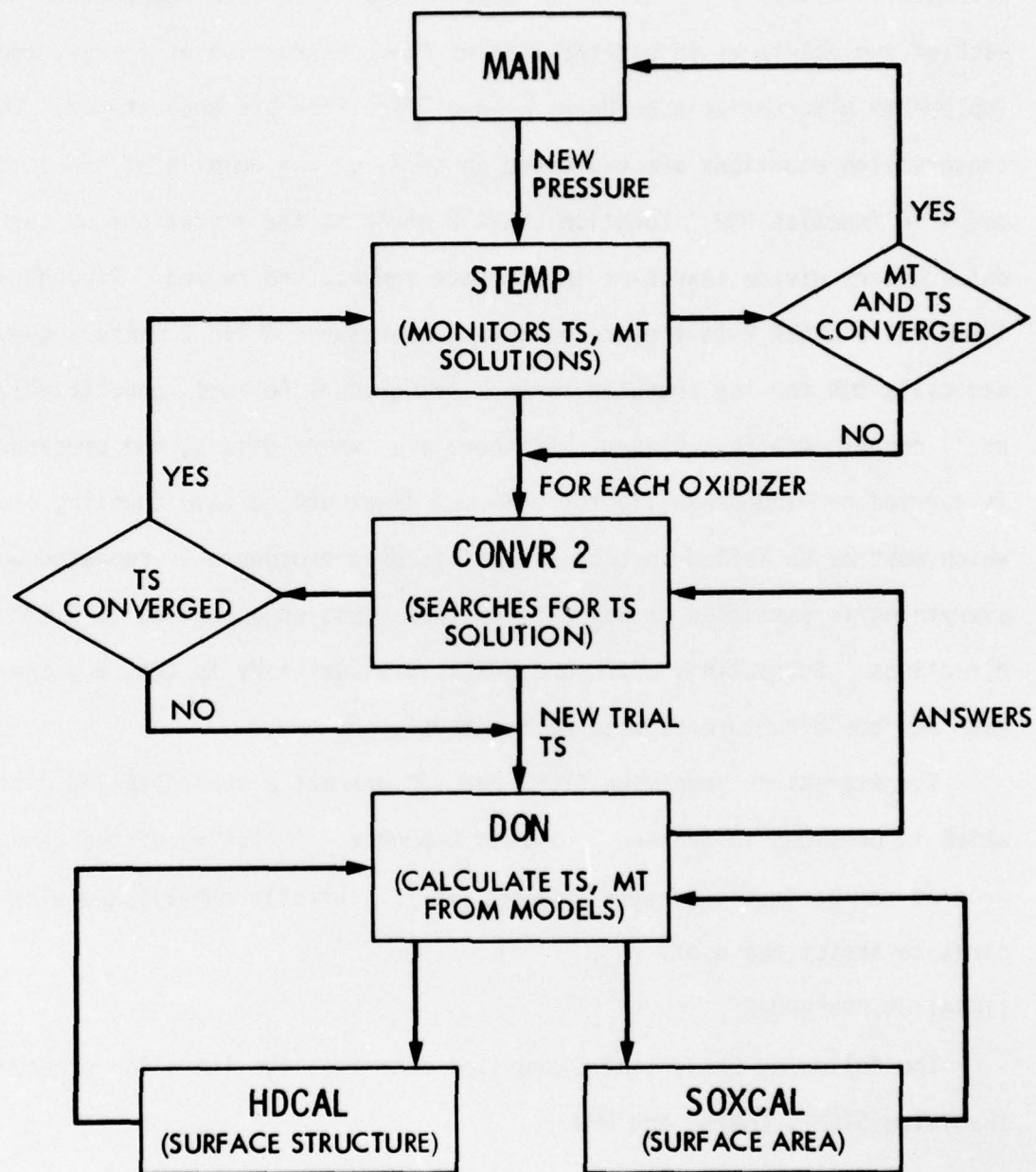


Figure B-2. Inner Loop Solution Logic

model executions which are provided by subroutine STEMP. The final calculation is keyed by the input value for final pressure.

Subroutine STEMP directs the combustion model calculations at each pressure. Basically, it calls for convergence of surface temperature for each of two oxidizers in satisfaction of the conservation of energy, and implements alternative procedures when difficulties are encountered. The conservation equations are expressed in terms of the details of the combustion model in function DON. Function CONVR 2 performs the iterations by carrying out a binary divide search of the surface temperature regime. Procedurally, STEMP calls CONVR 2 to iterate surface temperature; CONVR 2 makes a guess and calls DON for the computed surface temperature (error), repetitively, until convergence is achieved. If there are two oxidizers, the procedure is carried out independently for each but there are certain coupling elements which must be satisfied in each case; this dual procedure is repeated until everything is satisfied or any difficulties resolved according to STEMP directions. Subroutines HDCAL and SOXCAL are auxiliary to DON, and are concerned with surface structure aspects of the model.

The iterations involving STEMP and DON warrant a more detailed discussion, which is provided in Section 2 of this Appendix. A listing of the computer program can be furnished upon request; it is liberally embellished with comment cards to assist the user.

B-2 ITERATION PROCEDURE

The following sequential discussion describes the iteration procedure involving STEMP, CONVR2 and DON.

1. GUESS TS (1)

For one oxidizer, I=1 is the only problem. For two oxidizers, I=1 is computed first.

2. CALCULATE MOX (1)

3. CALCULATE HDP (1), HDN (1), EACH PARTICLE

For AP, the original BDP expressions are used; there is no planar melt and no deep penetration. For inert binder, RF is calculated from an Arrhenius expression using TS(1); for active binder, it is interpolated from an input table for binder rate.

4. CALCULATE SOXM(1), SOXF(1)

For AP, only SOXF applies. For nitramine, it is first assumed that SOXM applies. Particle contributions are weighted according to volume fraction.

5. CALCULATE MT

The contribution from the other oxidizer is first guessed on the basis of concentration ratio, then the previous answer is used for all subsequent trials. For inert binder, continuity establishes the binder contribution. For active binder, the binder contribution is determined from the input burning rate table and residual SOX.

6. CALCULATE R=MT/RHOP

7. DO MELT/FROZE TEST FOR EACH NITRAMINE PARTICLE

This is inoperative for AP.

8. IF FROZE, SOXF(1) APPLIES WITH EXEF (DEEP PENETRATION) SUBSTITUTED FOR HD FOR THAT PARTICLE; OTHERWISE SOXM(1) IS RETAINED

If there has been a shift from melt to froze, go back to Step 5 and repeat.

9. CALCULATE XSTARD

The final diffusion flame has little quantitative significance, but has been retained in the form of a single averaged flame. For the first trial, it is computed only on the basis of I=1; it is averaged on subsequent trials.

10. CALCULATE XSTPD(1), XSTPF(1)

AP and nitramine use different primary flame expressions. For AP, the characteristic diffusion dimension is based on DELDI; for nitramine, it is based on \sqrt{BSQR} . Kinetics also differ. For MT dependencies, MT is treated as above and then partitioned according to the relative mass flow contribution of this oxidizer.

11. CALCULATE XSTAP(1)

12. CALCULATE BETAF(1)

13. CALCULATE DIMENSIONLESS FLAME HEIGHTS

14. CALCULATE XTS

The energy balance is partitioned for this oxidizer. The relative impacts of the flames are determined by the BETA_F for this oxidizer. For certain oxidizer-active binder combinations, the diffusion flame heat release may be set to zero (no diffusion flame).

15. COMPARE TS(1)-XTS

Go back to Step 1 and repeat until convergence.

16. IF SOLUTION CANNOT CONVERGE FOR MELT OR FROZE, REITERATE UPON AN INTERMEDIATE SOX(1), CODE TRAN (TRANSITION), KFLG(1)=1
A nitramine break point may cause an endless flip-flop between melt and froze which prevents a TS solution. If this occurs, the remedy is as follows. STEMP directs a partition of SOXF and SOXM for that particle, in DON, by XK9. CONVR2 then iterates XK9 for that intermediate surface structure which will converge TS. In other words, the particle undergoing transition is deemed to be part melted and part frozen for purposes of Step 8. If this occurs, the output will note CODE=TRAN for that particle and print the value of XK9. If both particles (bimodal) are TRAN, each is partitioned the same way.

17. UPON CONVERGENCE OF TS(1), STORE MT AS MTTST
18. REPEAT STEPS 1-16 FOR THE SECOND OXIDIZER

The contributions from the first oxidizer are taken from the above answer. If there is only one oxidizer, the first completes the problem.

19. UPON CONVERGENCE OF TS(2), COMPARE NEW MT WITH MTTST

The convergence of TS(2) will yield a new MT. If this differs from MTTST beyond a certain tolerance, go back to Step 1 and recalculate the first oxidizer based on the results for the second. Repeat until MT and MTTST agree within the tolerance.

20. IF MT CONVERGENCE CANNOT BE ACHIEVED, IMPLEMENT ALTERNATIVE PROCEDURE, KMIX

Break point transitions sometimes cause problems in MT convergence as well as in TS convergence because results for one oxidizer may cause another to flip between melt and froze. If MT and MTTST cannot agree, STEM directs the iterations to begin all over again with all nitramine particles forced to be melted (KMIX=1). Upon solution, STEM tests the melt criterion (analogous to Step 7) and forces a melt, or frozen condition to exist, as applicable, in a next round of iterations (KMIX=2 or 3- one oxidizer has a frozen particle, or KMIX=4- both oxidizers have a frozen particle). This procedure is repeated as long as a melted particle would become a frozen particle in a subsequent round. If a KMIX condition is returned to STEM unchanged, the solution for that condition is accepted. If there is no solution, or if a frozen particle would flip back to a melted particle in a subsequent round, the second alternative is

implemented. The first alternative seeks to assist the iterations by forcing what the state of the particle must logically be, and is usually satisfactory.

21. IF MT CONVERGENCE STILL CANNOT BE ACHIEVED, IMPLEMENT ALTERNATIVE PROCEDURE, CODE ADJ (ADJUST)

As a last resort, STEMP will accept those answers which come closest to converging MT. A running survey is made to update the best answers. (Coding associated with statement DIFF.) These answers are returned to MAIN which then performs an adjustment (Code ADJ). The weaker mass flux component is adjusted to the extent that convergence would have been achieved. If this occurs, the output will note FACT=ADJ1 or ADJ2, depending upon which was adjusted, for that condition. The answer should be suspect, and perhaps bypassed in handplotting the results if it appears unreasonable.

B-3 CARD INPUT SEQUENCE AND STANDARD VALUES

The following describes input cards in sequence, with appropriate comments and numerical values which have been used.

JOB CARD

SEQUENCE OF TAPE CONTROL CARDS

EXECUTION CARD

<u>CARD</u>	<u>COLUMN</u>	<u>ENTRY</u>	<u>SYMBOL</u>	<u>UNITS</u>
1	2	Plot Format	IPLCT	-
	4	Extra Printout for Debug Analysis	IBUG	-
		COMMENT: IPLCT=1, Each case plotted separately. IPLCT=2, More than one case plotted together. IBUG=1, Printout of parameters tracing iterations. IBUG=Blank, No trace printout.		
2	3	Title of Case or Group	ITIT	-
3	2	Number of Oxidizers	NOX	-
		COMMENT: NOX=1, Single Oxidizer. NOX=2, Two Oxidizers, or Single Oxidizer with . more than two particle sizes.		
4	3	Name of First Oxidizer	ITIT1	-
5	2	Concentration of Fine Size of Oxidizer 1	ALF(1,1)	fraction
		COMMENT: In running multiple powders, the finest particle size should be the fine size of Oxidizer 1		
12		Particle Size of Fine Size of Oxidizer 1	D(1,1)	microns
22		Density of Oxidizer 1	RHOX(1)	g/cc
32		Concentration of Coarse Size of Oxidizer 1	ALF(1,2)	fraction
		COMMENT: If unimodal, input as zero.		
42		Particle Size of Coarse Size of Oxidizer 1	D(1,2)	microns
		COMMENT: If unimodal, input as zero.		

<u>CARD</u>	<u>COLUMN</u>	<u>ENTRY</u>	<u>SYMBOL</u>	<u>UNITS</u>
5 (contd)	52	Activation Energy of Decomposition of Oxidizer 1	E0X(1)	cal/mol
		COMMENT: 22000 has been used for AP; 50000 for Nitramine.		
	62	Prefactor for Decomposition of Oxidizer 1	A0X(1)	g/cm ² -sec
		COMMENT: 0.3000E+06 has been used for AP; 0.5000E+10 for HMX and RDX; 0.5000E+11 for TAGN		
6	2	Rate Constant for Monopropellant Flame of Oxidizer 1	KAP1(1)	g/cc-sec-atm ²
		COMMENT: 1.12 has been used for AP; 0.246 for HMX and RDX; 1.23 for TAGN		
12		Order of Monopropellant Flame Reaction for Oxidizer 1	XN2(1)	-
		COMMENT: 1.80 has been used for AP; 2.00 for Nitramine.		
22		Primary Flame Rate Constant for Oxidizer 1	KAPF(1)	g/cc-sec-atm ²
		COMMENT: A value of 30 has been used for AP; in the absence of better information, the same value has been used for Nitramine.		
32		Primary Flame Reaction Order for Oxidizer 1	XN1(1)	-
		COMMENT: 1.5 has been used for AP; 2.0 for Nitramine.		
42		Monopropellant Flame Temperature for Oxidizer 1	TAP(1)	°K
		COMMENT: 1400 has been used for AP; 3275 for HMX; 3292 for RDX; 2700 for TAGN		
52		Heat of Decomposition for Oxidizer 1	QL(1)	cal/g
		COMMENT: -120 has been used for AP; -225 for HMX and RDX; -185 for TAGN.		
62		Melting Point of Oxidizer 1	TMELT(1)	°K
		COMMENT: The value for HMX is 551; 467 for RDX; 400 for TAGN. For AP, zero should be input in order to key the program logic away from the Nitramine models based on particle melting.		

<u>CARD</u>	<u>COLUMN</u>	<u>ENTRY</u>	<u>SYMBOL</u>	<u>UNITS</u>
7	2	Heat of Fusion of Oxidizer 1	QLM(1)	cal/g
		COMMENT: 132.5 has been used for HMX and RDX, 30 for TAGN; for AP, zero should be input.		
12		Depth of Allowable Penetration of the Fine Size of Oxidizer 1	XN(1,1)	-
		COMMENT: It has been the practice to input 1 for sizes of the order of units of microns, 2 for tens of microns and 3 for hundreds of microns; for AP, which does not use this model, input 1.		
22		Repeat for the Coarse Size of Oxidizer 1	XN(1,2)	-
32		Thermal Diffusity of Oxidizer 1	XKAPO(1)	cm ² /sec
		COMMENT: 0.1100E-02 has been used for HMX and other Nitramines; the same value can be input for AP, which does not use this model.		
42		Thermal Conductivity of Oxidizer 1	XLAMO(1)	cal/cm- sec-°K
		COMMENT: 0.4900E-03 has been used for HMX and other Nitramines; the same value can be input for AP, which does not use this model.		
52		Average Flame Height Factor for Oxidizer 1	AFH(1)	-
		COMMENT: 0.3 has been used for AP; 1.0 for Nitramines.		
62		Primary Diffusion Flame Key for Oxidizer 1	KAP2(1)	-
		COMMENT: If the oxidizer is a stoichiometrically balanced Nitramine and the binder is active, input 0. to eliminate the diffusion flame; otherwise input 1. to retain the flame.		
8	3	Name of Second Oxidizer	ITIT2	-
		COMMENT: If NOX=1, this card and the following three cards are not necessary.		
9		Analogous to Card 5 for Oxidizer 2		
10		Analogous to Card 6 for Oxidizer 2		
11		Analogous to Card 7 for Oxidizer 2		
		COMMENT: Symbols are ALF(2,1), D(2,1), RHOX(2), ALF(2,2), D(2,2), EOX(2), AOX(2), etc.		

<u>CARD</u>	<u>COLUMN</u>	<u>ENTRY</u>	<u>SYMBOL</u>	<u>UNITS</u>
12	2	Concentration of Metal	BETA	fraction
		COMMENT: The provision for aluminum is invalid in those special situations where aluminum behavior has a significant effect upon the combustion process. The inclusion is proper where, as has usually been the case, the aluminum merely occupies space, absorbs its heat of fusion and raises the propellant flame temperature.		
12		Density of Metal	RHOM	g/cc
22		Metal Heat of Fusion	QM	cal/g
		COMMENT: A value of 200 has been used for aluminum.		
13	3	Name of Binder	ITIT3	-
14	2	Binder Density	RHOF	g/cc
		COMMENT: For various constants associated with various inert binders, see AFRPL-TR-72-96, "Role of Binder in Solid Propellant Combustion"; a value of 0.92 has been used for HTPB.		
12		Binder Heat of Decomposition	QFUEL	cal/g
		COMMENT: As above; a value of 569 has been used for HTPB. For active binder, a value of -170 has been used to represent NC; assume proportional to binder flame temperature.		
22		Activation Energy of Binder Decomposition	EF	cal/mol
		COMMENT: As above, a value of 16900 has been used for HTPB.		
		COMMENT: For active binder, input zero in order to key the logic for it.		
32		Prefactor for Binder Decomposition	AF	g/cm ² -sec
		COMMENT: A value of 299 has been used for HTPB; for active binder, which does not use this model, the same value can be input.		
42		Binder Thermal Conductivity	XLAMF	cal/cm-sec-°K
		COMMENT: As above; a value of 0.4410E-03 has been used for HTPB.		

<u>CARD</u>	<u>COLUMN</u>	<u>ENTRY</u>	<u>SYMBOL</u>	<u>UNITS</u>
14 (contd)	52	Binder Thermal Diffusity	XKAPF	cm ² /sec
		COMMENT: As (42); a value of 0.1100E-02 has been used for HTPB.		
15	2	Gas Molecular Weight	GMW	g/mol
		COMMENT: This would come from a thermochemical calculation for the propellant; typical values range from 16 - 28.		
12		Molecular Weight for the Gases in the Primary Flame	PMW	g/mol
		COMMENT: For Nitramines, it has been assumed that PMW=GMW. For AP, a value of 30 has been used assuming the primary flame to involve a perchloric acid - hydrocarbon reaction. For mixed AP-Nitramine, input a weighted average.		
22		Diffusion Correction	Y	-
		COMMENT: This parameter in part corrects for the uncertainty in mixing lengths; a value of 10.5 has been used.		
32		Diffusion Coefficient	GAMMA	cm ² -atm/sec- °K
		COMMENT: A high value, typically 1000, has been input in accordance with Beckstead's modification to the basic Burke-Schumann model of mixing. If this causes an overflow on some computers, because of the enormous values of components that result, reduce to 100 or 10. A value of the order of 0.001 would begin to upset the modification.		
42		Propellant Stoichiometric Ratio	XNU1	-
		COMMENT: For various inert binders with AP, see AFRPL-TR-72-96; for HTPB, the value is 9.30.		
		For Nitramines, the value is calculated from the oxidizer content of the Nitramine and the fuel content of the binder; the premise is that an active diffusion flame can exist. For HMX/HTPB, the value is 53.		

CARD	COLUMN	ENTRY	SYMBOL	UNIT
15	42	COMMENT: For active binder with KAP2=0, the model is (contd) (contd) not used so 53 can be input. For active binder with AP, the value is calculated from the oxidizer content of the AP and the fuel value of the binder; the premise is that an active diffusion flame can exist. On this basis, a typical value for AP/NC-NG is 8.8. Note that AP with active binder is analogous to HMX with inert binder in that a stoichiometrically balanced system is combined with an unbalanced system. For HMX or RDX with active binder, both are balanced and so a diffusion flame is presumed absent.		
		COMMENT: For mixed AP-Nitramine and active binder, use the value for AP and active binder. For mixed AP-Nitramine and inert binder, a weighted average may be used in lieu of a detailed analysis.		
52		Primary Flame Stoichiometric Ratio	XNUP	-
		COMMENT: For Nitramines, it has been assumed that XNUP=XNUL. For AP, a value of 5.37 has been used assuming the primary flame to involve a perchloric acid-hydrocarbon reaction. For mixed AP-Nitramine, input a weighted average.		
16	2	Gas Thermal Conductivity	XLAMB	cal/cm-sec-°K
		COMMENT: A value of 0.0003 has been used.		
12		Average Heat Capacity	CSUBP	cal/g-°K
		COMMENT: A value of 0.3 has been used.		
22		Diffusion Pressure Dependence	PXP	-
		COMMENT: For Nitramine, 0.625 has been used; for AP, this model will not be used and zero may be input.		
		COMMENT: For mixed AP-Nitramine, input 0.625 and it will properly be used for Nitramine and bypassed for AP.		
32		Nitramine Diffusion Correction	FAC99	-
		COMMENT: For Nitramine, a value of 17.0 has been used; for AP, it will not be used and zero may be input.		

<u>CARD</u>	<u>COLUMN</u>	<u>ENTRY</u>	<u>SYMBOL</u>	<u>UNITS</u>
16 (contd)	32 (contd)	COMMENT: For mixed AP-Nitramine, input 17.0 and it will properly be used for Nitramine and bypassed for AP.		
	42	Nitramine Surface Structure Exponent	FACB	-
		COMMENT: For Nitramine, a value of 0.25 has been used; for AP, it will not be used and zero may be input.		
		COMMENT: For mixed AP-Nitramine, input 0.25 and it will properly be used for Nitramine and bypassed for AP.		
	52	Flame Shape Key	CONF	-
		COMMENT: A value of zero has been used to key a parabolic shape; a value of unity would key a conical shape.		
17	2	Oxidizer Ignition Constant	CIGN	$\text{sec-atm}^{0.72}/\text{cm}^{0.8}$
		COMMENT: A value of 190 has been used for AP; the same has been assumed for Nitramines.		
	12	Ignition Pressure-Dependence	POWIGN	-
		COMMENT: A value of 0.721 has been used for AP; the same has been assumed for Nitramines.		
	22	Ignition Diameter-Dependence	POWD	-
		COMMENT: A value of 0.8 has been used for AP; the same has been assumed for Nitramines.		
	32	Nitramine Surface Structure Coefficient	FAC77	$\text{microns}^{-0.25}$
		COMMENT: A value of 0.8759 has been used; for AP, it will not be used and zero may be input.		
		COMMENT: For mixed AP-Nitramine, input 0.8759 and it will properly be used for Nitramine and bypassed for AP.		
	42	Propellant Bulk Temperature	TZERO	$^{\circ}\text{K}$
	52	Diffusion Exponent	EPS	-
		COMMENT: A value of 1.0 has been used for AP; input 0.0 for Nitramine and mixed AP-Nitramine.		

<u>CARD</u>	<u>COLUMN</u>	<u>ENTRY</u>	<u>SYMBOL</u>	<u>UNITS</u>
18	2	Starting Pressure	PSTART	atm
	12	Final Pressure	PSTOP	atm
COMMENT: A factor of from 200 - 300 has been used for the pressure range.				
19	2	Number of Entries (Cards) for Table of Flame Temperature Versus Pressure	NPP	-
	COMMENT: For low pressure calculations, it was desired to account for changes in flame temperature with pressure; input a value of at least 2.			
20	2	Pressure	PFP(1)	atm
	12	Flame Temperature	TFP(1)	°K
	COMMENT: This constitutes the first table entry. The flame temperatures are obtained by thermo-chemical calculation.			
21	Repeat for Data at the Second Pressure; PFP (2) and TFP(2).			
	COMMENT: Unless a low pressure study is planned, this will suffice. For high pressure work, the two temperatures have been taken as equal.			
22	2	Number of Entries (Cards) for Table of Burn Rate Versus Pressure for Active Binder	NPD	-
	COMMENT: This card and the companion sequence are omitted for inert binder.			
23	2	Pressure	PJX(1)	psia
	12	Burning Rate	RJX(1)	in/sec
24	Repeat for Data at the Second Pressure; PJX(2) and RJX(2).			
	COMMENT: Ten cards or less should suffice to adequately describe the burn rate curve for the binder by itself.			
LAST	2	\$NAM1		
	8	NJOB=4,\$END		
	COMMENT: For multiple cases, this last card is preceded by the following sequence of cards.			

<u>CARD</u>	<u>COLUMN</u>	<u>ENTRY</u>	<u>SYMBOL</u>	<u>UNITS</u>
MULTIPLE 1	2	\$NAM1		
8		COMMENT: Begin all changes that are desired for the new case, running them consecutively in any order, using SYMBOL= , interspersing with a comma rather than a space. Do not go beyond column 72.		
MULTIPLE 2	3	Continue Changes.		
		COMMENT: If a parameter is not changed, the value from the previous case will be used.		
END OF MULTIPLE	3	Complete changes, including keying any title and plot changes, followed by \$END.		
		COMMENT: The case or group header title is changed with the key ITIT=1,. This may be changed after each case if plotted separately, or after the first of a subsequent group of cases to be plotted together. Otherwise do not change.		
		COMMENT: To key the plot for the last of several cases to be plotted together, include IPLOT=4,. If a subsequent group of cases is then to be plotted together, the first of that group should include IPLOT=2,.		
		COMMENT: The name of oxidizer 1 is changed with the key ITIT1=1,. The name of oxidizer 2 is changed with the key ITIT2=1,. The name of the binder is changed with the key ITIT3=1,.		
TITLE	3	The New Title (If ITIT=1)		
NAME	3	The Name of the New Oxidizer (If ITIT1=1)		
NAME	3	The Name of the New Oxidizer (If ITIT2=1)		
NAME	3	The Name of the New Binder (If ITIT3=1)		
NEXT		Repeat the above for each new case.		
MULTIPLE 1				
LAST		Insert the last card at this point for multiple cases.		